SET - Brazilian Society of Television Engineering

SET INTERNATIONAL JOURNAL OF BROADCAST ENGINEERING

SET IJBE v. 1, 2015

ISSN Print 2446-9246

ISSN Online 2446-9432

SET INTERNATIONAL JOURNAL OF

BROADCAST ENGINEERING

SET IJBE v. 1, 2015

volume 07 - número 07 - 2013

ISSN print: 2446-9246
ISSN online: 2446-9432

Online version available at www.set.org.br/IJBE

Rio de Janeiro/RJ
Rua Jardim Botânico,700 - Sala 306 | 22461-000
Phone.: + 55 (21) 2512-8747
www.set.org.br | set@set.org.br

São Paulo/SP
Av. Auro Soares de Moura Andrade, 252- Cj. 11 | 01156-001
Phone: +55 (11) 3666 9604
www.set.org.br | set@set.org.br

SET INTERNATIONAL JOURNAL OF BROADCAST ENGINEERING

SET IJBE v. 1, 2015, 75 pages, 10 articles.

EDITORIAL BOARD

CORPORATE AUTHOR AND EDITOR

SET - Brazilian Society of Television Engineering, or, in portuguese, **SET - Sociedade Brasileira de Engenharia de Televisão.** Address: Av. Auro Soares de Moura Andrade, 252, cj 11 – CEP (zip code): 01156-001 – São Paulo - SP - Brazil.

JOURNAL'S PRESENTATION

The **SET IJBE, SET International Journal of Broadcast Engineering**, is a peer-reviewed, Open- Access, article-at-a-time publishing, International Scientific Journal with the objective to cover engineered communications knowledge in the Broadcasting field. SET IJBE seeks the latest and most compelling current research and state of the art technologies.

PUBLISHING SCHEDULE AND SCHEMA

Online version – Once an article is accepted and its final version approved by the Editorial Board it will be immediately published online on an article-at-a-time basis. **Printed version** – Yearly, all articles accepted and published online over the last 12 months will be assembled together to be published in its printed version.

TYPES OF PAPERS

Regular Papers (Full papers) - Traditional and original research. [6 to 20 pages]
Tutorial Papers - Brand new OTT (Over The Top) detailed implementation and state of the art systems full setup. [4-6 pages]
Letters - Short notes and considerations about current and relevant techniques, technologies and implementations on engineered solutions. [1-3 pages]

ONLINE ARTICLE SUBMISSION

If you wish to submit your manuscript to SET IJBE, SET International Journal of Broadcast Engineering, please access the Journal's website at: www.set.org.br/IJBE

OPEN ACCESS POLICY

If the manuscript is accepted to be published, the article will be made free to read and reuse under a Creative Commons Attribution (CC-BY) license.

EDITORIAL OFFICE

If you have any need for additional information please contact SET IJBE administrative staff, **SET International Journal of Broadcast Engineering** administrative staff: Address: Av. Auro Soares de Moura Andrade, 252, cj 11 - CEP(zip code): 01156-001 - São Paulo - SP – Brazil. Email: IJBE@set.org.br

AIMS AND SCOPE ARE AS FOLLOWS, BUT ARE NOT LIMITED TO

Advanced audio technology and processing
Advanced display technologies
Advanced RF Modulation Technologies
Advanced technologies and systems for emerging broadcasting applications
Applying IT Networks in Broadcast Facilities
Broadcast spectrum issues – re-packing, sharing
Cable & Satellite interconnection with terrestrial broadcasters
Cellular broadcast technologies
Communication, Networking & Broadcasting
Content Delivery Networks – CDN
Digital radio and television systems: Terrestrial, Cable, Satellite, Internet, Wireless.
Electromagnetic compatibility issues between collocated services (e.g. broadcast and LTE)
General Topics for Engineers (Math, Science & Engineering)
Hybrid receiver technology
Interactive Technology for broadcast
IP Networks management and configuration
Metadata systems and management
Mobile DTV systems (all aspects, both transmission and reception)
Mobile/dashboard technology
Next-gen broadcast platforms and standards development
Non-real time (NRT) broadcast services
Ratings technology Second screen technology and services
Secondary service system design; mitigation of interference to primary services
Securing Broadcast IT Networks
Signal Processing & Analysis
Software Defined Radio - SDR Technologies
Streaming delivery of broadcast content
Transmission, propagation, reception, re-distribution of broadcast signals AM, FM, and TV transmitter and antenna systems
Transport stream issues – ancillary services
Unlicensed device operation in TV white spaces

SUMMARY

[Journal Page Number located at the bottom right of the footnote] - Content

Current Issue	**05**	**Editorial**
Article 1	**06**	**Quality Assessment of Video in Digital Television** Roberto N. Fonseca and Miguel A. Ramirez
Article 2	**19**	**Transmission and Reception Tests of Digital Terrestrial TV in the Metropolitan Region of Curitiba** Célio Lúcio Vasco, José Frederico Rehme, Ruth Angelina Martins, Elias Agostinho, Alexandre de Almeida Prado Pohl, Richard Demo de Souza, Keiko Verônica Ono Fonseca, and Marcelo Eduardo Pellenz
Article 3	**26**	**Simulation Software for the ISDB-T_B Modulation System** Cristiano Akamine and Yuzo Iano
Article 4	**37**	**IP Transmission over ISDB-T_B** Gustavo de Melo Valeira, Cristiano Akamine, Edson Lemos Horta, Fujio Yamada, and Rodrigo Eiji Motoyama
Article 5	**43**	**Objective Analysis of HDTV H.264 x MPEG-2 with and Without Packet Loss** Eduardo Santos Bueno, Cristiano Akamine, Renato de Mendonça Maroja, and Gustavo de Melo Valeira
Article 6	**48**	**Passive Reception of Digital TV Signals with an Antenna** Fujio Yamada, Cristiano Akamine, Rodrigo Eiji Motoyama, and Gustavo de Melo Valeira
Article 7	**52**	**Experimental Investigation of Digital TV Signals with Multipath in Curitiba** Marco Antônio Costa de Borba, Carlos Eduardo Neves Mayer, Keiko Verônica Ono Fonseca, Alexandre de Almeida Prado Pohl, Karine de Ramos Good, Luciano Mildemberg, Deisi Luiza Wosch, and Ruth Angelina Martins
Article 8	**58**	**Factors that Influence the Performance of Terrestrial Digital TV Receivers in São Paulo** Paulo Guedes Esperante, Raquel Cymrot, Cristiano Akamine, Fujio Yamada, Rodrigo Eiji Motoyama, and Fabio Raia
Article 9	**64**	**Digital TV Signal Reception Testing in a Device with Spatial Diversity** Eduardo Romani, Wyllian Bezerra da Silva, Marco Antônio Costa de Borba, Keiko Verônica Ono Fonseca and Alexandre de Almeida Prado
Article 10	**70**	**Results of Field Tests of the ISDB-T_B System at 8 MHz in Botswana** Eduardo S. Bueno, Gunnar Bedicks, Jr., Cristiano Akamine, and Edson L. Horta

Current Issue **EDITORIAL**

Dear reader,

In this issue of SET IJBE we proudly bring to you our first edition, this project required dedication and support from SET personnel, our associates and non-associates. And, to all these people, we from SET, and we believe the worldwide community working in the Broadcast Engineering field would like to show our appreciation and express our gratitude towards them. For those who are not yet fully acquainted with our mission, we would like to explain that the Brazilian Society of Television Engineering (SET) is a Technical-Scientific Association, non-profit organization, founded in 1988, conveying together professionals, academics and companies, dedicated to the engineering studies, developments, refinement of technical, operational and scientific knowledge, in the fields of Radio, Television, Telecommunications, Film and New Medias. In this 2015 Edition we've conveyed an attention-grabbing series of articles regarding Digital Television, the reason for such emphasis is to collaborate with the current Analogic Television switch off process recently started in Brazil and supplement the technology unceasing development. In addition to this, the prominent adoption of the ISDB-T standard in most South-American countries and its expansion towards African and Asian regions enhanced the reason for this choice in this issue. We hope you enjoy and take advantage of these papers and feel motivated to submit us yours in the future.

Best wishes,

SET IJBE Staff

Quality Assessment of Video in Digital Television

Roberto N. Fonseca and Miguel A. Ramirez

***Abstract*—This article is based on the assessment of the quality of video signals, specifically an objective evaluation of completely referenced video signals in standard definition. The most reliable way to measure the difference in quality between two video scenes is using a panel made from television viewers, resulting in a subjective measure of the difference in quality. This methodology requires a long period and has an elevated operational cost; this makes it an unpractical method to be used. This article will present the relevant aspects for the assessment of video application in standard definition digital television and the validation of these methodologies. The objective is to test metrics below the computational cost that evaluate the peak signal-to-noise ratio (PSNR) and measures the structural similarity index measure (SSIM). One methodology for the validation of these metrics is presented and is based on the scenes and the results of subjective tests performed by VQEG. The scenes for these metrics are prepared by the equalization of brightness, detail smoothing, and edge detection. Controlling the intensity of these filters, a new set of measures is obtained. Performance comparisons are made between these new sets of measures and the set of measures obtained by VQEG. The results showed that the objective measures are easily implemented from the computational point of view, and can be used to compare the quality of video signals, if properly combined with techniques for the adequacy of the human visual system like the mitigation and extraction of contours.**

***Index Terms*—Color image analysis, Mean square error (MSE), Objective quality, Video quality, Visual system.**

I. Introduction

THE transmission of television signals in Brazil began in 1950, changing to color television signals in 1972. In 1996, a joint operation between Grupo Abril and Grupo Hughes, a subsidiary of General Motors (GM) in the United States of America, began the transmission of digital television signals via satellite in Brazil. From the end of the 1960s until the middle of the 1980s, various formats were developed for the capture, storage, processing and transmission of television signals around the world. This stimulated researchers, industries, and developers to search for ways to reconcile a generation of television programs that were growing in number.

Even though the capture, processing and transmission of television signals in a digital format are more complex, there are certain advantages such as robustness to noise and interference, efficient regeneration of coded signals, privacy of transmitted information, and a uniform format for various types of services (video, audio, and data) meant that these types of signals were implemented worldwide. Simply, the digital system can be divided into three large blocks, (1) capture or generation of television signals, (2) processing, and (3) transmission. The source encoders or video compressors are part of the processing stage and enable, for example, the simultaneous transmission of various programs in one transport stream with a reduced rate in relation to the original signal.

The compression or encoding of video signals based on the limitations of the human visual system is a process that can cause irreparable loss to the original signal. It significantly reduces its bit rate using sampling rate conversion techniques, processing digital images and eliminating spatial and temporal redundancy using domain transformation. In the specific case of video signal to television, the viewers perceive the loss as degradation, which may be acceptable because of the numerous advantages that the system can offer as a whole. [2]

With the introduction of television signals with digital encoding, the measures of object distortion used previously are no longer sufficient to determine with precision the quality perceived by the end user, due to non-linear distortions caused mainly by the techniques used for reducing the rate occupied by these digital signals. [3] [4]

An objective evaluation of video signals can be classified into three categories: (1) completely referenced, known as FR or Full Reference, when both signals, original and processed, are available for assessment; (2) partially referenced, known as RR or Reduced Reference, when only some samples or certain characteristics of the original signal are available; and (3) not referenced, also known as NR or No Reference, when only the processed signal is available.

In 1997, a group of experts from the International Telecommunication Union (ITU) met in Turn, Italy and formed the VQEG (Video Quality Experts Group). The VQEG has projects for applications in television and multimedia, in the three groups previously cited. In the objective evaluation of completely referenced (FR) for the application of television with standard definition (SDTV) the VQEG completed two projects, those being completed in 2000 and 2003, the reports are available in [5] and [6], respectively. These reports resulted in a recommendation of the ITU to specifically assess standard definition television signals. Four models were recommended for implementation via recommendation ITU-R BT.1683 in 2004 [7]. VQEG also released, in 2000, the entire set of data used in its first assessment, including the original and processed video scenes, and the results of the subjective experiments with these scenes, allowing other researchers to

Roberto N. Fonseca
Miguel A. Ramirez

doi: 10.18580/setijbe.2015.1 Web Link: http://dx.doi.org/10.18580/setijbe.2015.1

develop and test alternative methodologies and innovative approaches to this type of assessment, as in the work carried out by Gunawan, 2008 [8], Ong, 2007 [9], Sheikh, 2006 [10], Seshadrinathan, 2008 [11] and Gou, 2004 [12].

II. Objectives

Considering the introduction of non-linear distortions in the video signal, the perception of these non-linear distortions by human beings and as the content has a significant influence on the parameterization of these distortions, the most reliable form to measure the impact caused by the processing phase on the quality of the video signal is through subjective experiments. These experiments involve people considered to have normal vision in controlled environments, following internationally accepted standards, ITU-R BT.500-11 [13] and ITU-T P.910 [14], both from the International Telecommunication Union. The subjective evaluation demanded sophisticated resources, a high degree of ability and experience of those conducting the evaluation, besides a long time to reach a conclusion. Recently various studies demonstrated prospects in the development of algorithms with the capacity to simulate and estimate the subjective measures with a high degree of certainty that increases each time. This work only addresses the relative aspects of the objective evaluation of completely referenced (FR) video signals in standard definition (SDTV). To validate this type of evaluation, six distinct phases are needed, these are:

- Selecting the scenes. A set of short video scenes is chosen. These scenes should not be distorted and represent excerpts characterizing the context being evaluated. Natural and artificial scenes containing strong colors, diverse textures, camera movements and objects from various directions, soft and strong contrasts should be part of these set of scenes;
- Processing the scenes. These scenes are then subjected to similar processes that they would experience along their path to the being seen by the viewers: capture, processing and transmission;
- Subjective evaluation. Each pair of scenes, an original and processed, are reviewed by a panel of viewers who give their opinions within a predetermined, specific context for the experiment being conducted. The opinions about the original and processed scenes result in two scores. The mean score and standard deviation is calculated for each score, resulting in an average variable grade from the opinion of the observers, mean opinion score (MOS).
- Obtaining differences. The difference between the scores assigned to the original processed scenes and results in another variable is called the difference mean opinion score (DMOS). As the opinions expressed by the observers are interpreted in values from 0 to 100, the DMOS can range from -100 to 100. Values near to zero signify that little difference was perceived between the original and processed scene while a high values signify that a big difference was perceived between the scenes. Negative values are rare and signify that the processed scene was perceived as a better quality than the original;
- The proposed method. The same pair of scenes is submitted to the subjective evaluation method proposed. The method should represent the differences measured between the scenes on the DMOS scale, estimating another variable represented by $DMOS_p$ (prediction of DMOS). If the objective measurement is not represented in the same subjective space, form mapping must be completed to obtain a prediction of the DMOS on the same scale;
- Validation of the method. In this last step, a set of statistical descriptions is chosen to evaluate the performance of the proposed method. In this work, the mean square error, the Pearson correlation coefficient, Spearman rank order, coefficient correlation, and outliers ratio were the validation metric adopted.

In Fig. 1 a simplified diagram shows this process. Two distinct types of experiments were completed as part of this work. The first approach was to utilize the measurements obtained by PSNR, SSIM, and S-CIELAB as a starting point to confirm and extend the results obtained by VQEG in [5]. The second approach was to optimize these measurements for typical standard definition television scenes with 525 interlaced lines (NTSC-M 480i). The main contributions were using the measure of quality based on S-CIELAB color space in video scenes and the optimization of the objective measure PSNR maintaining its low computational complexity and increasing its correlation with the subjective measure (human perception).

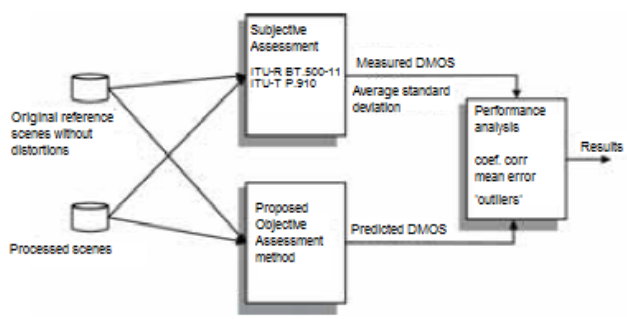

Fig. 1. Process for comparing the performance metrics for the assessment of video quality.

III. Video Signals

Video signals are a form of electrical waves that enable the image sequence transportation from one location to another. By observing the scene, a two-dimensional image is generated in each retina in the human eye. As this varies with time, three-dimensional information is obtained. The combination of images generated by the two retinas create a stereoscopic image [2]. Because the tension various over time, an electrical waveform is two-dimensional. To convert this two-dimensional information into three-dimensional information compatible with the retina, a resource called scan is used. Using the scan feature makes a video scene that can be reproduced line by line, image after image. Each image is scanned from left to right and from top to bottom, one line at a time. This type of scan is called horizontal linear scan. The

frame rate in television systems was derived from a combination of the frequency used in electricity supply networks and the first cinema systems, where the frames were displayed at 48 frames per second. Even though only 24 frames per second were needed to cause the eyes the sensation of movement, the frame rate in cinemas was doubled to avoid a flicker effect during the screening of the film, mainly in scenes with high levels of illumination [21]. Starting with the frame rate and the desired resolution, the horizontal and vertical scanning frequencies can be used as a basis for monochrome television systems, launched commercially in the 1940s.

A. Analog video

Conventional analog television systems follow ITU and SMPTE recommendations for standard definition. The recommendations ITU-R BT470-7 [22] and ITU-R BT1700 [23], both recommendations from 2005, defined the most common video composite formats used, while the document SMPTE 170M-2004 [19] characterizes in detail the signal of standard video NTSC.

In interlaced scanning systems, as is the case with all analog video systems used in television, firstly it must be transmitted to all lines of a field, and then start the transmission of the next field. The intensity along a scan line is represented by an electrical voltage; lower voltages represent dark areas, and higher voltages represent lighter areas.

1) Synthesis

The composite video signal must contain an electrical representation of the brightness and the color of a given scene. These signals must also include references that allow reconstruction on a screen. These references will be used for synchronization and should not be visible on a well-adjusted system. Some parts of the composite signal have no information about the scene and should be forced to a level even blacker than the reference (base), so that the scanning beams of the capture and reproduction equipment function perfectly [22].

A composite video signal, fundamentally, has two difference components:

- Luma component, represented by Y
- Color difference component, represented by Cr e Cb or U and V

Fig. 2 shows an example of the system to obtain a video composite signal NTSC from their RGB nonlinear colors.

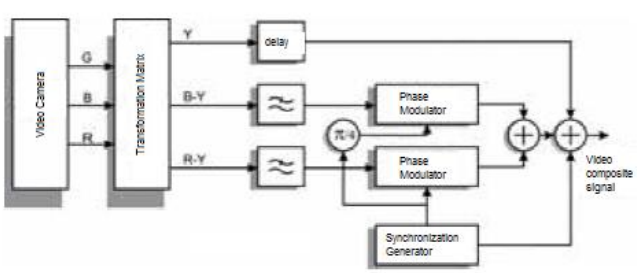

Fig. 2. Obtaining a composite video signal

In this system, the reference signals G, B, and R must be synchronized with equal amplitude for the representation of an image without color information. These signals are usually described as corrections with gamma factor, represented in old documents like E'_G, E'_B, and E'_R [19]. The definition of gamma correction is described by SMPTE, in SMPTE 170M-2004 [19] and by the International Telecommunication Union, in ITU-R BT709-5 in 2002 [20]. The equations that define this transfer function for the intervals $0.018 \leq L \leq 1$ and $0.0812 \leq V \leq 1$ are:

$$V = 1.099 \cdot L^{0.45} - 0.099 \quad (1)$$

$$L = \left[V + \frac{0.099}{1.099}\right]^{\frac{1}{0.45}} \quad (2)$$

where V represents the electrical signal of components G, B, and R corrected by the gamma factor and L indicates the brightness when entering the capture system for each of the components Red (R), Green (G), and Blue (B). Outside the indicated interval the relationship is V=4.5L, then L=V/4.5.

According to Poyton, 1996 [16], the combination of two effects, those being the physical origin and the perceptive origin, were responsible for the gamma factor conception. The effect of the physical origin is related to the fact that the cathode ray tubes (CRT) used in television have an exponential transfer curve between the input voltage and output brightness, the perceptive origin factor is that human beings do not perceive linear variations of brightness.

These signals must be transformed into two components, luminance (Y) and chrominance (R-Y and B-Y). The term chrominance is defined as the difference between two colors with the same luminosity, one being a reference color [17]. After filtering to elimate high frequencies, the signals of different color (B-Y and R-Y) are sent to a quadrature modulator, which will modulate the I and Q vectors resulting in a phase modulation of the color subcarrier. This color subcarrier having been modulated is added to the luminance signal, as well as the synchronization signal of luminance, chrominance, deletion, and pedestal.

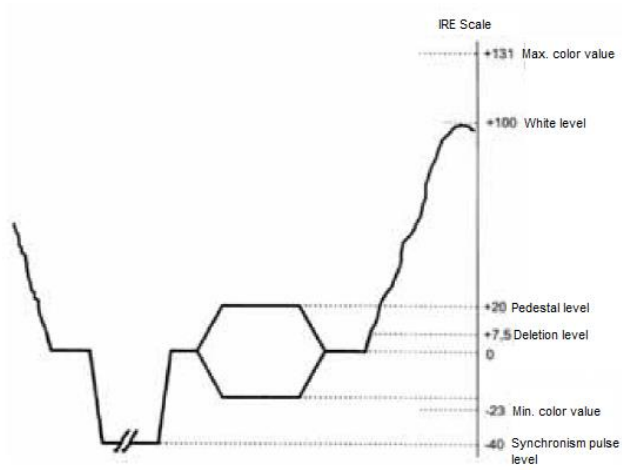

Fig. 3. Waveform of the composite video signal

doi: 10.18580/setijbe.2015.1 Web Link: http://dx.doi.org/10.18580/setijbe.2015.1

A representation of the electrical video signal can be seen in Figs. 3 and 4. In Fig. 3 the vertical axis represents the voltage, converted to the standard IRE, and the horizontal axis represent time, shown at an interval of the horizontal line. In Fig. 4 the representation is polar, where the magnitude is the color intensity and phase represents hue.

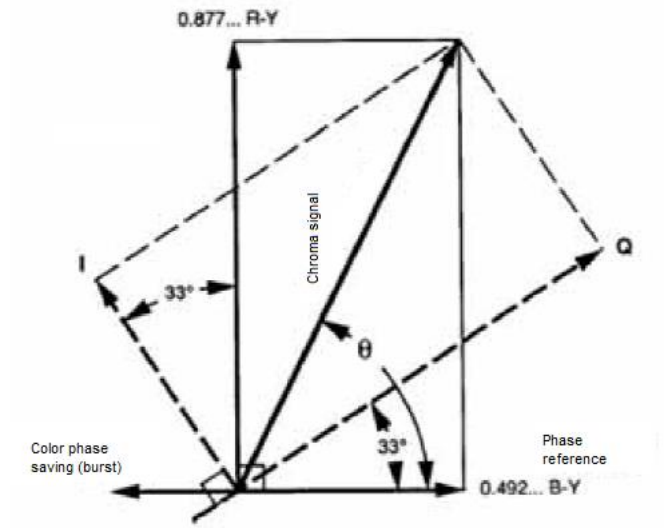

Fig. 4. Vector representation of color components in a composite video signal

In terms of the spectral components, the video signal can be described by the sum of a luma signal as two color difference signals [19]. The following equation shows a composite video signal $E'_M(t)$ formed by its components $E'_Y(t)$ $U'(t)$ and $V'(t)$.

$$E'_M(t) = E'_Y(t) + U'(t)sen\left(2\pi f_{SC}t\right) + V'(t)\cos(2\pi f_{sc}t) \quad (3)$$

The synchronization of these signals is of fundamental importance for the reproduction of video signals. The synchronization of analog television signal is done through horizontal and vertical synchronism pulses and saves color synchronism. These synchronism pulses are linked to each other by the definition of each pattern and color system. In NTSC-M systems, for example, the frequencies of color synchronization f_{sc}, horizontal synchronization f_H, and vertical synchronization f_V are given by the following equations [19]:

$$f_{sc}\ (MHz) = 5 \cdot \frac{63}{88} = 3.579\overline{54} \quad (4)$$

$$f_H(Hz) = \frac{2}{455} \cdot f_{sc} = 15734.\overline{265734} \quad (5)$$

$$f_V(Hz) = \frac{2}{525} \cdot f_H = 59.\overline{940059} \quad (6)$$

B. Digital video

In applications for standard definition digital television, the signals used are classified according to the color space used, the sampling frequency, and the aspect ratio. Fig. 5 was adapted from [24] and shows how the various color spaces are used in typical digital video applications. The upper part of Fig. 5 represents the synthesis process of a typical video signal, and the lower part is a representation of the process for image display.

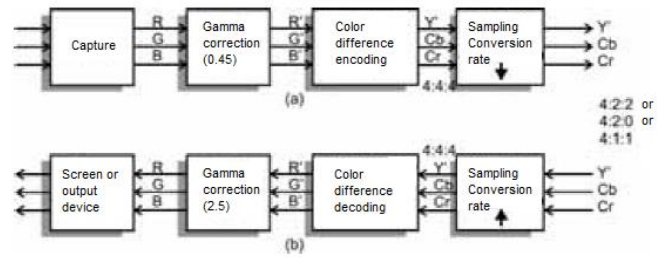

Fig. 5. Color spaces used in a digital television system

Although the RGB color space presents advantages when used for computer graphics (mainly because the screens use the same space to display the colors created), its efficiency in terms of the bit rate is reduced [18]. In this color space, each component uses the same rate, i.e., R, G, and B are the color components of a given pixel to be displayed. If we consider that each of the three components occupy 1 byte, 3 bytes are required to represent each pixel.

As human vision is more sensitive to the perception of detail rather the perception of colors, various shapes that represent a variation of light intensity in a component and the variation of colors in others were created. The color space of YUV, YIQ, and YCbCr are examples of this type of approach. To represent digital video signals, it is very common to use the color space of YCbCr, formed by the luma component (Y') and color difference (Cb and Cr).

Television studios employ digital signals in the Abekas format, also known as big YUV, where the samples of each line are sequentially arranged bytes, starting with a color sample, followed by a luma sample, and so forth. Fig. 6 shows the structure used for the transportation of digital video signals in 4:2:2 formats uncompressed with the aspect ratio 4:3 [25]. The Abekas format uses the same sequence for storing the digital video signal byte by byte in binary files, without bytes for appropriate synchronism.

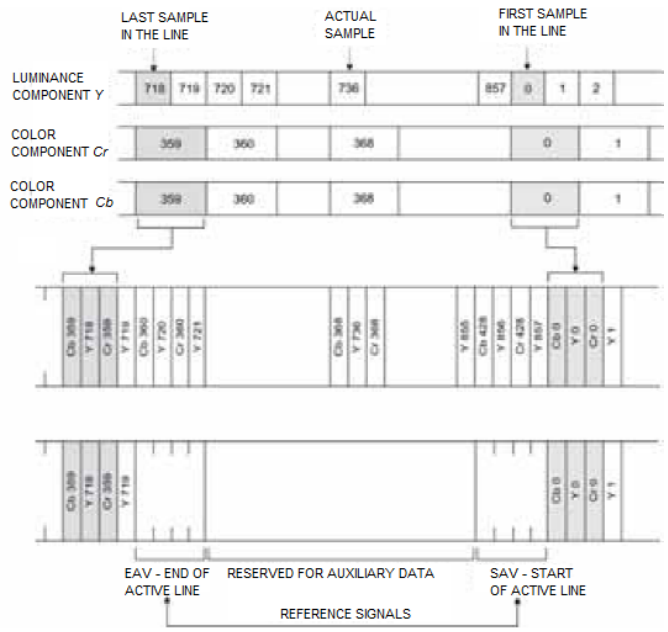

Fig. 6. Sequence of bytes for digital video applications in format ITU-R BT601-5

This file format for storing digital video allows the storage of video scenes without being compressed occupying 16 bits per pixel. Each byte in the file represents a color component or a luma (gray level corrected by the gamma function Y') of an image. In this way, the space occupied by each pixel is 2 bytes, made up of one for the luma and the other for the color (or Cb or Cr). One television frame of standard definition SDTV with 486 lines and 720 pixels per line occupies 350kb (720x486x2=699,840bytes).

One scene with 260 frames occupies, therefore, 182MB (720x486x2x260=181,958,400bytes).

In the files made available by VQEG in [5], the gamma correction was previously applied to the luminance samples, this being known as color format Y'CbCr. The frames are in sequence from the left to right and from top to bottom, starting with the upper field and following this frame sequence by frame, noting that this is an M standard 525 lines and 59.94 fields per second, interlaced. This storage format is described and standardized by ITU in recommendation ITU-R BT601-5 [26] and the protocols used for transportation are described in recommendations ITU-R BT656-4 [25] and ITU-R BT1302-0 [27].

IV. Processing Digital Images

A. Filtering in space domain

Filtering in the space domain consists of carrying out operations directly on the pixels in the image.

$$g(x,y) = T[f(x,y)] \tag{7}$$

Where T is the operator of $f(x,y)$.

In this type of filtering, the value of each pixel in the processed image, $g(x,y)$, is obtained by mathematical operations performed directly on the pixels in image f. To obtain the value of each pixel g, the operator T can be applied to only one-pixel f or to a set of pixels, referred to as a window.

The most used filtering method is that which smooths the images, to simply its scale, thereby reducing entropy. In this type of filtering, the operator T uses a window with several pixels f to calculate the value of each pixel g.

$$g(i,j) = \sum_{i=x-a}^{x+a}\sum_{j=y-a}^{y+a} f(i,j)w(i,j) \tag{8}$$

Where $w(i,j)$ is an operator in the window, and a, b are the limits of the desired window.

Another very common type of filtering is analogous to smoothing, but with the exact opposite effect. They are filters that use derivatives to enhance the outlines of the images. The most common method in this type of application is using the gradient.

The discrete convolution between two grayscale images $f(I,j)$ and $w(I,j)$ of MxN size is represented by $f(I,j)*w(I,j)$ and defined by the expression:

$$g(i,j) = f(i,j) * w(i,j) = \frac{1}{MN}\sum_{m=0}^{M-1}\sum_{n=0}^{N-1} f(m,n)w(i-m,j-n) \tag{9}$$

B. Edge detection

The image edge is defined as the boundary region where there is a significant change in some aspect of the image, leading to a change in intensity, color or texture [28]. In this work, only edge detection in relation to the intensity was used. Two of the most used methods for edge detection will be applied in this paper, the gradient method and the Laplacian method.

1) Gradient method

Considering the function $f(x,y)$, where x and y, the gradient of f at the co-ordinates x and y in the direction formed by the unit vectors $\hat{\imath}_x$ and $\hat{\imath}_y$ can calculated as:

$$\nabla f(x,y) = \frac{\partial f(x,y)}{\partial x}\hat{\imath}_x + \frac{\partial f(x,y)}{\partial y}\hat{\imath}_y \tag{10}$$

Initially the magnitude of $\nabla f(x,y)$ is calculated, and then this value is compared with a reference to determine whether this point is a possible edge. In general the edges found in the images of natural scenes are smooth, so that an edge band would be found and not a defined boundary edge. The thinning process is necessary to turn a band of pixels detected as contours into a contour line. A common approach for edge detection is to verify if $\nabla f(x,y)$ has a local maximum in any direction.

In processing digital images, $f(x,y)$ is substituted for a two-dimensional discreet sequence $f(n_1,n_2)$, and $\frac{\partial f(x,y)}{\partial x}$ and $\frac{\partial f(x,y)}{\partial y}$ can be substituted by a difference, for example:

$$\frac{\partial f(x,y)}{\partial x} \leftrightarrow [f(n_1+1,n_2+1) - f(n_1-1,n_2+1] + [f(n_1+1,n_2) - f(n_1-1,n_2)] + [f(n_1+1,n_2-1) - f(n_1-1,n_2-1]. \tag{11}$$

doi: 10.18580/setijbe.2015.1 Web Link: http://dx.doi.org/10.18580/setijbe.2015.1

This difference can be seen as a discrete convolution between $f(n_1,n_2)$ and the filter impulse response $h(n_1,n_2)$. For the equation above, for example, the filter impulse response is given by the coefficients

-1	0	1
-1	0	1
-1	0	1

Specifically, in this case, this set of coefficients for specifying the Prewitt edge detection operator in the horizontal direction of an image (Prewitt, 1970 cited by Gonzalez and Woods, 2000) [1]. The contours in the vertical direction of a given image can be detected by another operator obtained by transposing $h(n_1,n_2)=h(n_2,n_1)$. The fact that the contour detection can be given in a specific direction causes the operator to be called a directional operator. Non-directional operators can be developed by the discreet approximation of $f(x,y)$. The following approximation was used by Duda and Hary, 1973 cited by Lim, 1990 [28] to define two different pairs of operators, called the Sobel operator and the Roberts operator.

$$|\nabla f(x,y)| \rightarrow \sqrt{f_x(n_1,n_2)^2 + f_y(n_1,n_2)^2} \quad (12)$$

where:
$f_x(n_1,n_2) = f(n_1,n_2) * h_x(n_1,n_2)$ and
$f_y(n_1,n_2) = f(n_1,n_2) * h_y(n_1,n_2)$

The following are samples of the Sobel operators (3x3) and the Roberts operators (2x2):

-1	0	1
-2	0	2
-1	0	1

1	2	1
0	0	0
-1	-2	1

1	0
0	-1

0	1
-1	0

2) Laplacian method

Another way to detect contours in an image is to look for second order zero crossing differences. One issue that arises with this approach is that noise would be detected as contours, due to the sensitivity of the second derivative. One way to minimize this issue is by applying smoothing filters before submitting the image to contour detection. The equation below shows how to calculate the Laplacian of function $f(x,y)$ [28]:

$$\nabla^2 f(x,y) = \nabla\big(\nabla f(x,y)\big) = \frac{\partial^2 f(x,u)}{\partial x^2} + \frac{\partial^2 f(x,y)}{\partial y^2} \quad (12)$$

Similar to what was seen in the gradient method, (9) can be approximated for digital images, represented by $f(n_1,n_2)$, as follows:

$$\nabla^2 f(x,y) \rightarrow \nabla^2 f(n_1,n_2) = f_{xx}(n_1,n_2) + f_{yy}(n_1,n_2) \quad (13)$$

where $f_{xx}(n_1,n_2)$ and $f_{yy}(n_1,n_2)$ can be approximated by the difference in relation to previous and subsequent pixels, thus:

$$\nabla^2 f(n_1,n_2) = f(n_1+1,n_2) + f(n_1-1,n_2) + f(n_1,n_2+1) + f(n_1,n_2-1) - 4f(n_1,n_2). \quad (14)$$

Similar to the gradient method, operators may be used to approximate the second-order derivative to be used in a discrete convolution. In the previous approach, for example, the Laplacian is calculated from a discrete convolution with the operator:

0	-1	0
-1	4	-1
0	-1	0

Applications using the pure and simple Laplacian method in the detection of contours are not very common, due to the sensitivity to noise mentioned earlier. A common approach is to use the Laplacian method combined with a Gaussian smoothing filter, a technique known as Laplacian-of-Gaussian or simply LoG. Fig. 13 shows an example using the first image of a scene used in this work. In this Fig. one can see the original image (a), a version smoothed by a Gaussian filter (b), the result of the convolution with a Laplacian filter (c), and finally the extraction of the edges using the zero-crossing technique after convolution with the result of the convolution between the response impulses of the Laplacian and Gaussian filters (d).

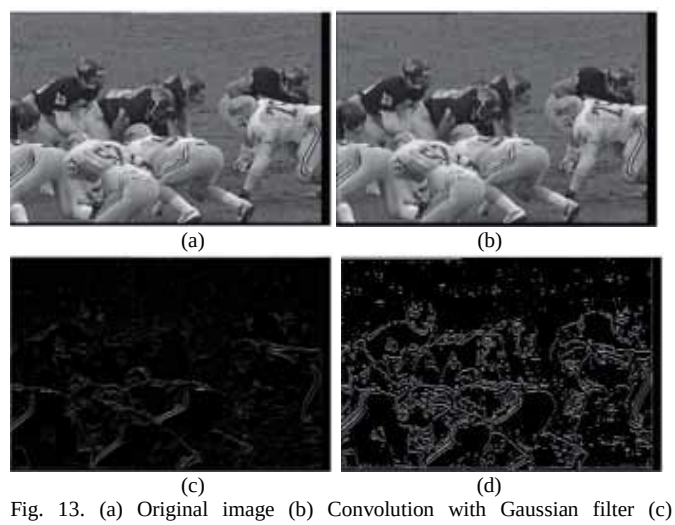

Fig. 13. (a) Original image (b) Convolution with Gaussian filter (c) Convolution with Laplacian filter (d) Edge detection using the convolution from the LoG filter (Laplacian-of-Gaussian).

It is important to highlight that the gradient of a two-dimensional image is in shades of gray and is a vector field in shades of gray while the Laplacian in the same image is a scalar field.

doi: 10.18580/setijbe.2015.1 Web Link: http://dx.doi.org/10.18580/setijbe.2015.1

V. Video Signal Quality

Usually, the viewer is interested in watching a two-dimensional representation of the real world that is as faithful as possible. The video signals are subject to degradation during capture, processing, storage, and transport. In composite video signals, analog television linear distortion and time invariants are inserted during these steps, allowing the utilization of a set of well-defined tests widely accepted by the community. Measured in terms of amplitude, frequency, and complete phase characterization of this type of signal and its distortions [29].

Recommendation ITU-R BT1204, 1995 [30] defines the techniques, test signals, and methodologies used to characterize these analog signals. Measures such as signal-to-noise ratio (S/N), differential gain (DG), phase gain (DP), impulsive characteristics (K2T and P/B), and linearity of the luma component are specified in this recommendation and are used to characterize video signals in the analog domain with high precision.

With the introduction of new digital techniques for the processing and compression of video signals, these measures are no longer sufficient to characterize the new forms of distortion inserted. According to Wang et al., 2003 [31]: "A video signal or image whose quality is being evaluated can be thought of as the sum of a perfect reference signal and an error signal". With this in mind, the most intuitive way to measure the video signal quality would be to quantify the error that is inserted in this signal. This task would be even simpler in the case of completely referenced video assessment since the reference signal is available.

According Jayant and Noll, 1984 [32]: "The evaluation of faithfulness or the degree of degradation that a given system causes in a video signal can be made objectively or subjectively." The subjective evaluation involves a number of people in a controlled environment, following a certain methodology and being conducted by experts with extensive experience in this type of activity. Objective evaluation is performed automatically and requires an algorithm performing measurements of certain video signal characteristics, resulting in a measure of quality.

A. *Subjective Evaluation*

In this type of evaluation, the scenes to be evaluated are presented to a panel of observers, who judge the quality of the scenes presented in certain well-defined aspects, under certain conditions also previously set according to the application. Recommendation ITU-R BT.500-11 defines five basic methodologies for subjective quality assessment for standard definition television - SDTV:

• Method 1:

• DSIS (Double Stimulus Impairment Scale-) mainly used to measure the robustness of systems, or to characterize transmission failures;

• Method 2:

• DSCQS (Double-Stimulus Continuous Quality Scale) mainly used for measurement of degradation caused by systems with respect to a reference;

• Alternative methodologies:

• SS (Single Stimulus);

• SSCQE (Single Stimulus Continuous Quality Evaluation) used when you want to subjectively evaluate a scene without considering a reference;

• SDSCE (Double-Simultaneous Stimulus for Continuous Evaluation) used for assessments where long scenes are required.

For applications in high-definition television (HDTV), video conferencing and multimedia applications, other ITU groups describe their evaluation methodologies. Pinson and Wolf carried out a comparison between these methodologies in 2003, verifying the sensitivity of each of them for certain applications, concluding that, among other things, for assessments using double stimuli (such as the DSCQS methodology) a duration of 15 seconds is a limiting factor due to the effect of the evaluators memory [33].

The evaluation of fully referenced digital television signal quality is of particular interest to the DSCQS methodology, in which pairs of scenes with short duration of time, typically 10 seconds, is presented to a panel of viewers, they attach notes to each scene pair . Using well-defined techniques for preparing the environment, choice of individuals, execution of experiments, and compilation of the results, the assessment methodology presents results in a consistent and well-defined way.

Although the evaluation of video signal quality in accordance with the perception of the viewer is defined by recommendation ITU-R-BT.500-11, new forms of assessment considering the compressed digital signal have been developed based on three main analysis techniques for the image quality in digital video [4]:

• Use dynamic synthetic video signals for measuring the distortions caused by signal compression;

• Make distortion measurements to determine how the original signal was distorted;

• Use real video scenes and analyze a set of parameters to correlate with the subjective image quality [34] [35].

B. *Objective Evaluation*

In this evaluation, there is a set of original and processed scenes, the fully referenced (FR) objective evaluation methods usually perform the comparison of scenes frame by frame, extracting features that can represent the effect of processing to the same extent that the human eye perceives them. Fig. 7 is adapted from [15] and shows a general diagram for obtaining an objective quality measure of the fully referenced video signal.

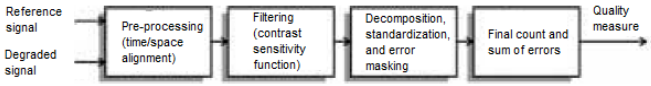

Fig. 7. Simplified diagram to obtain an objective measure of fully reference video signal quality.

In this diagram the first step is the pre-processing of the input signals to eliminate possible misalignments between the signals in spatial terms (horizontal and/or vertical displacement of all the pixels of a frame in relation to the same frame from the referenced video signal) and time (delay of a signal relative to the other).

1) ITU Models

The objective of VQEG was to define and standardize the correlations between the subjective evaluation of video quality and proposals for the objective evaluation of video quality from various laboratories. For the fully referenced (FR) objective evaluation in standard definition television - SDTV, VQEG performed two separate evaluations, called Phase I and Phase II. In the first phase VQEG analyzed 10 different algorithm proposals to objectively evaluate video quality, and in the second phase six proposals were evaluated. In 2000, VQEG released the final report on the first phase of the objective validation models for assessing video quality, concluding that none of the proposed models were materially superior to the traditional PSNR measure in all aspects, demanding a new phase of tests [5].

In 2003, the final report of the second phase was released, in which VQEG improved the tests performed and selected 6 models, suggesting the possibility of inclusion in ITU regulations, as the measures using PSNR were exceeded statistically [6]. In 2004, ITU published the recommendation ITU-R BT.1683, in which four models were described and approved for implementation [7]:

• BTFR (British Telecommunication Full Reference)
• EPSRN (Edge Peak Signal-to-Noise Ratio)
• CPqDIES (Centro de Pesquisa e Desenvolvimento: Image Evaluation based on Segmentation)
• NTIAVQM (National Telecommunications and Information Administration: Video Quality Metric)

The following will present the three distortion measures for objective evaluation using full reference that were utilized in this study, PSNR, SSIM, and S-CIELAB.

VI. Distortion Measurements

A. PSNR

The peak signal-to-noise ratio between two images or PSNR can be defined as starting from the mean square root error calculated pixel by pixel. [1] The following equation shows the calculation of the mean square distortion between two images f e g in size M x N pixels in grayscale:

$$f_{f,g} = \frac{1}{MN}\sum_{i=0}^{M-1}\sum_{j=0}^{N-1}[f(i,j) - g(i,j)]^2 \quad (14)$$

The PSNR has been used as a quality measurement reference for images and videos for many years. The following equation shows the calculation of PSNR between two images sampled with 8-bit resolution.

$$P_{f,g} = 10\log_{10}(\frac{255^2}{d_{f,g}}) \quad (15)$$

The main problem with this measure is that it does not take into account the limitations of the human visual system (HVS). The image compression algorithms and video compression algorithms use these limitations to act efficiently in the compression of these images and videos.

B. SSIM

Based on structural similarity, this method was first proposed by [37], but has been reviewed by [38] for better definition of the indexes. This approach has been published in literature in 2005 [39], and has been the basis for more improved methodologies for measuring the quality of an objective image like the E-SSIM [40] and the M-SSIM [41].

This measure is based on the assumption that the human visual system (HVS) is highly prepared to extract information about the structures present in its field of vision.

To define the SSIM index (Structural SIMilarity) between two images in grayscale *f(i,j)* and *g(i,j)*, it is first necessary to define three basic quantities for each image block of 8x8 pixels of these images (1) comparing the luminance *I(f,g)*, (2) comparing the contrast *c(f,g)*, and (3) structure comparison *s(f,g)*. The SSIM index for a pair of images is calculated by the following expression:

$$S(g,g) = [l(f,g)]^{\alpha} \cdot [c(f,g)]^{\beta} \cdot [s9f,g)]^{\gamma}. \quad (16)$$

For the calculation of the SSIM index, the author suggests a simplified version of (3), where $\alpha = \beta = \gamma = 1$. Equation (4) shows a simplified version of this expression, which was used in the experiments reported in this article.

$$S(f,g) = \frac{(2\mu_f\mu_g + C_1)(2\sigma_{fg} + C_2)}{(\mu_f{}^2 + \mu_g{}^2 + C_1)(\sigma_f{}^2 + \sigma_g{}^2 + C_2)} \quad (17)$$

Where: μ_f and μ_g are the average of the gray levels in each of the pair of images being compared, and $\sigma_f{}^2$ and $\sigma_g{}^2$ are the variances of these values, and σ_{fg} refers to the cross-covariance gray levels of these images.

In a sequence containing T images or frames, the SSIM index is calculated by averaging *S(f,g)* as shown in the following equation:

$$\bar{S}(f,g) = \frac{1}{T}\sum_{t=0}^{T-1} S_t(f,g). \quad (18)$$

C. S-CIELAB

The comparison of the quality of color images can be made based on the differences between the opposite color space components L*, a*, and b*. The International Commission on Illumination, known as CIE (Commission Internationale de l'éclairage), in 1976, originally defined one approach for this type of evaluation. This standard has been updated by S014-4/E:2006, published in 2006 by CIE [42]. In this document, a color space called CIE 1976 L* 2* b* is defined, which became known internationally as CIELAB. In this space, the component L* represents white to black variations and assumes values between 0 and 100. The component a* represents red tint changes to green, assuming values between -500 and +500 and the component b*, variations of yellow hue to blue, varying its value from - 200 to +200. The following equations specify the transformation between the color model based on three stimuli (CIEXYZ) and the CIELAB [24]:

doi: 10.18580/setijbe.2015.1 Web Link: http://dx.doi.org/10.18580/setijbe.2015.1

$$L^* = 116\left(\frac{Y}{Y_n}\right)^{1/3} - 16$$
$$a^* = 500\left[\left(\frac{X}{X_n}\right)^{1/3} - \left(\frac{Y}{Y_n}\right)^{1/3}\right]$$
$$b^* = 200\left[\left(\frac{Y}{Y_n}\right)^{1/3} - \left(\frac{Z}{Z_n}\right)^{1/3}\right] \quad (19)$$

Where X, Y, and Z are the three stimuli and X_n, Y_n and Z_n are the values of the three stimuli of standard white (maximum value of X, Y, and Z).

CIELAB is, therefore, a color space formed by the components L*, a* and b*. The color difference between two CIELAB space images is calculated as a Euclidian distance, pixel to pixel and is referred to as ΔE.

The meaning of ΔE can be understood as follows: considering two colors closely defined by their coordinates L*, a* and b*, the ΔE value will be smaller the closer these colors are. The value of ΔE<1 indicates that the difference between these colors is not noticeable. The value of ΔE=1 indicates that the difference between these colors is less than can be perceived, being called JND (Just Noticeable Difference).

Several psychophysical experiments involving people's perception of differences between colors are conducted to arrive at a definition of ΔE. In 1996, Zhang and Wandell defined an extension of the CIELAB color space, called S-CIELAB. The difference of the S-CIELAB color space resulted in the measure ΔE_S [43].

To specify the color differences in the S-CIELAB space, smoothing filters are applied to the opposite color system components. In this work, for example, the filters that were adopted are described in [43]. The equation below shows the transformed CIEXYZ color system to the opposite color system formed by components O1, O2 and O3, which represent, respectively, the differences between white-black (W-B), red-green (R-G) and blue-yellow (B-Y).

$$O_1 = 0.279X + 0.72Y - 0.107Z$$
$$O_2 = -0.449X + 0.29Y - 0.077Z$$
$$O_3 = 0.086X - 0.59Y - 0.501Z \quad (20)$$

(20)

For each of these components, a two-dimensional filter is applied to adequately represent the sensitivity of human vision. The following equation describes the filter used in this work. The parameters k and ki were adopted as described in [43].

$$f = k\sum_i w_i E_i$$
$$E_i = k_i \exp\left[-\frac{(x^2+y^2)}{\sigma_i{}^2}\right] \quad (21)$$

(21)

Once filtered, the components O1, O2 and O3 of both images, original and processed, are compared, resulting in the color difference S-CIELAB. The following equation shows how to calculate this difference:

$$\Delta E_5 = \sqrt{(\Delta O_1)^2 + (\Delta O_2)^2 + (\Delta O_3)^2}. \quad (22)$$

For a pair of video scenes composed of N images, each containing i lines and j columns, this process must be repeated N.i.j times. In this work, pairs of scenes, an original and a processed were subjected to the S-CIELAB comparison and a difference for each pair of scenes was obtained.

Tests for the application of this perceptual color difference measure in the assessment of images and video footage were made by Fonseca and Ramírez, 2008, and are available in [44]. In these tests, it was concluded that the use of S-CIELAB space for the assessment of color images significantly increases the degree of correlation with perception, but this does not happen for color video scenes.

VII. Simulation Results

The experimental part of this work was divided in two stages. In the first stage, we used the evaluation methods PSNR, SSIM, and S-CIELAB as a starting point to confirm and extend the results obtained by VQEG in [5]. In the second stage, we used the resources and methods described in Chapter IV to create new evaluation methods based on the comparison of the pixel by pixel error and structural similarity, adjusting for typical TV scenes in standard definition. The first frame of each scene is shown in Fig. 8.

Fig. 8. The first frame of each scene used in the tests

A. Part I

The scenes used in this study were the same as those used in the initial assessment phase by VQEG, in which ten proposed algorithms for objective measurement of video quality were evaluated with respect to PSNR. The tests described were compared with the best reslut that VQEG found in each evaluation. Table I shows the results of the proposals submitted to VQEG using the set of M standard scenes.

doi: 10.18580/setijbe.2015.1 Web Link: http://dx.doi.org/10.18580/setijbe.2015.1

TABLE I
RESULTS OBTAINED BY VQEG FOR STANDARD M SCENES (60HZ)

Metric	cc Spearman (r_s)	cc Pearson nonlinear (r)	points outside	observation
P0	-0.71	0.76	58%	PSNR
P1	-0.75	0.84	56%	CpqD
P2	-0.77	0.84	54%	JND
P3	-0.63	0.73	65%	NHK
P4	-0.57	0.62	69%	KDD
P5	-0.80	0.87	52%	PDM
P6	-0.22	0.42	76%	Tapestries
P7	-0.74	0.78	57%	DVQ
P8	-0.69	0.77	53%	PVQM
P9	-0.70	0.77	65%	NTIA

It can be seen, as concluded by VQEG in [5], that none of the metrics were significantly better than PSNR, which is computationally more efficient than any other metric. Table II shows the comparison between the performance measurements obtained using PSNR, SSIM, and S-CIELAB in relation to the performance obtained by the P5 metric that is the best case that VQEG reported, utilizing the set of scenes used in this work. The P5 metric was developed by Winkler, 1999, and is described in [45]. In the Winkler metric, 4 different stages were used, including: (1) the perception of colors in opposite components, (2) spatial and temporal mechanism for filtering (3) masking and sensitivity of contrast and forms, and (4) response sensitivity of neurons in the primary visual cortex.

Although the results obtained by the P5 metric were better than those obtained using PSNR, SSIM, and S-CIELAB, it should be noted that only S-CIELAB uses the Cr and Cb components in the assessment. The assessment using SSIM and PSNR only includes the luma component (Y'), and they had similar results to those obtained with the use of color components. This is because the distortions inserted into the evaluated scenes cause similar degradation effects, to the perceptual point of view, in the three components Y', Cb, and Cr.

TABLE II
PERFORMANCE OF METRICS; PSNR, SSIM, AND ΔE_S (S-CIELAB)

Metric	cc linear (r_s)	cc nonlinear (r)	points outside	rms error
PSNR	0.76	0.79	59%	6.2
PSNR (only Y')	0.74	0.78	55%	6.3
SSIM (only Y')	0.77	0.85	54%	5.4
S-CIELAB	0.75	0.78	61%	6.8
P5 (BW, RG, BY)	0.80	0.87	52%	nd

Following are the individual effects of each scene (SRC) and each frame individually compared to the performance of each of the metrics so that the influence of these variables is clearly understandable.

This analysis was completed to have an understanding of how each scene individually contributes to the total mean error, as well as the contribution of each frame in the scene. In the first experiment, the average error was obtained with the PSNR and SSIM metrics only using the luma component of the images. Table III shows the results obtained.

TABLE III
PERFORMANCE OF METRICS; PSNR, SSIM, AND ΔE_S (S-CIELAB)

Scene	rms using PSNR	rms using SSIM
SRC13	6.81	4.94
SRC14	5.62	4.69
SRC15	5.56	6.37
SRC16	5.12	5.94
SRC17	7.00	4.69
SRC18	4.87	2.87
SRC19	8.62	9.00
SRC20	8.06	4.19
SRC21	4.69	7.31
SRC22	7.00	4.00

As can be seen, SRC19 is the biggest contributor to the total mean error. This scene contains images of an American football game, with horizontal camera movements and players. The errors in this type of scene type are not detectable by the human visual system with the same intensity that the PSNR and SSIM metrics detect.

The following are performance results obtained using each scene individually. With these results, a simplification of the metric is possible, where only a few frames of each scene could be used to obtain the objective measure. Fig. 9 shows the Pearson correlation coefficient calculated between the subjective DMOS and the results obtained by the PSNR and SSIM metrics. This result was obtained using only the luma component, calculated over all 160 pairs of scenes, one frame at a time. The horizontal axis shows the frame that was used to calculate the correlation coefficient and the vertical axis the obtained correlation module.

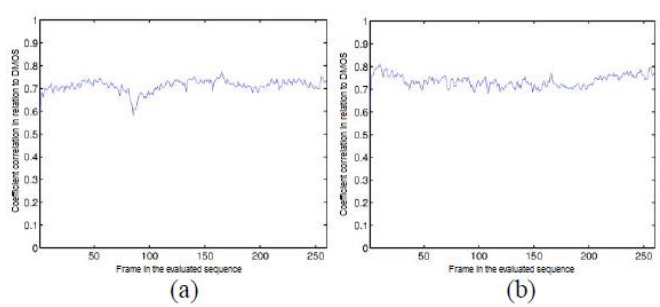

Fig. 9. Spearman linear correlation module for each frame (a) PSNR and (b) SSIM

It is observed in these Figs. that, even though, some of the scenes contain movements and sudden cuts, if the measurements were calculated using the average frame sample it would be possible to obtain a very close correlation using the mean of all the frames in calculation. To confirm this hypothesis, the objective quality measures were calculated using only the luma component through the SSIM and PSNR metrics. To calculate the PSNR, (14) has been replaced by:

$$\bar{d}_{f,g} = \frac{\tau}{MNT}\sum_{i=0}^{M-1}\sum_{j=0}^{N-1}\sum_{k=0}^{\frac{T}{\tau}-1}[f(i,j,\tau k) - g(i,j,\tau k)]^2 \qquad (23)$$

doi: 10.18580/setijbe.2015.1 Web Link: http://dx.doi.org/10.18580/setijbe.2015.1

where $f(i,j,\tau k)$ is the pixel value at coordinate (i,j) of frame τk of the scene f; $g(i,j,\tau k)$ is the pixel value at coordinate (i,j) of frame τk of scene g; τ is the sub-sampling value, or is only measured in τ frames.

The calculation of the SSIM mean value between scenes has similarly been completed, by substituting (18) for:

$$\bar{S}(f,g) = \frac{\tau}{T}\sum_{k=0}^{\frac{T}{\tau}-1} S_{\tau k}(f,g). \quad (24)$$

Table IV shows the results obtained by the objective metrics PSNR and SSIM using only Y' values for τ equal to 2, 5, 10, 20, 50 and 100, ie 50%, 20%, 10%, 5% , 2% and 1% of total 260 frames in each of the scenes.

TABLE IV
PERFORMANCE OF EACH METRIC ACCORDING TO THE NUMBER OF FRAMES USED

Metric	Frames used	cc Spearman (r_s)	cc Pearson nonlinear	points outside	rms errors
Y'_PSNR	100%	-0.74	0.78	56%	6.4
Y'_PSNR	50%	-0.74	0.78	57%	6.4
Y'_PSNR	20%	-0.74	0.79	57%	6.3
Y'_PSNR	10%	-0.74	0.78	58%	6.3
Y'_PSNR	5%	-0.74	0.78	59%	6.3
Y'_PSNR	2%	-0.72	0.77	61%	6.6
Y'_PSNR	1%	-0.69	0.74	61%	6.9
Y'_SSIM	100%	-0.77	0.85	53%	5.4
Y'_SSIM	50%	-0.77	0.85	55%	5.5
Y'_SSIM	20%	-0.77	0.85	51%	5.4
Y'_SSIM	10%	-0.76	0.85	52%	5.5
Y'_SSIM	5%	-0.76	0.85	52%	5.5
Y'_SSIM	2%	-0.76	0.84	54%	5.6
Y'_SSIM	1%	-0.75	0.83	56%	5.8

These results suggest that for applications in SDTV two simplifications can be made without significant loss of performance in the tested metrics:
• Use only the luma component (Y') and
• Use only 5% of the frames in the scene.

B. Part II

In this part of the work, the experiments were performed to verify how a metric can have its correlation with the subjective measure improved with a pre-set adjustment to the scenes to be evaluated. There are three different types of adjustments in this work: (1) standardization of brightness, (2) filter enhancement for edge detection, and (3) a smoothing filter.

Table V shows the results obtained after standardization of each frame in all scenes. The first line refers to the PSNR performance results applied only in luma without the standardization of brightness and the second line refers to the PSNR performance only in luma with the brightness differences corrected.

TABLE V
PERFORMANCE COMPARISON OF PSNT AFTER STANDARDIZATION

Metric	cc Spearman (r_s)	cc Pearson nonlinear (r)	points outside	rms error
Y-PSNR	-0.74	0.78	55%	6.3
Y-PSNR standardized	-0.71	0.75	61%	6.8

Edge detection was completed using the filtering techniques presented in [36]. Five different methods for extracting contours were tested: (1) Sobel, (2) Canny, (3) Roberts, (4) Prewitt, and (5) Laplacian of Gaussian (also known as LoG). The performance metric was performed on images containing only the original image contours, which are shown in Table VI.

TABLE VI
PERFORMANCE OF EACH METRIC ACCORDING TO THE NUMBER OF FRAMES USED

Detection Method	cc Spearman (r_s)	cc Pearson nonlinear (r)	points outside	rms error
Sobel	-0.78	0.84	52%	5.5
Canny	-0.57	0.64	71%	8.2
Roberts	-0.80	0.84	52%	5.5
Prewitt	-0.79	0.84	53%	5.5
LoG	-0.70	0.77	66%	6.8

Note the significant improvement in correlation with the subjective measure when using Sobel and Roberts edge detection methods. This is consistent with the fact that the human visual system is adapted to extract the structural forms of the images that are captured by the eyes. These methods for extracting contours when optimally applied require few computational resources.

The effects of using a smoothing filter before the execution of the PSNR and SSIM metrics in correlation with the subjective measurements are shown in Tables VII and VIII.

TABLE VII
EFFECT OF A SMOOTHING FILTER ON THE PERFORMANCE OF THE $DMOS_{PSNR}$ MEASURE COMPARED TO THE DMOS MEASURE

σ of the filter	cc Spearman	cc nonlinear	points outside	rms error
no filter	-0.74	0.77	55%	6.3
0.5	-0.76	0.81	55%	6.0
1.0	-0.75	0.79	53%	6.2
1.5	-072	0.76	54%	6.5

TABLE VIII
EFFECT OF A SMOOTHING FILTER ON THE PERFORMANCE OF THE $DMOS_{SSIM}$ MEASURE COMPARED TO THE DMOS MEASURE

σ of the filter	cc Spearman	cc nonlinear	points outside	rms error
no filter	-0.57	0.59	70%	8.4
0.5	-0.76	0.85	49%	5.3
1.0	-0.78	0.86	51%	5.1
1.5	-0.77	0.85	54%	5.4

doi: 10.18580/setijbe.2015.1 Web Link: http://dx.doi.org/10.18580/setijbe.2015.1

VIII. CONCLUSION

A comparison of the objective evaluation metrics of video quality was presented. The performance metrics PSNR, SSIM, and S-CIELAB, were presented. It has been shown that for typical TV scenes in standard definition, subjected to typical distortions for this type of application, that it is still possible for more simplification of the types of metrics used to be completed, enabling their use in practical applications in real time. In addition, the results of the comparison with the subjective measurements showed that these simple metrics can be significantly improved when better adapted to the spatial contrast sensitivity and the structural recognition capability of the human visual system.

The adaptation to spatial contrasts was completed with the use of image smoothing filters. The image recognition structures were tested with the use of filters for extracting contours and also with a metric that has this intrinsic characteristic (SSIM).

These metrics are not able to replace the subjective evaluation of video quality, but complement this type of evaluation, estimating its results to a correlation of around 85%. Other approaches suggested to continue this work:

• Provide other databases with previously evaluated video scenes to supply the scientific community with shared resources of good quality, like the VQEG scenes used in this work;

• Test other filter types that are related to the extraction of structural information of video scenes;

• Complete the same tests for applications in high-definition television HDTV;

• Partially referenced or even non-referenced implementations can be tested, visualizing applications in remote monitoring.

REFERENCES

[1] R.C. Gonzalez and R. E. Woods, *Processamento de Imagens Digitais*, 1st ed,. São Paulo, Brazil: Edgard Blücher, 2000, p. 509.

[2] J. Watkinson, "The Art of Digital Video,". *Revista de radioifusão* vol. 03, no. 0330, p. 774, 2000.

[3] M. Pinson and S. Wolf, "A new standardized method for objectively measuring video quality," *IEEE Transactions on Broadcasting*, vol. 50, no. 3, pp. 312–322, 2004.

[4] W. Y. Zou and P. J. Corriveau, "Methods for evaluation of digital television picture quality," presented at the 138th SMPTE Technical Conference and World Media, 1996.

[5] Video Quality Experts Group, "Final Report from the Video Quality Experts Group on the Validation of Objective Models of Video Quality Assessment," VQEG, March 2000. Available: <ftp://vqeg.its.bldrdoc.gov/>.

[6] Video Quality Experts Group, "Final Report on the Validation of Objective Models of Video Quality Assessment, Phase II," March. 2003. Available: <ftp://vqeg.its.bldrdoc.gov/>.

[7] *Objective perceptual vqm techniques for digital broadcast television in the presence of a full reference*, Recommendation ITU-R BT1683, 2004.

[8] I. P. Gunawan and M. Ghanbari, "Reduced-reference video quality assessment using discriminative local harmonic strength with motion consideration," *IEEE Transactions on Circuits and Systems for Video Technology*, vol. 18, no. 1, pp. 71–83, 2008.

[9] E. P. ONG et al, "Video quality metrics - an analysis of low bit-rate videos," *in IEEE International Conference on Acoustics, Speech, and Signal Processing - ICASSP*, vol. 1, pp. I–889–I–892, 2007.

[10] H. Sheikh and A. Bovik, "Image information and visual quality," *IEEE Transactions on Image Processing*, vol. 15, no. 2, pp. 430–444, 2006.

[11] K. Seshadrinathan, and A. C. Bovik, "A structural similarity metric for video based on motion models," in *IEEE International Conference on Acoustics, Speech, and Signal Processing*, vol. 1, no. 1, pp. 869–872, 2007.

[12] J. Guo, M. V. Dyke-Lewis, and H. R. Myler," Gabor difference analysis of digital video quality," *IEEE Transactions on Broadcasting*, vol. 50, no. 3, 2004.

[13] *Methodology for the assessment of the quality of television pictures*, Recommendation ITU-R BT500-11, 2002.

[14] *Subjective video quality assessment methods for multimedia applications*, Recommendation ITU-T P910, 2008.

[15] T. N. Pappas and R. J. Safranek, "Perceptual criteria for image quality evaluation," *Handbook of image and video processing*. Academic Press, 2000. ch. 8, sec. 2, pp. 669–684.

[16] C. A. Poynton. (1996). *A Technical Introduction To Digital Video*. [Online]. Available: <http://www.poynton.com/ PDFs/GammaFAQ.pdf>.

[17] K. B. Benson and J. K. Whitaker, *Television Engineering Handbook: Featuring HDTV systems*. New York: Mc Graw-Hill, 1992.

[18] K. Jack, *Video Demystified: A Handbook for the Digital Engineer*. 3rd ed., Eagle Rock: LLH Technology Publishing, 2001, p. 759.

[19] *Composite analog video signal*, SMPTE 170M-2004, 2004.

[20] *Parameter values for the HDTV standards for production and international programme exchange*, Recommendation ITU-R BT709-05, 2002.

[21] B. Grob, *Televisão e Sistemas de Vídeo*, 5th ed,. Rio de Janeiro, Brazil: Guanabara S.A, 1989, p. 385.

[22] *Conventional analogue television systems*, Recommendation ITU-R BT470-7, 2005.

[23] *Characteristics of composite video signals for conventional analogue television systems*, Recommendation ITU-R BT1700, 2005.

[24] C. A. Poynton. (1997). *Frequently Asked Questions about Color*. [Online]. Available: <http://www.poynton.com/PDFs/ColorFAQ.pdf>.

[25] *Interfaces for digital component video signals in 525-line and 625-line television systems operating at the 4:2:2 level of recommendation ITU-R BT.601 (part a)*, Recommendation ITU-R BT656-4, 1998.

[26] *Studio encoding parameters of digital television for standard 4:3 and wide-screen 16:9 aspect ratios*, Recommendation ITU-R BT601-5, 1995.

[27] *Interfaces for digital component video signals in 525-line and 625-line television systems operating at the 4:2:2 level of recommendation ITU-R BT.601 (part b)*, Recommendation ITU-R BT1302-0, 1997.

[28] J.S. Lim, *Two-Dimensional Signal and Image Processing*, 2nd ed., Englewood Cliffs: [s.n.], 1990, p. 694.

[29] D. K. Fibush, "Tutorial paper - video testing in a dtv world," *SMPTE Journal Society of Motion Pictures and Television Engineers*, no. 109, pp. 661–667, 2000.

[30] *Measuring methods for digital video equipment with analogue input/output, Rec*ommendation ITU-R BT1204, 1995.

[31] Z. Wang, H. R. Sheikh, and A. C. Bovik, "Objective video quality assessment," in *The Handbook of Video Databases: Design and applications*, 1st ed., Austin: [s.n.], 2003.

[32] N. Jayant and P. Noll, *Digital Coding of Waveforms: Principles and Applications to Speech and Video*. 2nd ed., Englewood Cliffs: [s.n.], 1984, p. 688.

[33] M. H. Pinson and S. Wolf, "Comparing subjective video quality testing methodologies," in *VCIP*, [S.l.: s.n.], 2003, pp. 573–582.

[34] M. C. Q. Farias, M. Carli, and S. K. K. Mitra, "Video quality objective metric using data hiding," in *IEEE International Workshop on Multimedia and Signal Processing*, [S.l.: s.n.], 2002.

[35] M. C. Q. Farias, J. M. Foley, and S. K. Mitra," Perceptual contributions of blocky blurry and noisy artifacts to overall annoyance," in *International Conference on Multimedia and Expo*, Baltimore: [s.n.], 2003.

[36] R. Arthur, "Avaliação Objetiva de Codecs de Video," M.S. thesis, UNICAMP, Campinas, São Paulo, Brazil, 2002.

[37] Z. Wang and A. C. Bovik, "A universal image quality index," *IEEE Signal Processing Letters*, vol. 9, pp. 81–84, March. 2002.

[38] Z. Wang, L. Lu, and A. C. Bovik, "Video quality assessment using structural distortion measurement," in *International Conference on Image Processing*, vol. 3, pp 65-68, [S.l.: s.n.], 2002.

[39] Z. Wang, A. C. Bovik, and E. P. Simoncelli, "Structural approaches to image quality assessment," in *Handbook of Image and Video Processing*, 2nd ed., San Diego: [s.n.], 2005.

[40] G. H. Chen et al. "Edge-based structural similarity for image quality," in *IEEE Transactions on Acoustics, Speech, and Signal Processing*, vol. 2, no. 1, pp. II–II, 2006.

[41] Z. Wang, E. P. Simoncelli, and A. C. Bovik, "Multiscale structural similarity for image quality assessment," in *Conference Record of the Thirty-Seventh Asilomar Conference on Signals, Systems and Computers*, vol. 2, pp. 1398-1402, [S.l.: s.n.], 2003.

[42] *Colorimetry - Part 4: Cie 1976 l*a*b* colour spaces*, CIE S 014-4/E:2007, 2007.
[43] X. Zhang and B. A. Wandell, "A spatial extension of cielab for digital color image reproduction," *Society for Information Display Symposium Technical Digest*, vol. 27, pp. 731–734, 1996.
[44] Roberto N. Fonseca and Miguel A. Ramírez, "Using SCIELAB for image and video quality evaluation," in *ISCE 2008. IEEE International Symposium*, 2008, pp.1 – 4.
[45] S. Winkler, "A perceptual distortion metric for digital color video," in *Proc. SPIE Human Vision and Electronic Imaging Conference*, San Jose: [s.n.], 1999, vol. 3644, pp. 175–184.

Cite this article:
Fonseca, Roberto N. and Ramirez, Miguel A. .; 2015.Quality Assessment of Video in Digital Television. SET INTERNATIONAL JOURNAL OF BROADCAST ENGINEERING. ISSN Print: 2446-9246 ISSN Online: 2446-9432. doi: 10.18580/setijbe.2015.1. Web Link: http://dx.doi.org/10.18580/setijbe.2015.1

Transmission and Reception Tests of Digital Terrestrial TV in the Metropolitan Region of Curitiba

Célio Lúcio Vasco, José Frederico Rehme, Ruth Angelina Martins, Elias Agostinho, Alexandre de Almeida Prado Pohl, Richard Demo de Souza, Keiko Verônica Ono Fonseca, and Marcelo Eduardo Pellenz

***Abstract*—This paper describes the preliminary test results of the transmission and reception of Digital TV signals, on Channel 41, in the metropolitan region of Curitiba, in the state of Paraná, Brazil. It describes the equipment configuration deployed to carry out the tests, with the objective of mapping signal levels in the field and carrying out objective (channel power received, C/N, MER) and subjective measures (signal quality and observation of artifacts) in 200 selected locations in the metropolitan region of Curitiba. A propagation model is discussed (based on the Log-distance and Okumura-Hata models), as a function of the received channel power values measured in some selected locations. The results should allow the calculation of the coverage area, and the identification of the shadowed areas and critical reception points.**

***Index Terms*—**

I. Introduction

THE standard for digital TV in Brazil is set by a regulatory framework in the country, as well as increasing activity in the broadcasting area. With the introduction of new standards in audio and video encoding, middleware and transmission of RF signals, intensified research, project implementation and consequently trade in this area, including new receivers.

The definition of the Brazilian Digital Television Terrestrial System - SBTVD-T was determined by Decree No. 5820 [1] on 06/29/2006, which established the Japanese system ISDB-T (Integrated Services Digital Broadcasting Terrestrial) as the transmission standard and also a transitional period of ten years for the transition from analog and digital. The official start of digital TV transmissions in Brazil [2] took place on December 2, 2007, when it began broadcasting in the city of São Paulo, since followed by other state capitals in the country.

One of the challenges that this new technology brings is to determine if the coverage of the digital signal will have the same range as analog broadcasting since the cost benefit between quality and robustness of the signal can cause differences in the signal coverage area. Coupled with the fact that with digital receivers, images can freeze when the reception level meets the reception threshold, unlike analog receivers.

With this in focus, this paper describes the preliminary results of the transmission and reception tests for a digital TV channel in the metropolitan region of Curitiba, the state capital of Paraná, the focus is the determination of an empirical propagation model that will agree with the measurements taken.

The purpose of surveying the digital TV broadcast signals in Curitiba is to know the propagation characteristics within the region of the new modulated digital signals to determine if there are critical points or shadow areas. This study is of interest to all broadcasters wishing to deploy digital TV systems in the region.

The tests are being conducted in a partnership between the Universidade Tecnológica Federal do Paraná (UTFPR) and the Associação das Emissoras de Radiodifusão do Paraná (AERP), with assistance from Rede Paranaense de Communicação (RPC).

This article describes the infrastructure used for the survey, the propagation models used, the analysis of the collected data, the estimated signal coverage and conclusions.

II. Infrastructure

The early trials of Digital TV transmission in Curitiba took place with the authorization for the UTFPR to run the Special Service for scientific or experimental purposes conforming to Act no. 1388 [3] on 03/12/2008, issued by the Agência Nacional de Telecommunicações (Anatel).

The feasibility study was made possible by RPC, one of the main Paranaense broadcasters associated with AERP, which

Célio Lúcio Vasco, Universidade Tecnológica Federal do Paraná (UTFPR) (e-mail: celiov@yahoo.com.br)
José Frederico Rehme, Rede Paranaense de Comunicação (RPC) (e-mail: fredrehme@gmail.com)
Ruth Angelina Martins, Rede Paranaense de Comunicação (RPC) (e-mail: ruthm@tvparanaense.tv.br)
Elias Agostinho, Associação das Emissoras de Radiodifusão do Paraná (AERP) (e-mail: elias@sertpr.org.br)
Alexandre de Almeida Prado Pohl, Universidade Tecnológica Federal do Paraná (UTFPR) (e-mail: pohl@cpgei.cefetpr.br)
Richard Demo de Souza, Universidade Tecnológica Federal do Paraná (UTFPR) (e-mail: richard@cpgei.cefetpr.br)
Keiko Verônica Ono Fonseca, Universidade Tecnológica Federal do Paraná (UTFPR) (e-mail: keiko@utfpr.edu.br)
Marcelo Eduardo Pellenz, Pontificia Universidade Católica do Paraná (PUC-PR) (e-mail: marcelo@ppgia.pucpr.br)

doi: 10.18580/setijbe.2015.2 Web Link: http://dx.doi.org/10.18580/setijbe.2015.2

provided the necessary infrastructure, i.e., the transmitter and the radiant system installed on a tower, operating on UHF channel 41. The survey began in June 2008 and is still ongoing during the period of this article being written. Therefore, the results discussed in this paper are only partial.

A. Transmission

The transmission system characteristics are described in Act no. 1388 issued by Anatel [3], as follows:

a) The transmitter equipment used is manufactured by Linear Electronic Equipment SA, Model IS74K1 with power operation up to 4.1 kW tuned to channel 41, occupying the range of frequencies between 632-638 MHz;

b) The radiant system used is manufactured by Transtel Conti & Cia Ltda., model TTSL8 U0 - 41-10D, omnidirectional, with 8 slots, with a total gain of 10.89 dBd;

c) The geometric center of the radiating system is installed 90.0m above the quota basis, 950m above sea level. The azimuth orientation is 0° NV.

The transmitter was tested in five different configurations, for the configuration levels analyzed the transmission power is 4.1 kW, the modulation is 64QAM, the guard interval is 1/16 and FEC rate is 3/4. Video content was transmitted in a sequence of different scenes, which were non-commercial.

B. Reception

The collection of reception data is being completed in a vehicle called the mobile field measurement unit from RPC, equipped with:

a) an 8m telescopic mast, equipped with a log-periodic antenna manufactured by Proeletronic with full UHF band for the reception of channel 41. It was also equipped with an antenna for the reception and evaluation of analog signals from channel 12, not forming part this study;

b) a manufacturer's spectrum analyzer, Agilent ESA model E 4405 B for measuring the reception power;

c) a digital television receiver connected to a display with the aspect ratio of 16: 9. This allows the subjective quality scoring of the received signal;

d) a laptop for data collection;

e) a GPS receiver for measuring location coordinates;

f) A thermohygrometer for measuring temperature and humidity;

The height of an 8m mast antenna on the mobile unit, as seen in Fig. 1 allows the simulation of a residential receiving antenna. Fig. 2 shows the inside of the mobile unit, where the equipment layout can be seen.

Fig. 1. Mobile field measurement unit

Fig. 2. Interior of the mobile unit

III. Data Analysis

The database considered consists of the measurements collected in 87 locations assessed from June 13 until July 17, distributed around the city of Curitiba.

In this study only the 6MHz bandwidth channel power was analyzed, measured at the receiver, with the transmission at 4.1kW, broadcasting in high definition, which allows evaluation of the propagation characteristics in the region of Curitiba in normal operating conditions.

A. Propagation model choice

The initial comparison of the receiving power measurement was with the free space propagation model, which enables the prediction of signal attenuation in an unobstructed line of sight between the transmitter and the receiver.

Using Friis' free space equation, described by Rappaport [4], the reception power P_r is given by:

$$P_r(d) = \frac{P_t G_t G_r \lambda^2}{(4\pi)^2 d^2 L} \quad (1)$$

where P_t is the transmitter power, G_t is the gain of the transmitting antenna, G_r is the gain of the receiving antenna, λ is the wavelength of the transmitted signal, d is the distance

doi: 10.18580/setijbe.2015.2 Web Link: http://dx.doi.org/10.18580/setijbe.2015.2

between the transmitter and receiver, and L is other losses not related to the propagation.

This model considers the transmitter power, the antenna gain, and operating frequency, as the received power decreases with the square mean of the distance. In the results from the implementation of this model, shown in Fig. 3, it is observed that the position of the curve is well above the plotted locations, indicating that this prediction model is far from the real situation.

As the received signal level decreases logarithmically with the distance, the Log-distance path loss model was used, as described by Rappaport [4] and is calculated by:

$$\mathrm{PL}(d) = \mathrm{PL}(d_0) + 10n\log(d/d_0) \quad (2)$$

where PL is the propagation loss between the distances of d and d_0, where: d is the distance from the transmitter to the measured location, d_0 is the distance to the nearest transmitter reference, and n is the propagation loss exponent. In the evaluation, it was considered that d_0 is equal to 200m, that is, the distance from the transmitter to the measured location nearest to the antenna and PL(d_0) the average propagation loss at the measured locations to 200m.

The exponent n of the Log-distance model was obtained using the minimum-mean-square-error method (MMSE), where n = 2.8267 is obtained, as shown in Fig. 3. This value indicates that the decay of the reception level is greater than in the in the case of free space attenuation, or that the environment causes more severe losses than in free space conditions. According to Rappaport [4], $2.7<n<3.5$ indicates an environment in urban areas, consistent with the calculated value. To analyze the dispersion values around the mean, the standard deviation was calculated, and as shown in Fig. 3 the value found was σ = 10.1dB, indicating that the reception power may have considerable variation around the mean.

This normalization logarithmic model in which the propagation loss is characterized by an attenuation factor, which, in this case, is the distance exponent n is a non-frequency dependent model that can be used in various transmission bands, and the value of n intrinsically contains the effect of all propagation mechanisms [5].

The Hata model [6] is a mathematical formula for empirical graphic base of attenuation losses provided by Okumura, and valid for the range of 150MHz to 1500MHz, this was implemented as described by Rappaport [4] and is calculated by:

$$L_{50} = 59.55 + 26.16\log f_c - 13.82\log h_{te} - \mathrm{a}(h_{re}) + (44.9 - 6.55\log h_{te})\log d \quad (3)$$

where L_{50} is the propagation loss in dB; f_c is the operating frequency; h_{re} is the height of the transmission antenna, h_{re} is the height of the receiving antenna, and d is the distance from transmitter to receiver. The correction factor for a large city and frequency greater than 300MHz, is given by:

$$a(h_{re}) = 3.2(\log 11.75\, h_{re})^2 - 4.97. \quad (4)$$

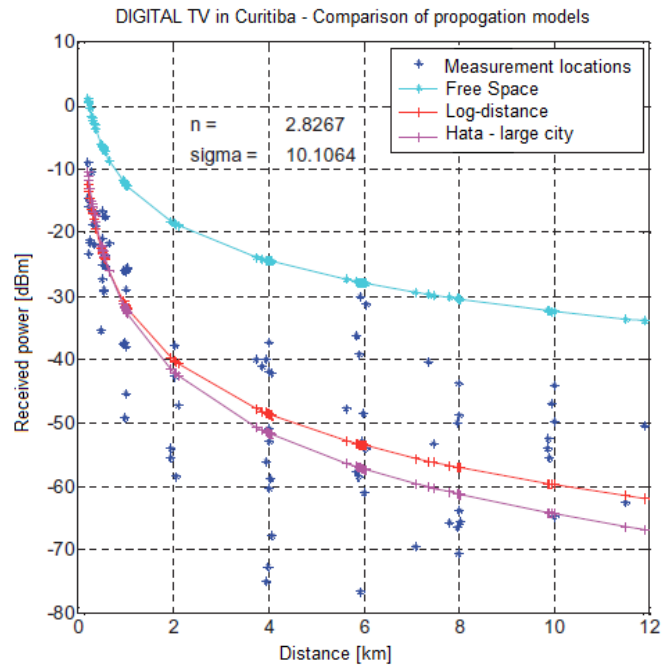

Fig. 3. Analysis of reception power for the free space, Log-distance, and Hata models

B. *Improving the estimation of received power*

The evaluation of the reception power data indicates that the Log-distance and Hata models can be adopted by Curitiba, but it is observed that the standard deviation between the measured values were compared with the average estimated at 10.1dB, a value that would be wanted to be reduced. Therefore, we investigated a way to have a more detailed estimate of the estimated channel power values received at the considered locations.

In an attempt to minimize the standard deviation, stratification of the received power values was completed in three sets in relation to the average: a) within ± 10dB, b) above 10dB c) below 10dB. Fig. 4 presents this stratification.

doi: 10.18580/setijbe.2015.2 Web Link: http://dx.doi.org/10.18580/setijbe.2015.2

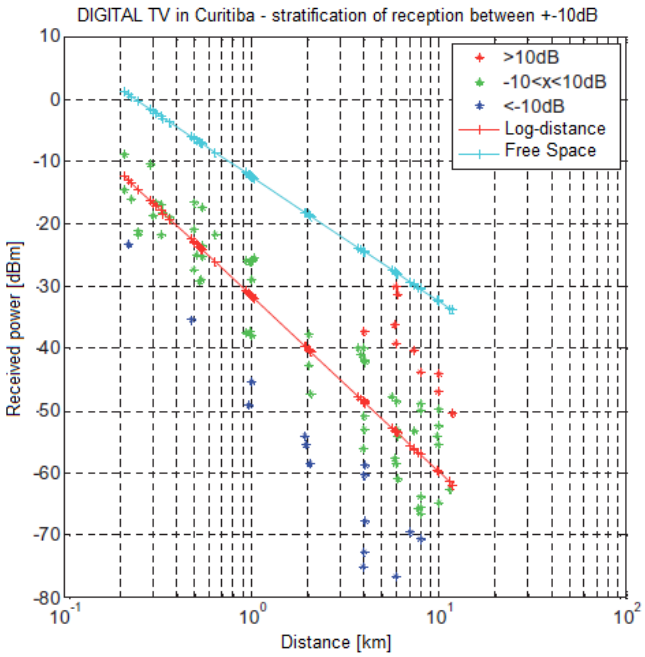

Fig. 4. Stratification of the received power within the standard deviation

It is observed that there are ten values above the standard deviation limit and fifteen values below the standard deviation limit. An interpretation of the values below the limit is the existence of other signal attenuations that have not been considered, such as, for example, losses due to obstruction. The values above the variance should indicate a line of sight situation between the receiver and the transmitter, approaching the free space model.

C. Obstruction by attenuation analysis

As the city of Curitiba does not have uniform topography, and because of the existence of concentrations of buildings along the line of sight of transmissions, a situatio typical of big cities, attenuation by obstruction was analyzed due to the signal diffraction phenomenon. This phenomenon is present when obstacles, such as hills blocking line of sight signals, causing attenuation that adds to the attenuation of free space propagation [7].

From terrain profile data obtained from the SIGAnatel system, it was possible to make a survey of Curitiba, shown in Fig. 5, with a radius of 12km, and with a precision of 90m. The Sistema de Informações Geográficas Anatel (SIGAnatel) [8] is an application available on the website of the National Telecommunications Agency (Anatel), which contains geographical and topographical data of Brazil, and enables a propagation analysis module.

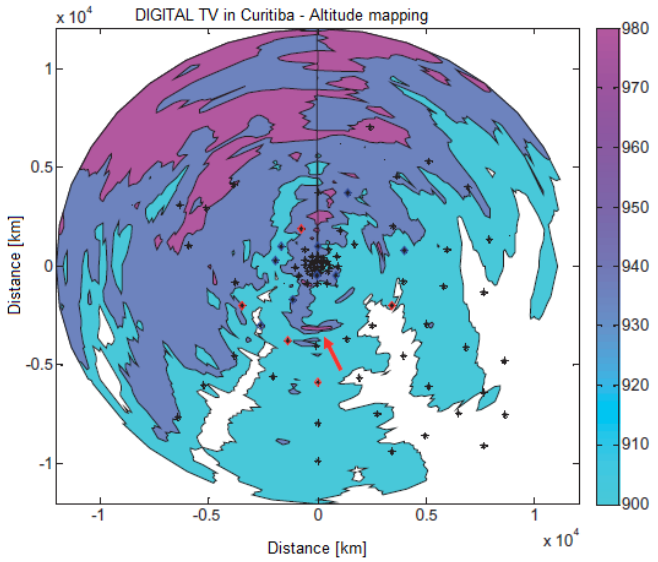

Fig. 5. Topographic map of Curitiba

It is observed that the transmitting antenna in the center of Fig. 5, is situated at a median altitude of the region, specifically 950m. To the north, there is a higher region and to the southeast there is a lower region. Approximately 3km south of the antenna, there is a region with a high concentration of buildings that are the same height as the atenna's base obstructing line of sight transmissions to the southern region.

In the map in Fig. 5, the altitude of some regions of Curitiba, which were considered relevant to the survey, those 60m above ground level mark the height of buildings. These regions were obtained through empirical analysis using GoogleEarth and are shown in Fig. 6. The marked areas indicate regions with concentrations of buildings, and the altitude of the region indicated by the arrow in the south azimuth has the same dimensions as the transmission antenna's base.

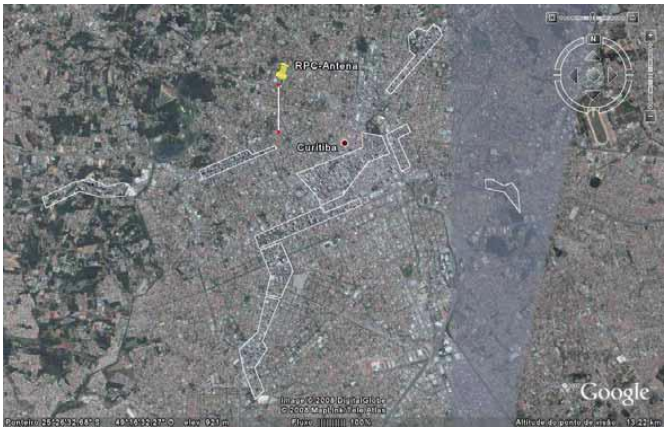

Fig. 6. Areas with high concentrations of buildings

From the terrain profile database and the marking of buildings, mapping of the loss due to obstruction in the city was completed, for each of the azimuths from 0° to 350°, in steps of 10°, and a variation of distance from 1km to 12km in

doi: 10.18580/setijbe.2015.2 Web Link: http://dx.doi.org/10.18580/setijbe.2015.2

90m steps. The v parameter from Fresnel-Kirchoff's diffraction was used, as described by Rappaport [4], and is calculated by:

$$v = h\sqrt{\frac{2(d_1+d_2)}{\lambda d_1 d_2}} \quad (5)$$

where v is the Fresnel-Kirchoff diffraction parameter, one-dimensional, λ is the signal wavelength transmitted, h is the obstruction height above the line of sight between the transmitting antenna and the receiving antenna, d_1 is the distance between the transmitting antenna and obstruction, and d_2 is the distance between the obstruction and the receiving antenna.

From the v diffraction parameter, the obstruction loss P_d in dB was calculated, as described by Rappaport [4] and is given by:

$$P_d = -20\log(0.5\exp(-0.95v)) \qquad 0 \le v \le 1 \quad (1)$$

$$P_d = -20\log\left(0.4\sqrt{0.1184-(0.38-0.1v)^2}\right) \qquad 1 \le v \le 2.4 \quad (2)$$

$$P_d = -20\log\left(\frac{0.225}{v}\right) \qquad v > 2.4. \quad (3)$$

The mapping of the loss by obstruction is shown in Fig. 7.

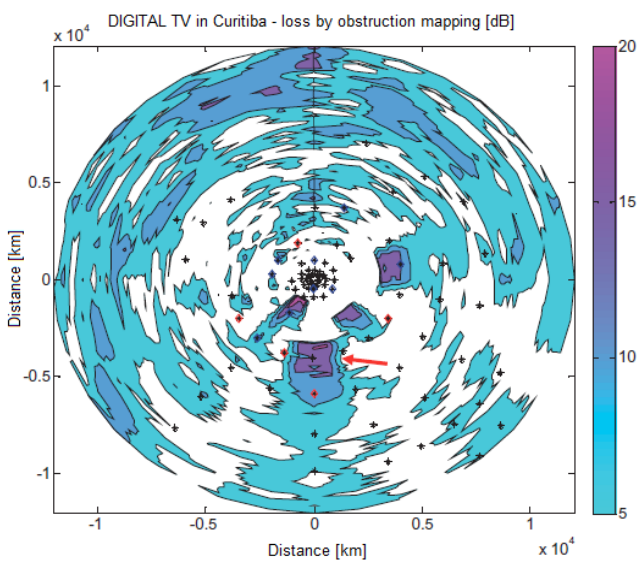

Fig. 7. Map of signal loss caused by obstructions in Curitiba

Of the 87 locations examined, 49 locations were found to have an attenuation loss greater than 0dB, with an average of 5.6dB and a standard deviation of 3.5dB. The maximum attenuation of 16.7dB was found in azimuth 181° at a distance of 4km (region marked by the arrow), followed by 15.2dB at 79° and 4km, and 12.6dB at 180° and 5.9km. These points are in agreement with those regions that were pointed out in Fig. 6.

It is observed in Fig. 7 that there are shadow areas caused by the density of buildings in some regions of the city, which can cause a greater loss than 15dB in signal strength. The arrow indicates the shadow region in the south azimuth caused by a cluster of buildings also marked in Fig. 6. The white regions indicate areas with obstruction loss less than 5 dB and must have lines of sight between the transmitter and the receiver, or is unobstructed.

D. Propagation model analysis considering loss by obstruction

With the calculation of loss by obstruction in the evaluated locations, the analysis was repeated with propagation models, and the results are presented in Fig. 8.

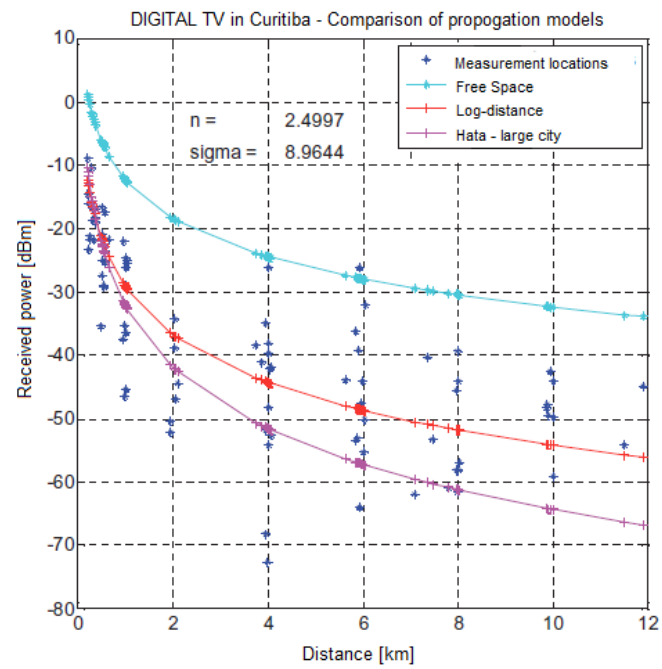

Fig. 8. Analysis of the received power, considering loss by obstruction, for the Free Space, Log-distance and Hata models

It was observed that there was an improvement of approximately 1 dB in the standard deviation of channel power values at the measured locations. The Log-distance curve indicates that the average scores are being less dispersed, i.e., these estimates are more precise. In relation to the stratification values, a new situation has been obtained.

doi: 10.18580/setijbe.2015.2 Web Link: http://dx.doi.org/10.18580/setijbe.2015.2

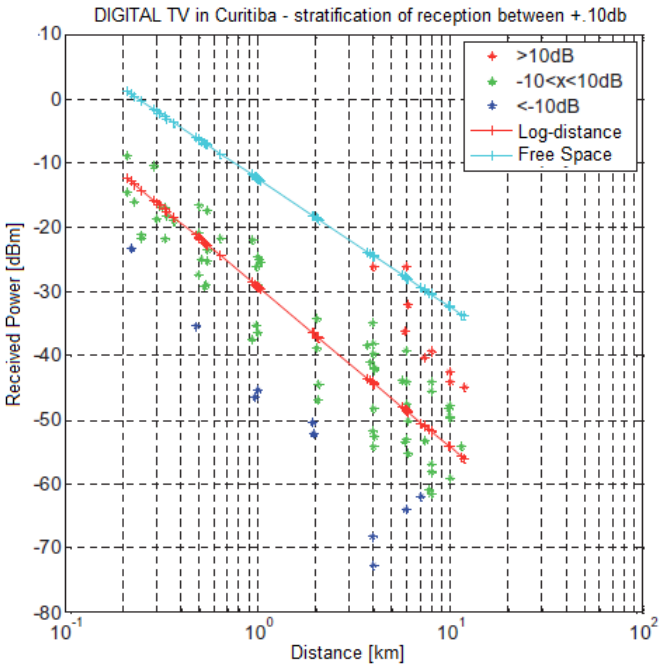

Fig. 9. Stratification of the powers received within the ±10dB deviation considering the loss by obstruction

It is observed that there are nine values above the standard deviation limit and ten below the standard deviation limit. There was an improvement in the dispersion of estimated values; however, there are still values that are outside the standard deviation. A location analysis is needed to check for possible loss by obstruction by local buildings, or other situations.

IV. Estimate of Signal Coverage

After obtaining a suitable propagation model for the city of Curitiba, it is possible to estimate the Digital TV signal coverage distance to the parameters considered.

According to standard ABNT NBR 15604 [9] which regulates digital TV receivers, the receiver sensitivity must be less than -77dBm at the receiver input.

Considering (2), the estimated Log-distance model in Section III.A, we have:

$$\mathrm{PL}(d) = \mathrm{PL}(d_0) + 10n\log(d/d_0). \tag{9}$$

Therefore, considering the practical data: transmission power of 4.1kW, i.e., 66.12dBm; reference power of 11.75dBm to 200m; minimum power reception of -77.0dBm; loss by propagation exponent of 2.8271; calculates the maximum distance of *d* as 40.6km.

Concluding that, according to the estimate made in this work, from the empirical obtainment of a propagation loss curve, the digital TV signal coverage would have an average distance of 40.6km for the region of Curitiba. Note that this estimate is in 50% of the cases, that is, values that are within the standard deviation from the evaluated locations and without a radial analysis, which could have different values.

To prove this estimate, a simulation of TV channel viability in the SIGAnatel system [8] was carried out with the same simulation data. This system has an application to simulate the coverage area of a digital TV channel, whereas the coverage area for the primary protection of transmission is the radius that the reception level threshold is -51dBμV (-56dBm). The result obtained in the SIGAnatel simulation, indicates that the average distance for the -56dBm receiving power is 47.0km.

It is observed that the mean radius of the primary boundary for the -51dBμV estimate generated by the SIGAnatel system is 47.0km, while the estimate according to the Log-distance curve field survey of reception power is -77dBm and 40.6km. This difference may be because the analysis completed by the SIGAnatel system follows recommendation ITU-R 1546, which has a different propagation condition in relation to urban density.

In accordance with annex 7 of recommendation ITU-R P.1546-1 [10], the equation to obtain the field strength for the Okumura-Hata method is given by:

$$\mathrm{E} = 69.82 - 6.16\log f + 13.82\log H_1 + a(H_2) - (44.9 - 6.55\log H_1)(\log d)^b \tag{10}$$

where E is the field strength in dBμV/m to 1 kW erp; *f* is the operating frequency; H_1 is the height of the transmission antenna, H_2 is the height of the receiving antenna, *d* is the distance from the transmitter to the receiver, and *b* is the correction factor dependent on H_1 and d, where b = 1 for d≤20km. The correction factor for the receiving antenna is given by:

$$a(H_2) = (1.1\log f - 0.7)H_2 - (1.56\log f - 0.8). \tag{11}$$

It is noted that in (11), the correction factor shown in recommendation ITU-R P.1546-1 is the same as that presented by Rappaport [4] and in (3.83), used for propagation in small and medium-sized cities. Therefore, it can be inferred that the model adopted by recommendation ITU-R P.1546-1 is equivalent to the Hata model for small and medium-sized cities.

In addition to the difference in density urban, according to recommendation no. 398 the coverage assessment is completed considering the height of the receiving antenna at 10m, which causes an increase in the level received at the receiver.

Therefore, the simulation completed by the SIGAnatel system considers a less rigid situation than observed empirically in Curitiba. Again, it is concluded that the estimated model for this work is suitable to be used in Curitiba.

V. Conclusion

The Log-distance propagation model is useful for providing an estimate from empirically collected data, the behavior of channel power in relation to distance. From this estimated model, we can also conclude that the Hata model used in urban areas of large cities, it is suitable for use in Curitiba.

In conclusion, according to the estimate made in this paper, the digital TV signal coverage for a city region would have a radius of 40.6km. Considering that this is a situation that will be needed in 50% of cases.

doi: 10.18580/setijbe.2015.2 Web Link: http://dx.doi.org/10.18580/setijbe.2015.2

There is a difference between the estimate obtained by this work and the estimate of coverage obtained by the SIGAnatel system, which adopts recommendation ITU-R P.1546-1 that considers average propagation conditions, ie, for small and medium-sized cities. While this work from local empirical data estimates that propagation conditions are more severe in the urban areas of large cities. This comparison will have a future breakdown.

This study, which is preliminary, may only be completed after the completion of data collection of the 200 locations it proposes in this research.

REFERENCES

[1] Presidência da República (2006). "Decreto nº 5.820," in *Diário Oficial da União de 30/6/2006*.

[2] Ministério das Comunicações (2007). "Ministro Hélio Costa fala sobre TV Digital." Available: <http://www.mc.gov.br/003/00301009.asp?ttCD_CHAVE=19242>

[3] Anatel (2008). "Ato nº 1388." in *Diário Oficial da União, nº 51, de 14/3/2008*.

[4] Rappaport, Theodore S. (1999). "Wireless Communications – Principles & Practice," Prentice Hall, USA.

[5] C. Perez-Vega and J.M. Zamanillo, "Path-loss model for broadcasting applications and outdoor communication systems in the VHF and UHF bands." *IEEE Trans. Broadcasting*, vol. 46, no. 2, pp. 91-96, June. 2002.

[6] M. Hata, "Empirical Formula for Propagation Loss in Land Mobile Radio Services," *IEEE Trans. Veh. Technol.*, vol.29, pp.317-325, Aug. 1980.

[7] *Propagation by Diffraction*, Recommendation ITU-R P.526-10, 2007.

[8] Anatel (2008). "SIGAnatel - Sistema de Informações Geográficas." Available at: http://sistemas.anatel.gov.br/siganatel

[9] ABNT (2007). "ABNT NBR 15604 – Televisão digital terrestre – Receptores," in *Associação Brasileira de Normas Técnicas*.

[10] Anatel (2005). "Rec. UIT-R P.1546-1 - Método de previsões ponto-área para serviços terrestres na faixa de freqüências de 30 a 3000 MHz" in *Anexo à Resolução Anatel n.º 398, de 7/4/2005, Anexo II.*

Cite this article:
Vasco,C.L., Rehme, J. F. , Martins, R. A., Agostinho, E., de Almeida Prado Pohl, A., Demo de Souza, Richard, Ono Fonseca, K. V., Pellenz, M. E.; 2015.Transmission and Reception Tests of Digital Terrestrial TV in the Metropolitan Region of Curitiba. SET INTERNATIONAL JOURNAL OF BROADCAST ENGINEERING. ISSN Print: 2446-9246 ISSN Online: 2446-9432. doi: 10.18580/setijbe.2015.2. Web Link: http://dx.doi.org/10.18580/setijbe.2015.2

Simulation Software for the ISDB-T_B Modulation System

Cristiano Akamine and Yuzo Iano

***Abstract*—This paper presents a simulation tool for the ISDB-T_B modulator, to perform complex analyses in each processing stage. From a Broadcast Transport Stream (BTS) file you can follow the processing performed in each modulator block to the final transmission stage. It is possible to make real transmissions with the RF files generated in the simulator with the use of a vector signal generator. A mathematical and practical approach to the operation of each modulator block is performed starting with the description of the BTS signal up to the final transmission stage.**

***Index Terms*—Broadcast Transport Stream – Orthogonal Frequency Division Multiplexing (BST-OFDM), Integrated Digital Broadcasting System – Terrestrial (ISDB-T), Modulator, Simulation.**

I. Introduction

THE Integrated Services Digital Broadcasting - Terrestrial (ISDB-T) modulation system [1] is designed to operate with various types of services occupying a TV channel with a bandwidth of 6, 7 or 8 MHz. The system is very flexible and allows the combination of multiple services, such as portable reception, mobile, and fixed with unequal protection errors on the same channel. The system uses the Band Segmented Transmission - Orthogonal Frequency Division Multiplexing (BST-OFDM) modulation in which each segment uses a wide band corresponding to 6/14 MHz = 428.57 kHz for 6 MHz bandwidth. The thirteen segments may be combined in up to three hierarchical layers called Layer A, Layer B, and Layer C. Recently, a modified version of the ISDB-T modulation system called ISDB-T version B (ISDB-T_B) [2] was developed and adopted in Brazil and many other countries. The main difference of the ISDB-T_B modulation system is the RF channel and transmission mask [2], [3]. The ISDB-T_B modulation system can be divided into three stages composed of the re-multiplexor, the channel encoder, and the modulator as can be seen in Fig. 1. The ISDB-T_B modulator cannot be configured locally and depends on the multiplexer/re-multiplexer to control and configure all the processing stages. To illustrate the operation of these stages, this article presents a software simulation of the ISDB-T_B modulator.

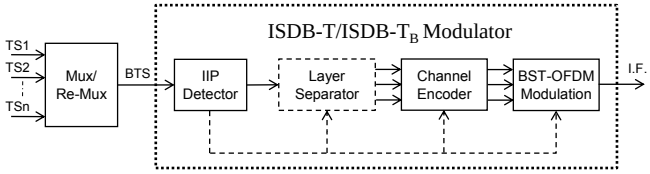

Fig. 1. Simplified diagram of the modulator.

From the Broadcast Transport Stream (BTS) that is generated in the multiplexing/re-multiplexing stage, all blocks that compose the modulator are described and analyzed using this computational tool. This simulator allows the monitoring of the input and output of all blocks in supported file formats with Matlab, C/C++ and support for Field Programmable Gate Array (FPGA). In addition, RF vectors can be created that can be transmitted by arbitrary signal generators. Fig. 2 shows a screenshot of this software, in which it is possible to select the file format, processing block, signal generator type and simulation time.

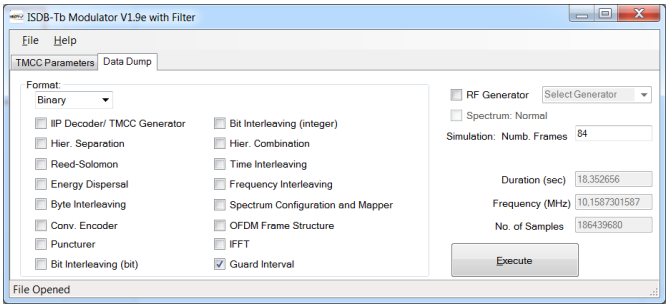

Fig. 2. Configuration screen of the ISDB-T_B simulator.

Thus, a review of the re-multiplexing stage is carried out in Section II. In Sections III and IV, the coding and modulation stages are presented. In Section V, the simulation tool is evaluated using an arbitrary signal generator and spectrum analyzer with an ISDB-T_B demodulator. Finally, in Section VI the conclusion is presented.

II. Re-multiplexing

To synchronize all the layers between the system source coding and modulation, the MPEG-2 TS 188 byte [4] from the source coding scheme, data carousel, etc. is multiplexed and re-multiplexed. The output of re-multiplexer is formed by a single TS with a size of 204 bytes and constant bit rate of four

This work was partly financed by FINEP and FOXCONN/MCT.
Cristiano Akamine is a Professor at the Engineering School of Mackenzie Presbyterian University, São Paulo, SP Brasil (e-mail: cristiano.akamine@mackenzie.br).
Yuzo Iano is a professor at UNICAMP in the Department of Communications for the Electrical Engineering and Computer Communications Faculty (DECOM / FEEC / UNICAMP), Campinas, SP, Brazil. (E-mail: yuzo@decom.fee.unicamp.br).

doi: 10.18580/setijbe.2015.3 Web Link: http://dx.doi.org/10.18580/setijbe.2015.3

times the sampling frequency of the Inverse Fast Fourier Transform (IFFT) modulator, or (4 x 512/63) = 32.5079Mb/s to 6 MHz bandwidth. Due to this characteristic the output signal of the re-multiplexer is called BTS [5]. The process of re-multiplexing is the positioning of each Transport Stream Packets (TSP) for each Layer and null TSP in a synchronized order with the demodulator of the receiver. The null TSP insertion maintains a constant BTS bit rate signal independent of the modulation parameters and channel coding. The packet order is required to secure the hierarchical transmission in a single TS and to minimize processing at the receiver [6].

The BTS signal is structured in a multiplexing frame in which the number of TSP depends on the mode and guard interval (GI) as can be seen in Table I [1], [2].

Additional the dummy byte, or 16 bytes in each BTS TSP is used to indicate the hierarchical layer that each TSP will be transmitted, TSP counter, frame headers, and the auxiliary data drivers, etc. Optionally, a Reed Solomon (RS) block code shortened (204,196,4) is applied and has correction capability of up to 4 bytes in a BTS TSP.

Fig. 3 shows an example of a TSP and multiplexer frame.

TABLE I
TSP NUMBERS INCLUDED IN A FRAME MULTIPLEXER

Mode	Guard interval reason			
	1/4	1/8	1/16	1/32
1 (2k)	1280	1152	1088	1056
2 (4k)	2560	2304	2176	2112
3 (8k)	5120	4608	4352	4224

The segment transmission order of the OFDM at the end of the modulation must be fully synchronized to the BTS signal frame multiplexer at the output of the re-multiplexer. Problems in the formation of the BTS signal multiplexer frame and clock and can generate a signal transmission error.

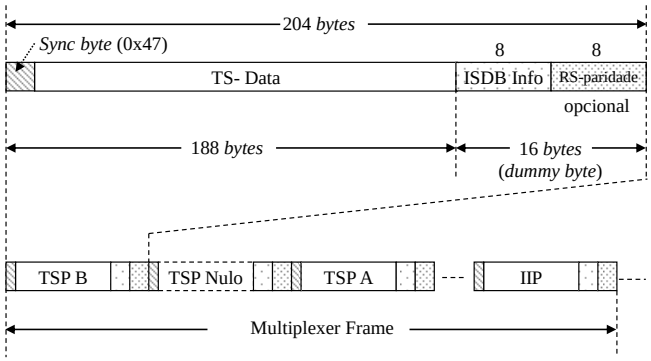

Fig. 3. BTS Frame Multiplexer.

Additionally the Modulation Configuration Control Information (MCCI) is sent in a package called ISDB-T Information Packets (IIP). The IIP is only transmitted once in the BTS signal multiplexer frame in which it has two descriptors that are called MCCI and Network Synchronization Information (NSI). The MCCI sets the modulation parameters and channel encoder as the size of IFFT, IG, modulation method, code rate, and the number of segments, etc. The NSI is used in the synchronization of the single frequency network in which the Synchronization Time Stamp (STS), maximum delay, control equipment, and product number, etc. are entered in this field.

Fig. 4 shows an example of an IIP for a BTS signal.

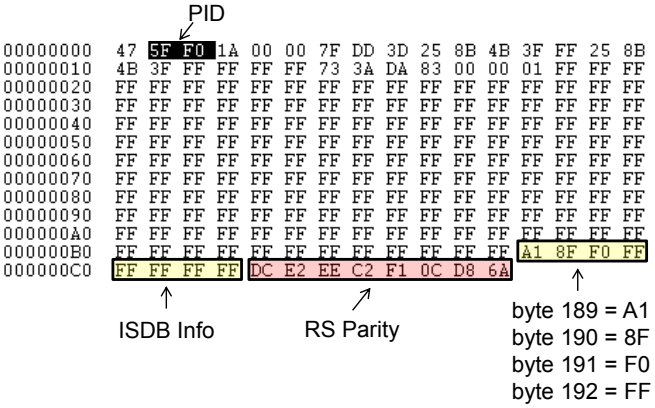

Fig. 4. IIP parameter identification.

III. ENCODER CHANNEL

The channel encoding process starts with IIP detection. The IIP can be identified by PID 0x1FF0 or by Layer 0x8 indication that can be obtained in the first four bits of byte 190. Reading descriptor IIP MCC, the TMCC generated is responsible for the configuration and control of all coding and modulation stages. In [1] and [2] it is possible to obtain the details of each bit for the MCCI and TMCC descriptors.

Fig. 5 shows the extracted IIP modulation parameters from Fig. 4 and Fig. 6 shows a simplified block diagram of the channel encoder. The detail of each of these blocks is presented in the following sub-sections.

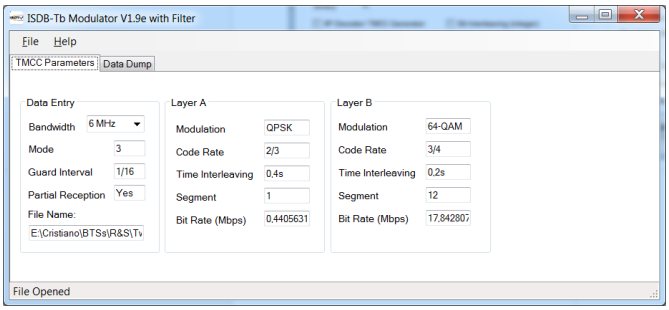

Fig. 5. Extracted IIP modulation parameters.

A. Layer Separator

The layer separator has the purpose of directing each BTS TSP to its respective layer. The separator reads BTS byte 190 and redirects each TSP according to the information contained in Table II. Null TSP and IIP are not transmitted in any of the hierarchical layers. The resulting output of the layer separator is an MPEG-2 TS, 188 bytes in size. Fig. 7 shows a Layer A TSP at the output of the separator.

doi: 10.18580/setijbe.2015.3 Web Link: http://dx.doi.org/10.18580/setijbe.2015.3

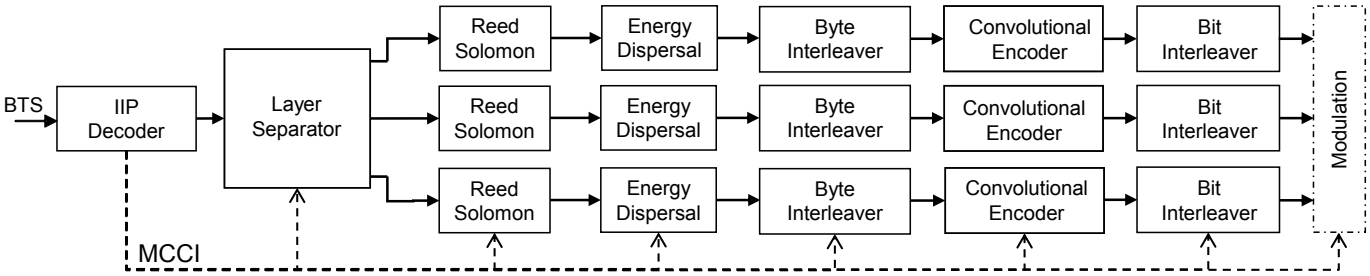

Fig. 6. Diagram of the channel coding stage.

TABLE II
ISDB FIELD LAYER INDICATOR INFO

byte 190 [7:4] (Layer Indicator)	**Description**
0000_b (0x0)	Null TSP
0001_b (0x1)	Layer A TSP
0010_b (0x2)	Layer B TSP
0011_b (0x3)	Layer C TSP
1000_b (0x8)	IIP TSP

```
00000000  47 01 01 20 B7 10 09 F5 D7 8C 00 FB FF FF FF FF
00000010  FF FF FF FF FF FF FF FF FF FF FF FF FF FF FF FF
00000020  FF FF FF FF FF FF FF FF FF FF FF FF FF FF FF FF
00000030  FF FF FF FF FF FF FF FF FF FF FF FF FF FF FF FF
00000040  FF FF FF FF FF FF FF FF FF FF FF FF FF FF FF FF
00000050  FF FF FF FF FF FF FF FF FF FF FF FF FF FF FF FF
00000060  FF FF FF FF FF FF FF FF FF FF FF FF FF FF FF FF
00000070  FF FF FF FF FF FF FF FF FF FF FF FF FF FF FF FF
00000080  FF FF FF FF FF FF FF FF FF FF FF FF FF FF FF FF
00000090  FF FF FF FF FF FF FF FF FF FF FF FF FF FF FF FF
000000A0  FF FF FF FF FF FF FF FF FF FF FF FF FF FF FF FF
000000B0  FF FF FF FF FF FF FF FF FF FF FF FF
```

Fig. 7. Layer A TSP.

B. Reed Solomon

The Reed Solomon (RS) block code was developed by two researchers, Irving S. Reed and Gustave Solomon in 1960 [7]. The RS code is considered a subclass of the Bose, Chaudhuri, and Hocquenghein (BCH) code for non-binary symbols [8]. The RS encoder is effective in correcting random errors and burst noise like the impulsive noise. The RS code is considered very powerful in relation to its error correction capability and is widely used in mobile communications; satellite; and storage devices such as CD, DVD; and bar codes.

ISDB-T uses an RS encoder (n=255, k=239, t=8), where n is the number of output symbols, k is the number of input symbols and t is the correction capability. Each symbol of this code uses m=8 bits. Due to this, MPEG-2 TS is standardized at 188 bytes, a modified version of this code called shortened RS is used with the following parameters RS(204,188,8). This version is obtained with the insertion and extraction of 51 null symbols at the beginning and end of the RS code.

The RS code uses algebra called Galois Field (GF) in which sum, subtraction, division, and multiplication are performed within this space. The GF(256) is generated from a field code generator *p(x)* described in (1).

$$p(x) = x^0 + x^2 + x^3 + x^4 + x^8 \tag{1}$$

Using (2) in GF(256) it is possible to calculate the polynomial generator g(x) in (3).

$$g(x) = (x + a^0)(x + a^1)(x + a^2) \dots (x + a^{2t-1}) \tag{2}$$

$$g(x) = x^{16} + 59x^{15} + 13x^{14} + 104x^{13} + 189x^{12} + 68x^{11} + 209x^{10} + 30x^9 + 8x^8 + 163x^7 + 65x^6 + 41x^5 + 229x^4 + 98x^3 + 50x^2 + 36x^1 + 59 \tag{3}$$

Considering the message to be coded *U(x)*, the encoded signal *V(x)* can be obtained using (4) and (5) where *q(x)* is the quotient and *r(x)* is the remainder of the division.

$$\frac{U(x) \times x^{n-k}}{g(x)} = q(x) + \frac{r(x)}{g(x)} \tag{4}$$

$$V(x) = U(x) \times x^{n-k} + r(x) \tag{5}$$

Fig. 8 shows the TSP in Fig. 7 in the output of RS code. The addition of 16 bytes and the displacement of 1 byte can be seen. This displacement is necessary to maintain the synchronism with the OFDM frame.

```
00000000  01 01 20 B7 10 09 F5 D7 8C 00 FB FF FF FF FF FF
00000010  FF FF FF FF FF FF FF FF FF FF FF FF FF FF FF FF
00000020  FF FF FF FF FF FF FF FF FF FF FF FF FF FF FF FF
00000030  FF FF FF FF FF FF FF FF FF FF FF FF FF FF FF FF
00000040  FF FF FF FF FF FF FF FF FF FF FF FF FF FF FF FF
00000050  FF FF FF FF FF FF FF FF FF FF FF FF FF FF FF FF
00000060  FF FF FF FF FF FF FF FF FF FF FF FF FF FF FF FF
00000070  FF FF FF FF FF FF FF FF FF FF FF FF FF FF FF FF
00000080  FF FF FF FF FF FF FF FF FF FF FF FF FF FF FF FF
00000090  FF FF FF FF FF FF FF FF FF FF FF FF FF FF FF FF
000000A0  FF FF FF FF FF FF FF FF FF FF FF FF FF FF FF FF
000000B0  FF FF FF FF FF FF FF FF FF FF FF 6F 15 AD 7C 9F
000000C0  BF F7 FF CD 5C 9D 71 D7 03 F4 43 47
```

Fig. 8. Layer A TSP output from the RS encoder.

C. Energy Dispersal

In one TS, there are many null packets or bytes with values 0xFF and 0x00 that are used to adjust the bit rate or compliment the number of bytes in a TSP. These packet sequences or bytes are often present at the source coding output and multiplexing.

To disperse these sequences, an interconnected energy dispersal at the RS output is used to reduce interference between symbols generated by the repetitive transmission of the same information.

This dispersal consists of a Pseudo Random Binary Sequence Generator (PRBS) and an adder module 2. The PRBS generator uses the polynomial generator $g(x) = 1 + x^{14} + x^{15}$. This generator consists of 15 shift registers and an adder module 2 that is connected to the output registers 14, 15

doi: 10.18580/setijbe.2015.3 Web Link: http://dx.doi.org/10.18580/setijbe.2015.3

and input register 1 as can be seen in Fig. 9. The sequence length of this generator is $2^{15} - 1 = 32767$, and is synchronized with the IIP and the TS clock of each layer. The disperser is initialized by a frame multiplexer with the word "100101010000000" and is disabled by a TSP synchronizing byte.

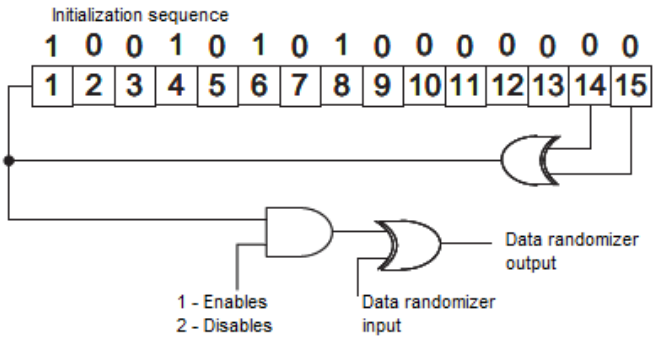

Fig. 9. Energy dispersal circuit.

Fig. 10 shows the TSP of Fig. 8 at the energy disperser output. It can be seen that the repetitive sequence of ones (0xFF) are dispersed.

```
00000000  02 F7 28 83 20 B1 56 44 45 68 4C 8C 4C D6 55 0
00000010  01 C3 FB 77 E4 CF A5 5E 20 3B 3F 65 7C A0 F4 3
00000020  C7 73 6C D4 95 04 81 E4 FB A5 E6 23 AB 36 05 4
00000030  E0 47 BE 6E 7A 9A E0 A1 BC 3A 77 62 CC B1 54 5
00000040  06 2F EB 1F 85 BE E2 79 B2 EA 51 82 1A F3 A1 D
00000050  3B 0B 65 C4 A3 64 34 A7 44 2C 67 16 AD 88 12 C
00000060  91 5E 98 38 AF 6C 1C 97 B4 8E 44 DA 65 22 A1 3
00000070  39 5F 68 3C 8F 74 DC C5 35 61 40 B8 7C 6E F6 9
00000080  C8 AB 4C 04 57 E6 0F AB DE 07 3B ED 67 90 AE 9
00000090  18 B7 AC 4E 16 5B 8A 26 C3 29 75 08 C1 CD 7B 5
000000A0  E4 1D A7 B2 2E 53 1A 15 A3 82 36 F3 49 D4 4B 0
000000B0  45 EA 63 82 B6 F0 49 DE 4B 3A 45 F2 8A E0 3F 3
000000C0  36 16 CB 8B E5 0A E4 A6 7C D3 41 47
```

Fig. 10. Layer A TSP at the energy disperser output

D. Byte interleaver

Interleavers are used in a wide variety of communication methods. An interleaver is a device that receives an alphabet of symbols and produces identical output symbols in a different order without increasing the bit rate. The interleaver disperses the bit sequences in order to minimize the block error effect in the middle of a data stream [9], [10].

These block errors are created from the impulsive noise of some equipment and selective fading in the communication channel. The error-correcting codes cannot correct errors that are concentrated in a sequence. Using interleavers, the sequence of symbols to be transmitted is scrambled and at the time that an accumulation of errors in the communication channel occurs, the decoder unscrambles the sequence spreading the errors. At that point, the error correcting codes can detect and correct errors.

The byte interleaver is a convolutional interleaver that uses time multiplexing and shift registers [11]. Each input multiplexer has a set of shift registers. The registers delay the bit sequence and then these bits are grouped again. In Fig. 11, it is possible to see how this interleaver is built. It has 12 branches *(B)* and 17-byte shift registers *(M)*. The *B* branches are cyclically connected to the energy disperser output and transfer 1 byte at a time via each branch. The first branch *(B_i=0)* has no memory, and the symbols are immediately transferred to the output. The byte interleaver aims to spread the packets from the Reed Solomon and the energy disperser to increase their efficiency before block errors occur.

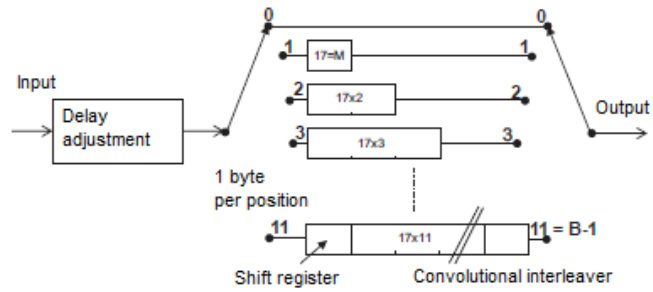

Fig. 11. Byte interleaver.

The maximum delay by the interleaver branch can be calculated by (6).

$$N = (B - 1) \times M \tag{6}$$

The delay generated by the convolutional interleaver can be calculated by (7) in which the equivalent of 2244 bytes is represented by 11 TSP consisting of 204 bytes each.

$$D = N \times B \tag{7}$$

However, to keep all blocks synchronized with the frame multiplexer, a delay adjustment is inserted to supplement the number of TSP in a multiplexer frame. It is possible to calculate the number of TSP used in a multiplexer frame with the use of (8). This way, the synchronization delay value can be calculated using (9), where N_s is the number of segments, N_c is the number of data carriers, b_{QAM} is the number of bits per symbol in the primary modulation and R_{cc} is the rate of the convolutional encoder.

$$N_{TSP} = \frac{N_s \times N_c \times b_{QAM} \times R_{cc}}{8} \tag{8}$$

$$D_{ajuste} = N_{TSP} - D \tag{9}$$

Fig. 12 shows the packet in Fig. 10 at the byte interleaver output after 48 packets.

```
00000000  E5 23 85 76 78 3C A7 FC 6C 0D D0 8C 78 AD B2 E
00000010  1C 7A 76 C9 31 B3 1C 5E 5E 4C FC AF D0 8B F1 8
00000020  58 96 C8 D4 63 05 A3 87 E8 5A C0 6D 1E B3 76 4
00000030  7F 63 24 FC 70 05 1C 4D 83 79 2C 62 E9 D9 9E 3
00000040  1B 24 0E 1E E8 ED E7 79 B7 FF 41 39 FB 45 4A E
00000050  39 0B 80 C4 9C 6F B9 17 AF A9 36 98 7F B6 F5 C
00000060  31 3E 6C A0 66 6E 03 E9 94 6C 56 DA 60 21 7D 5
00000070  62 FF 93 DE 29 3A F5 C5 B9 D2 65 99 F6 B8 B3 B
00000080  48 11 14 04 6C AA AD 92 8D D6 FA 6A 50 C8 D4 9
00000090  C2 CC C4 94 E6 BD AD 79 C1 6D CD 08 A3 3F C4 3
000000A0  44 B4 06 D6 F1 B4 B5 15 38 6D 5A 08 39 23 D6 B
000000B0  26 78 D1 82 64 AA BC BB 94 AF 0C 36 CA 9C D1 3
000000C0  66 51 95 16 91 D1 CD 1B 12 E7 3C 47
```

Fig. 12. TSP output from the byte interleaver.

E. Convolutional Encoder

The convolutional codes were introduced by Elias in 1955 as an alternative to the use of block codes [12]. The substantial difference between block codes and convolutional codes lies

doi: 10.18580/setijbe.2015.3 Web Link: http://dx.doi.org/10.18580/setijbe.2015.3

in the fact that convolutional codes make use of memories, thus a given output at a certain time depends on not only some inputs at that very time, but also a time in the past *m*, where *m* is the number of memories [8]. A convolutional encoder (*n*, *k*, *m*) with *k* inputs, *n* outputs, and *m* memories may be implemented as a combinatorial sequential circuit which makes use of registers comprised of flip-flops, adder module 2 (or exclusive), and multiplexers/re-multiplexers. The rate of the convolutional encoder *R=k/n* depends on the input *k* and the output *n*. Fig. 13 shows the combinational circuit used by ISDB-T_B [1], [2].

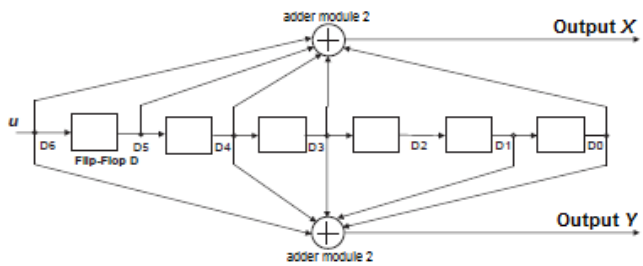

Fig. 13. Convolutional encoder (2,1,6) rate ½.

This convolutional code has mother rate R = 1/2, 64 states and its impulse response is expressed in (10).

$$g^{(0)} = 171_{oct}(1\,1\,1\,1\,0\,0\,1)$$
$$g^{(1)} = 133_{oct}(1\,0\,1\,1\,0\,1\,1) \quad (10)$$

Considering the input message u, X and Y outputs can be obtained using (11), where $\otimes$ represents the discrete convolution.

$$X = u \otimes g^{(0)}$$
$$Y = u \otimes g^{(1)} \quad (11)$$

Additionally, puncturing is used to discard some of the bits at the convolutional encoder output. This technique allows the bit rate to be varied, and the puncturing pattern can be seen in Table III. The P field indicates the bits that must be discarded and are represented by 0. The minimum free distance (dfree) of this convolutional code [13] is used as a performance parameter. In (12) it is possible to calculate the asymptotic gain of this code using a Viterbi decoder hard decision in relation to the uncoded modulation [14].

TABLE III
CONVOLUTIONAL ENCODER PUNCHING VALUES

Code rate (R)									
1/2		**2/3**		**3/4**		**5/6**		**7/8**	
P	**d_{free}**	**P**	**d_{free}**	**P**	**d_{free}**	**P**	**d_{free}**	**P**	**d_{free}**
X=1 Y=1	10	X=10 Y=11	6	X=101 Y=110	5	X=10101 Y=11010	4	X=1000101 Y=1111010	3

$$\delta = 10log_{10}\left(\frac{R \times d_{free}}{2}\right) \quad (12)$$

The bit interleaving is completed by a serial/parallel converter with variable size according to the modulation method. Thus, the input bits are converted from serial to parallel in dibit (2 bits), quadbit (four bits) or sixbit (6 bits) for the QPSK, 16-QAM, and 64-QAM modulations, respectively. The number of branches *B* of the interleaver is equal to the number of bits in each modulation method, and each branch has a specific delay. Because of these features, this interleaver is classified as a multiplexed convolutional interleaver [15]. The maximum branch delay is calculated using (13) and the total delay using (7).

$$N = \frac{120}{B-1} \quad (13)$$

TABLE IV
BIT INTERLEAVER DELAY ADJUSTMENT VALUE

Modulation	Mode 1(2k)	Mode 2 (4k)	Mode 3 (8k)
QPSK	$384 \times N_s - 240$	$768 \times N_s - 240$	$1536 \times N_s - 240$
16QAM	$768 \times N_s - 480$	$1536 \times N_s - 480$	$3072 \times N_s - 480$
64QAM	$1152 \times N_s - 720$	$2304 \times N_s - 720$	$4608 \times N_s - 720$

To maintain the synchronism with the multiplexer frame, an additional delay is inserted, and its value can be obtained in Table IV where N_s represents the number of segments. Fig. 14 shows the bit interleaver diagram used in the 64-QAM modulation.

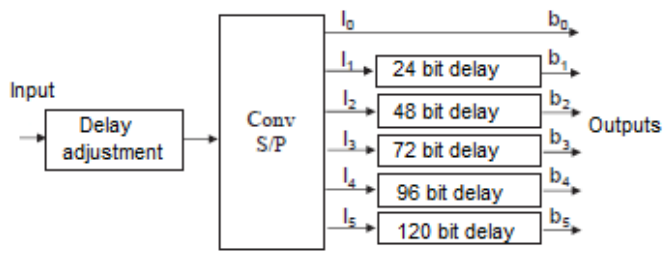

Fig. 14. Diagram of the bit interelaver used in the 64-QAM modulation.

IV. MODULATION

The ISDB-T_B modulation stage can be seen in Fig. 15 and will be detailed in the following subsections.

A. Layer Combiner

The set of bits entering the layer combiner are grouped, and in this article are called symbols. It may be noted that our proposal is different from [1] and [2] and aims to reduce memory usage. Thus, the layer combiner performs the concatenation of the data symbols in all segments. For example, Mode 3 has 384 data carriers in each segment, this block groups all the segments amounting to 4992 symbols (carriers). Table V shows the distribution of the pilots in the three ISDB-T_B modes.

doi: 10.18580/setijbe.2015.3 Web Link: http://dx.doi.org/10.18580/setijbe.2015.3

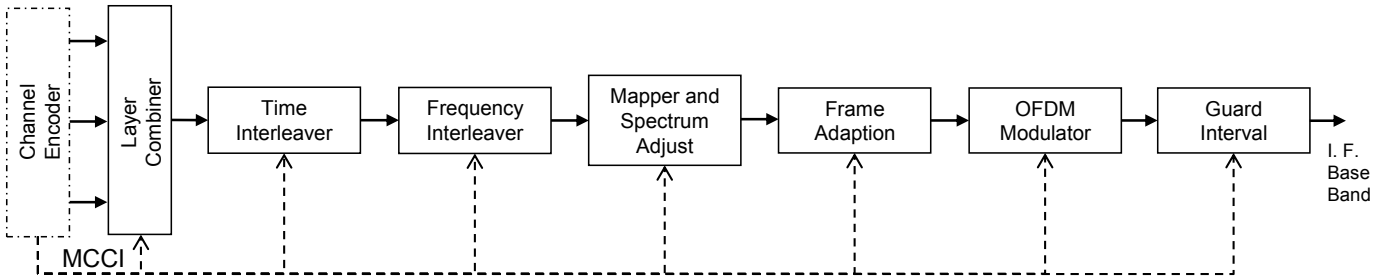

Fig. 15. Diagram of the modulation stage.

TABLE V
NUMBER OF CARRIERS USED IN THE COHERENT MODULATION

Carrier	Mode 1 (2k)	Mode 2 (4k)	Mode 3 (8k)
Total	108	216	432
Data (Nc)	96	192	384
SP	9	18	36
CP	0	0	0
TMCC	1	2	4
AC1	2	4	8
AC2	0	0	0

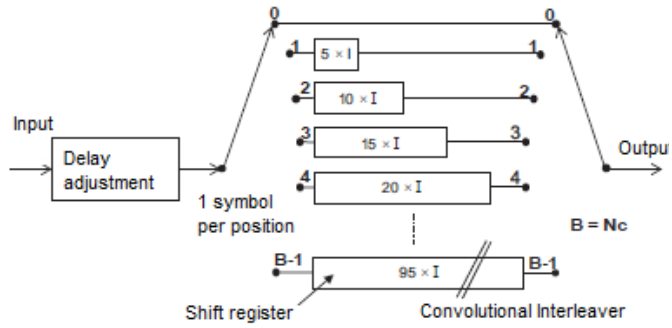

Fig. 16. Time interleaver.

B. *Time Interleaver*

After the layer combiner, the signal is interlaced. The time interleaver is formed by a convolutional interleaver that aims to interlace the carriers within various OFDM symbols. The time interleaver acts separately on each OFDM data segment and is cyclically combined at the output. The interleaving size can be adjusted by varying parameter *I*. In (14) it is possible to calculate the delay for each branch of the time interleaver, where *i* represents the number of each branch $i = 0, 1, 2, \ldots B - 1$ and mod is a function that returns the remainder of the division. The number of branches *B* of the time interleaver is equal to the number of data carriers.

$$D_i = mod(54 \times i, 96) \times 1 \quad (14)$$

Table VI indicates the maximum time interleaver delay and the delay adjustment that is required to synchronize symbols within an OFDM frame. Fig. 16 shows a diagram of the interleaver and in Fig. 17 a scatter plot of the time intereaver of a segment in Mode 3. The time interleaver spreads the symbols from the modulation in each layer in which the length can be chosen, for the approximate values 0, 100, 200 and 400ms. The time interleaver increases the robustness of the system against impulsive noise and improves performance of mobile reception [16].

TABLE VI
TIME INTERLEAVER PARAMETERS IN MODE 3 (8K)

I	Maximum delay (symbols)	Delay adjustment (symbols)
0	0	0
1	95	109
2	190	14
4	380	28

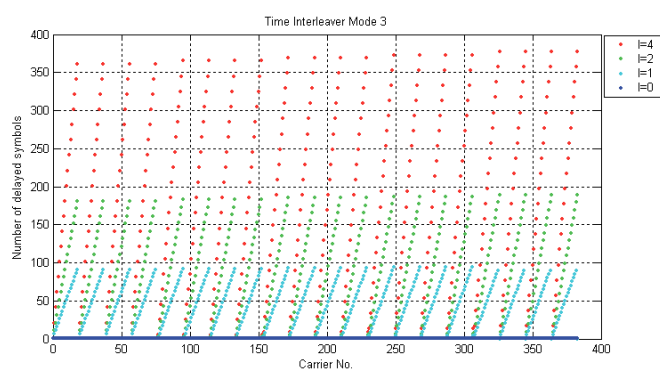

Fig. 17. Time interleaver scatter plot.

C. *Frequency Interleaver*

The frequency interleaver can be considered a block interleaver. In this interleaver symbols are written in a memory and read in a certain order. The frequency interleaver is performed in one OFDM symbol and is divided into three parts, as can be seen in Fig. 18.

doi: 10.18580/setijbe.2015.3 Web Link: http://dx.doi.org/10.18580/setijbe.2015.3

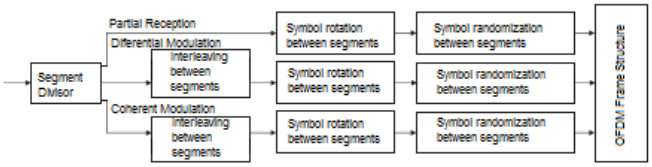

Fig. 18. Diagram of frequency interleaving.

The first type of interleaving performs carrier interleaving between the segments. If the partial reception option is enabled, the zero data segment is not scrambled. Fig. 19 shows the scatter plot of the interleaver used in the configuration shown in Fig. 5. It can be seen that symbols in the first segment enter and leave in the same order.

In Fig. 20, the carrier rotation within each segment can be seen. In Fig. 21, the carrier dispersion pattern within each segment can be seen. In [1] and [2] it is possible to obtain the tables and parameters of these interleavers. The final result, of frequency interleaving, can be seen in Fig. 22. Frequency interleaving is applied to the OFDM symbol that increases the system robustness against selective frequency fading [16]. Both the time interleaver and the frequency interleaver increase the error correction stage efficiency.

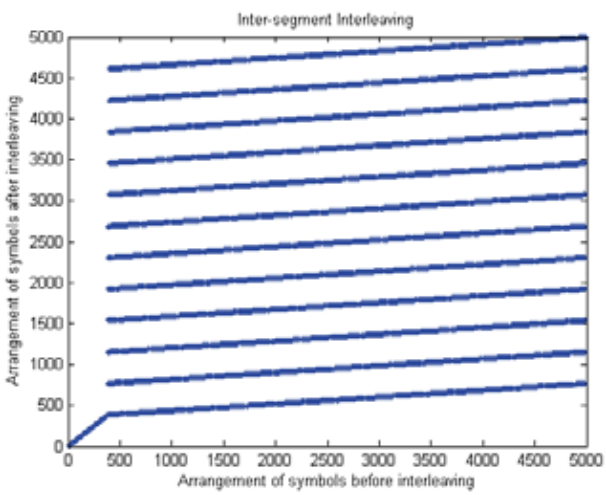

Fig. 19. Carrier dispersion interleaving between segments.

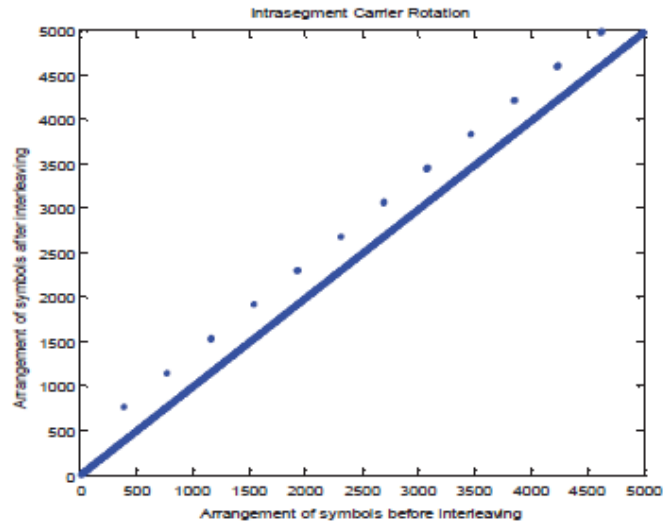

Fig. 20. Carrier rotation dispersion within each segment.

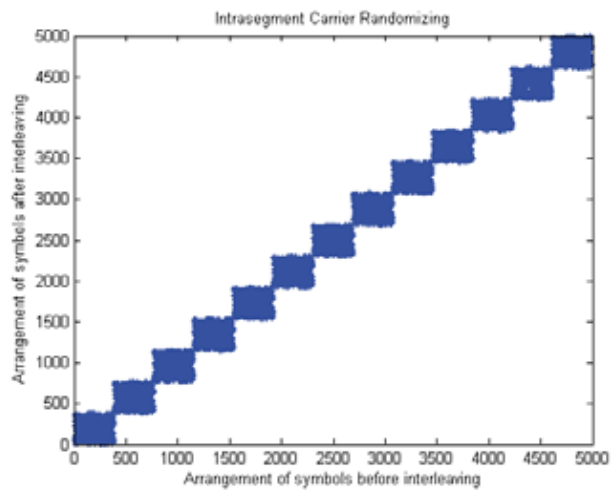

Fig. 21. Random interleaving dispersion between the segments.

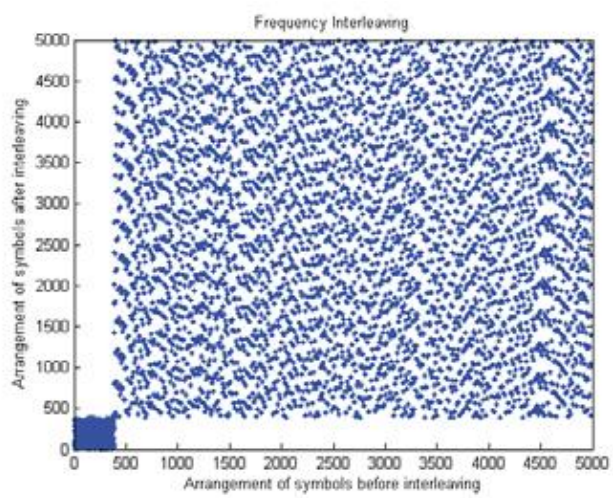

Fig. 22. Resulting dispersion from frequency interleaving.

D. Mapper and Spectrum Adjustment

After frequency interleaving, these symbols are modulated in QPSK, 16-QAM or 64-QAM through the use of a table.

doi: 10.18580/setijbe.2015.3 Web Link: http://dx.doi.org/10.18580/setijbe.2015.3

Table VII shows the bit values, and the symbols for the QPSK modulation standardized to the power of 1 Watt. The tables for modulations 16-QAM and 64-QAM can be extracted from [1], [2].

TABLE VII
QPSK MODULATION VALUES

bit[1], bit[0]	In-phase	Quadrature
0.0	$\sqrt{2}/2$	$\sqrt{2}/2$
0.1	$\sqrt{2}/2$	$-\sqrt{2}/2$
1.0	$-\sqrt{2}/2$	$\sqrt{2}/2$
1.1	$-\sqrt{2}/2$	$-\sqrt{2}/2$

Fig. 23 shows the constellations of the QPSK, 16-QAM, and 64-QAM modulations, respectively.

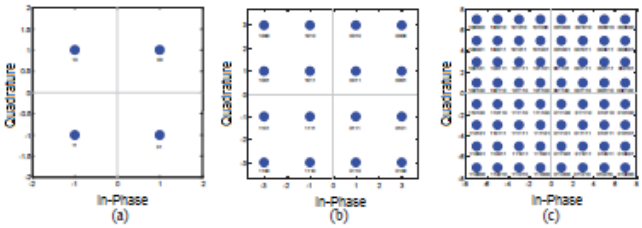

Fig. 23. ISDB-T system constellations: (a) QPSK (b) 16-QAM and (c) 64-QAM.

The spectrum adjustment is required to place the segments in the specific order established in [1] and [2]. Thus, the zero segment is positioned at the center of the spectrum and odd and even segments are distributed according to Fig. 24.

11	9	7	5	3	1	0	2	4	6	8	10	12

Fig. 24. Segment positions utilized after the spectrum adjustment.

E. Frame Adaption

The transmission signal is organized into frames. Each frame has a duration T_F and consists of 204 OFDM symbols. Each OFDM symbol has 13 segments and consists of a number of carriers, in Mode 1 K=1405 carriers (2k), K=2809 carriers in Mode 2 (4K), and K=5617 carriers in Mode 3 (8k) in which all are transmitted with the duration T_S. Fig. 25 shows an OFDM frame for a coherent modulation. Within the OFDM frame, Scattered Pilots (SP) and Continual Pilots (CP) are inserted and modulated in Binary Phase Shift Keying (BPSK) with a 33% power increase to guarantee the estimation and synchronization. The TMCC and Auxiliary Channel (AC) are inserted in the frame and modulated in Differential BPSK (DBPSK) with a 33% power increase for the purpose of signaling the modulation parameters, channel coding, frame synchronization, and transmission of auxiliary data. In total, 157 carriers out of 1405 carriers are used as pilots in Mode 1, 313 carriers out of 2809 carriers are used as pilots in Mode 2, and 625 carriers out of 5617 carriers are used as pilots in the Mode 3. In Fig. 26, the constellation of the frame adaption output can be seen. It can be seen that the SP pilots, TMCC, and AC are modulated in BPSK and possess greater potency than the QPSK and 64-QAM constellations.

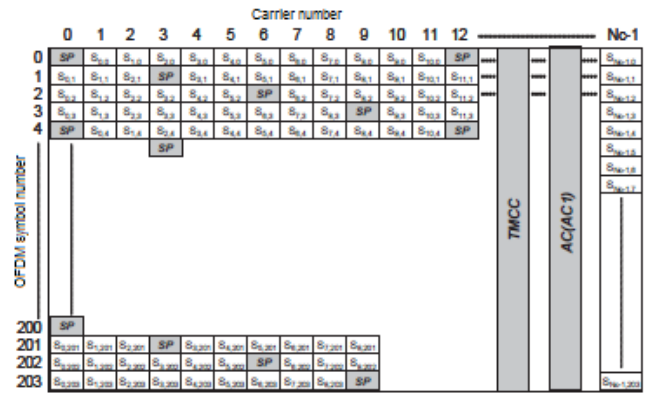

Fig. 25. OFDM frame structure for coherent modulation.

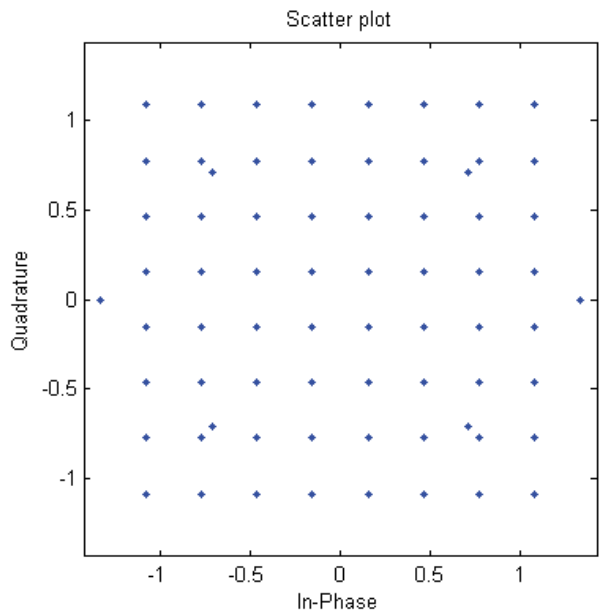

Fig. 26. Frame output adaptation constellation.

F. OFDM Modulation

The OFDM modulation appeared around the 1960s when Chang published his article on transmission synthesis with limited multi-channel bands [17]. He introduced the concept of transmitting messages across limited multiple channel bands without causing Inter-Carrier Interference (ICI) and Inter-Symbol Interference (ISI). In 1971, Weinstein and Ebert [18] used the Discrete Fourier Transform (DFT) to improve the performance of modulation and demodulation.

Due to the computational complexity of DFT and inverse DFT (IDFT), the Fast Fourier Transform algorithm (FFT) and Inverse Fast Fourier Transform (IFFT) discovered by Cooley and Tukey in 1965 [19] are used in modulation and demodulation, respectively. However, zeroes are added to the adapted frame output, to obtain the number of samples necessary to use IFFT and generate the useful part of the OFDM symbol (*Tu*). This technique is called zero padded

[20], and the OFDM modulator block diagram can be seen in Fig. 27, where *Nc* represents the number. The IFFT size can be configured to one of three values, Mode 1 = 2k; Mode 2 = 4k; and Mode 3 = 8k.

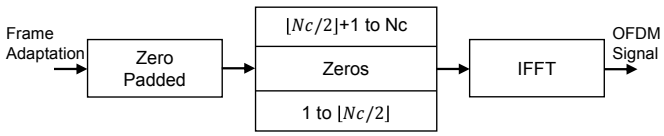

Fig. 27. OFDM modulator diagram.

G. Guard Interval

An important contribution to the OFDM modulation was made by Peled and Ruiz in 1980 [21], which introduced the cyclic prefix or cyclic extension, solving the orthogonality problem. Instead of using an empty guard space, they filled this space with a cyclic extension of the OFDM symbol.

The duration of the guard interval (Δ) is obtained by the duration $T_u \times k$, where k = 1/4; 1/8; 1/16; or 1/32. Thus, an OFDM symbol with duration T_s is composed of a guard interval with the duration Δ and T_u.

Fig. 28 shows an OFDM symbol with guard interval.

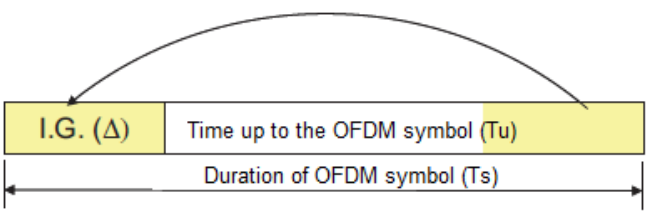

Fig. 28. Representation of the guard interval cyclic prefix.

In the BST-OFDM modulation, the common parameters for all layers are the IFFT size (Mode 1 = 2k, 4k Mode 2, and Mode = 3 = 8k) and the IG reason (1/4, 1/8, 1/16 and 1/32). The useful bandwidth used by ISDB-T is $6/14 \times 13$ corresponding to 5.57MHz.

In Fig. 29 the ISDB-T_B spectrum signal baseband in Matlab can be seen.

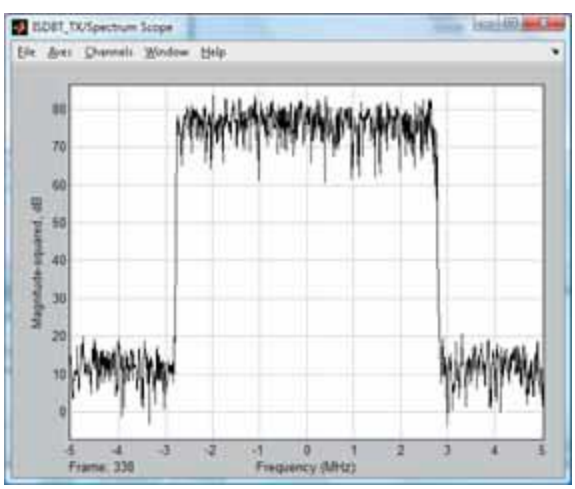

Fig. 29. ISDB-T_B spectrum baseband signal in Matlab.

V. Simulation Software

The simulator test was conducted with an arbitrary waveform generator and spectrum analyzer with an ISDB-T_B signal demodulation option. The RF vector from the simulator was installed in the generator and Bit Error Rate (BER), Modulation Error Rate (MER), and Mask Intermodulation tests were performed. Fig. 30 shows the equipment used in the tests.

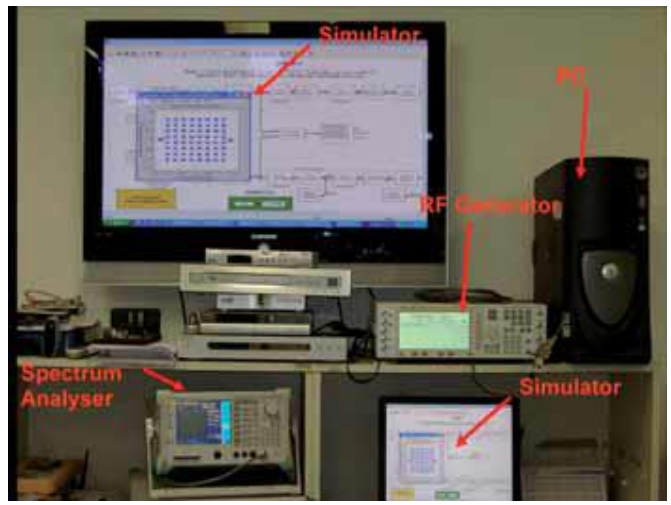

Fig. 30. Digital TV laboratory equipment used in the tests.

In the first test, it was verified that the ISDB-T_B signal generated by the simulator is within the mask transmission. Fig. 31 shows the result of this test.

In the Fig. 32, the measured bit error rate (BER) shows that the error is null before and after the RS in the two hierarchical layers. With this result, it can be concluded that all the stages of channel coding and simulated modulation function correctly. Furthermore, it can be seen that the modulation parameters detected through TMCC are the same as those in Fig. 5.

Figs. 33 and 34 show the MER measurement results. The value of MER is above 30 dB showing that any distortion in the modulation stage was introduced by the simulator.

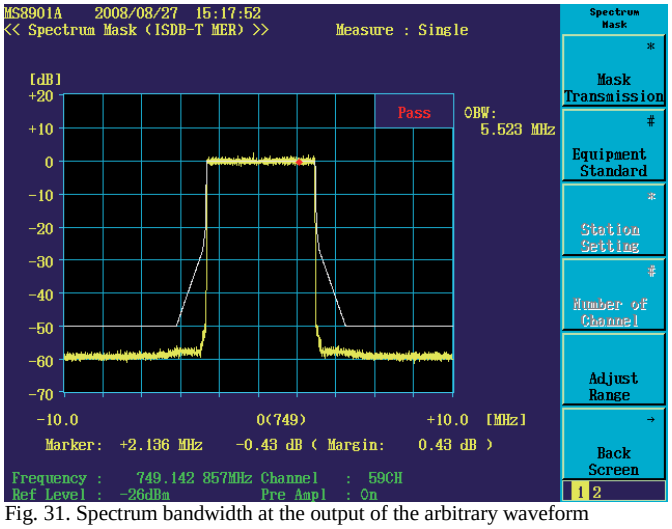

Fig. 31. Spectrum bandwidth at the output of the arbitrary waveform generator.

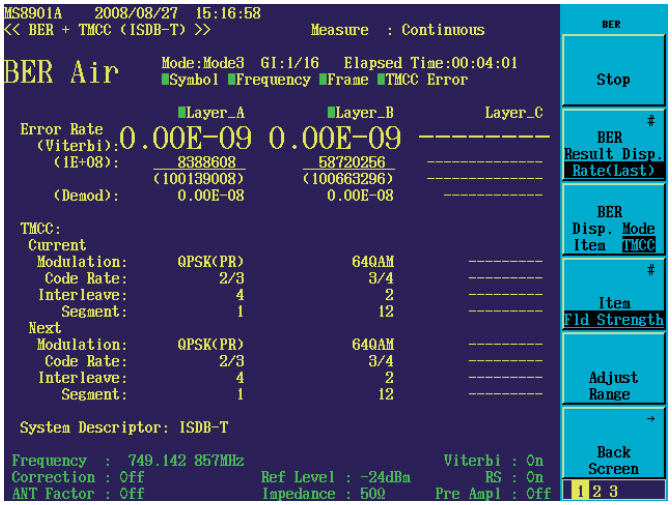

Fig. 32. Measurement of bit error rate before and after RS.

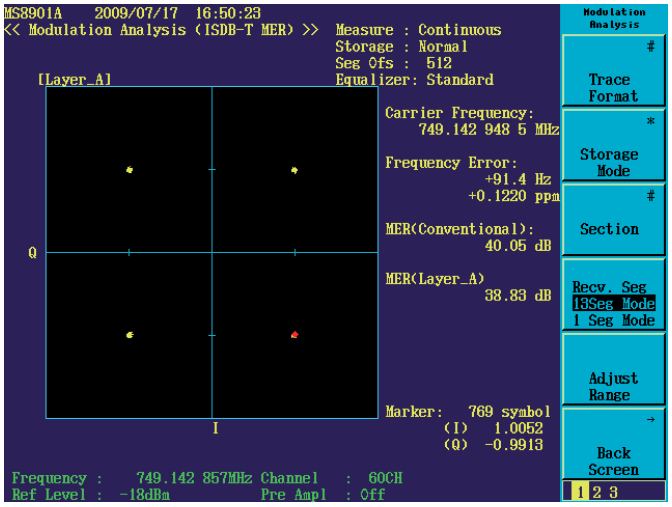

Fig. 33. MER measurements in Layer A.

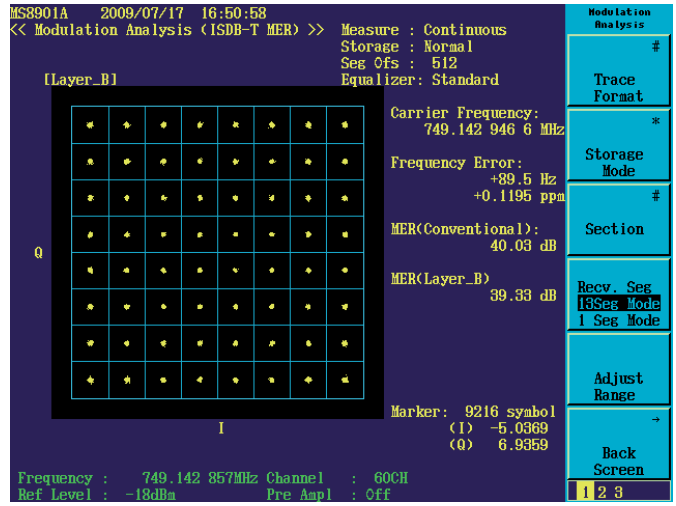

Fig. 34. MER measurements in Layer B.

VI. Conclusion

This paper presented a simulation tool that allows the analysis of all the blocks that make up an ISDB-T_B modulation to be completed. Numerical and graphical results were presented in order to illustrate the operation of an actual modulation system. Practical measures using an arbitrary waveform generator and spectrum analyzer were performed to demonstrate the compatibility of this simulation tool with the ISDB-T_B system.

Acknowledgment

The authors would like to thank RH-TVD CAPES and their colleagues at Mackenzie Digital TV Laboratory.

References

[1] *Transmission System for digital terrestrial broadcasting*, V1.6 E2 STD-B31, 2005.
[2] *Televisão digital terrestre – Sistema de transmissão*, ABNT NBR 15601:2007, 2007.
[3] G. Bedicks *et al.*, "Outlines of the Brazilian Digital Terrestrial Television Broadcasting System," presented at *57th annual IEEE Broadcasting Symposium*, Washington, DC, Oct. 1st–Nov. 2nd, 2007.
[4] *Generic coding of moving pictures and associated audio: Systems*, ISO/IEC 13818-1, Nov. 1994.
[5] C. Akamine *et al.*, "Re-multiplexing ISDB-T BTS into DVB TS for SFN," to be published in *IEEE Trans. Broadcasting* in December 2009.
[6] M. Uehara, "Application of MPEG-2 Systems to Terrestrial ISDB (ISDB-T)," *Proceedings of the IEEE*, vol. 94, no 1, 2006, pp. 261-268.
[7] I. S. Reed and G. Solomon, "Polynomial Codes over Certain Fields," *J. Soc. Ind. Appl. Math.*, vol. 8, pp. 300-304, 1960.
[8] S. LIN, D. Costello Jr, "*Error Control Coding: Fundamental and Applications"* 2nd ed. New York: Prentice Hall, 2004.
[9] SW. K. Andrews, C. Heegard, and D. Kozen, "A theory of interleavers," Department of Computer Science, Techical Report TR97-1634, June 1997.
[10] J. Ramsey, "Realization of optimum interleavers," *Information Theory, IEEE Transactions in*, vol.16, no.3, pp. 338-345, May 1970.
[11] G. D. Forney, "Burst-Correction Codes for the Classic Bursty Channel," *IEEE Transactions Communication. Technology.*, vol. COM-19, pp. 772-781, October 1971.
[12] P. Elias, "Coding for Noise Channels," *IRE Conv. Rec.*, Part 4, pp. 37-47, 1955.
[13] *Digital Video Broadcasting (DVB); Framing structure, channel coding and modulation for 11/12 GHz satellite services*, ETSI EN 300 421, 1997.
[14] S. Haykin, *Communication Systems*, 4th ed., New York: John Wiley & Sons, 2001.

[15] C. Heegard, and W. B. Stephen, *Turbo Coding*, Boston: Kluwer Academic Publishers, 1999.
[16] G. Bedicks *et al.*, "Results of the ISDB-T system tests, as part of digital TV study carried out in Brazil," *IEEE Trans. Broadcasting*, vol. 52, no.1, pp. 38–44, Mar. 2006.
[17] R. W. Chang, "Synthesis of band-limited orthogonal signals for multichannel data transmission," *Bell System Tech. J.*, vol. 45, pp. 1775-1796, Dec. 1966.
[18] S. B. Weinstein, and P. M. Ebert, "Data transmission by frequency division multiplexing using the discrete Fourier transform," *IEEE Trans.Commun*., vol. 5, pp. 628-634, Oct. 1971.
[19] J. Cooley and J. Tukey, "An Algorithm for the Machine Calculation of Complex Fourier Series," *Math. Comput.*, Vol. 10, no. 90, pp.297-301, Apr. 1965.
[20] R. V. Van Nee and R. Prasad, *OFDM for Wireless Multimedia Communications*, Norwood, MA: Artech House, 2000.
[21] A. Peled, and A. Ruiz, "Frequency domain data transmission using reduced computation complexity algorithms," in *Proc. IEEE Int. Conf.*Acoustic., Speech, Signal Processing, Denver, CO, 1980, pp. 964-967.

Cristiano Akamine received his B.Sc. degree in Electrical Engineering from Mackenzie Presbyterian University, São Paulo, Brazil, in 1999. He received his M.Sc. and Ph.D. degree in Electrical Engineering from the State University of Campinas (UNICAMP), São Paulo, Brazil, in 2004 and 2011 respectively. He is a professor of Embedded Systems, Software Defined Radio and Advanced Communication Systems at Mackenzie Presbyterian University. He is a researcher in the Digital TV Research Laboratory at Mackenzie Presbyterian University since 1998, where he has had the opportunity to work with many digital TV systems. His research interests are in system on chip for broadcast TV and Software Defined Radio.

Yuzo Iano graduated and obtained a doctorate at Universidade Estadual de Campinas (Unicamp) where he has acted as a professor since 1973. He is responsible for the Laboratório de Comunicações Visuais de Departamento Comunicações da Faculdade de Engenharia Eléctrica e de Computação de Unicamp (LCV/Decom/FEEC/Unicamp). His research covers telecommunications fields including digital signal processing, audio, video, and images.

Cite this article:
Akamine, C. and Iano, Y. ; 2015. Simulation Software for the ISDB-TB Modulation System. SET INTERNATIONAL JOURNAL OF BROADCAST ENGINEERING. ISSN Print: 2446-9246 ISSN Online: 2446-9432. doi: 10.18580/setijbe.2015.3 Web Link: http://dx.doi.org/10.18580/setijbe.2015.3

IP Transmission over ISDB-T_B

Gustavo de Melo Valeira, Cristiano Akamine, Edson Lemos Horta, Fujio Yamada, and Rodrigo Eiji Motoyama

***Abstract*—This paper presents a new application of the Integrated Services Digital Broadcasting - Terrestrial version B (ISDB-T_B) digital television system to transmit data in the Internet Protocol (IP) format encapsulated in the MPEG-2 Transport Stream (MPEG-2 TS). The use of this encapsulation technique ensures compatibility of the ISDB-T_B multiplexing system, allowing the transmission of IP packets. The proposed application is unidirectional, i.e., there is no return channel and the protocol used in the IP packets is the User Datagram Protocol (UDP).**

***Index Terms*—Digital Television, Integrated Services Digital Broadcasting - Terrestrial version B (ISDB-T_B), User Datagram Protocol (UDP).**

I. Introduction

IN Brazil, the digital terrestrial television system used is a modified version of the Japanese system called Integrated Services Digital Broadcasting - Terrestrial (ISDB-T). This version is called ISDB-T_B, and the main differences are, video (MPEG-4 part 10 or H.264) [1], audio (MPEG-4 HEAAC) [2], middleware (Ginga based on Java or NCL) [3], and the use of high VHF and UHF bands [4].

The ISDB-T_B system can offer reliability for both high-quality transmission of image and sound in fixed receivers, and in mobile receivers. Due to its flexibility, it is also possible to transmit multimedia content [5].

The transmission of data or multimedia content may be performed in one hierarchical layer or multiplexed with other services, such as audio, video, etc.

There are other systems that transmit data in IP, such as Digital Video Broadcasting - Handheld (DVB-H) and Internet Protocol Television (IPTV). DVB-H is a terrestrial standard that uses the IP protocol for applications in portable receivers [6]. IPTV is based on the current IP network, i.e. using the broadband connection for transmitting digital television services [7].

This article proposes data transmission using User Datagram Protocol/Internet Protocol (UDP/IP) format encapsulated in an MPEG-2 Transport Stream for the ISDB-T_B digital TV system. This encapsulation ensures compatibility with the transmission system and with the IP receiver. The transmission of IP packets can be used in digital terrestrial television for streaming and downloading various types of services, for example, audio/video in different encoding formats, music, web pages, free games, and applications directly to a computer. To maintain convergence between these different forms of media, one ISDB-T_B Full-segment demodulator with IP output is in development. This receiver will receive the ISDB-T_B signal and decapsulate the MPEG2-TS, distributing the output signal in UDP/IP format. The output is connected to a computer, and the computer receives data in UDP. In Section II, a quick review of the ISDB-T_B system is made. Some services that use the IP protocol are discussed in Section III. Details of the protocols to be used in ISDB-T_B are shown in Section IV. Finally, in Section V, the conclusions are presented.

II. ISDB-T_B System

The ISDB-T_B digital television system is flexible, allowing the use of different services on a single television channel with a bandwidth of 6 MHz. The modulation used is Band Segmented Transmission - Orthogonal Frequency Division Multiplexing (BST-OFDM), where the channel is divided into thirteen segments of 6000/14 = 428.6 kHz each. These segments are distributed in up to three hierarchical layers called Layers A, B, and C. The layers may have different robustness, allowing different services (mobile, fixed and/or portable) on the same channel. The useful bandwidth used by ISDB-T_B is 6/14 * 13/14 = 5.57 MHz of the 6 MHz available. For this reason it can be said that the 6 MHz channel is divided into fourteen parts, thirteen of which are used [4] [8].

The parameters in common with the BST-OFDM system is the size of the Inverse Fast Fourier Transform (IFFT) (Mode 1, 2 or 3), and the guard interval (1/32, 1/16, 1/8 and 1/4). The convolutional encoder rate (1/2, 2/3, 3/4, 5/6 and 7/8), the time interleaver length, and the modulation are specific to each layer, changing the robustness and bit rate between layers [4]. There is also the 1seg service, a layer that occupies one segment and is used to transmit the low definition video to portable receivers.

The ISDB-T_B system can be separated into the following blocks: source encoder, multiplexer/re-multiplexer, and modulator as in Fig. 1 [4] [8].

Gustavo de Melo Valeira is a researcher at Mackenzie Presbyterian University, São Paulo, Brazil (e-mail: gustavo.valeira@mackenzie.br).

Cristiano Akamine is a professor at Mackenzie Presbyterian University, São Paulo, Brazil (e-mail: cristiano.akamine@mackenzie.br).

Edson Lemos Horta is a researcher at Mackenzie Presbyterian University, São Paulo, Brazil (e-mail: gustavo.valeira@mackenzie.br).

Fujio Yamada is a researcher at Mackenzie Presbyterian University, São Paulo, Brazil (e-mail: fujio.yamada@mackenzie.br).

Rodrigo Eiji Motoyama is an engineer at SKY, São Paulo, Brazil (e-mail: rodgsp@gmail.com).

doi: 10.18580/setijbe.2015.4 Web Link: http://dx.doi.org/10.18580/setijbe.2015.4

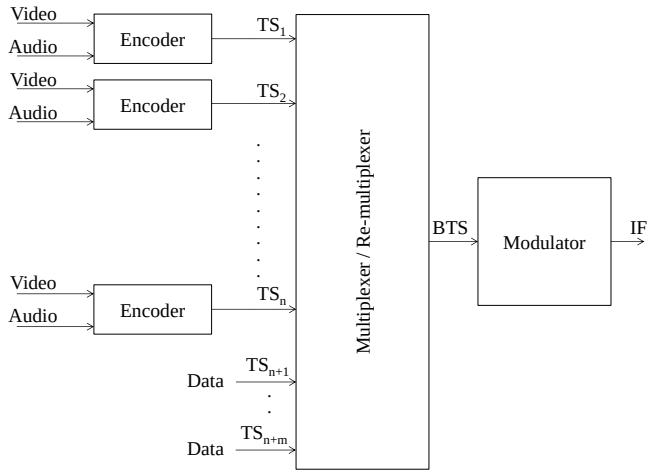

Fig. 1. Block diagram of ISDB- T_B

A. Source Encoder

Studio audio/video signals must be encoded in H.264 video standard [1] and audio MPEG4 HE-AAC v1 or MPEG4 AAC-LC for High Definition Television (HDTV) or Standard Definition Television (SDTV) and MPEG4 HE-AAC v2 for 1seg [2]. The MPEG-2 Transport Stream (MPEG2-TS) [9] is used at the output of encoders to maintain compatibility with the multiplexer/re-multiplexer, which uses the serial interface called Asynchronous Serial Interface (ASI) for transmitting MPEG2-TS. The TS packet size is 188 bytes, and its structure is shown in Fig. 2 [9] [10] [11].

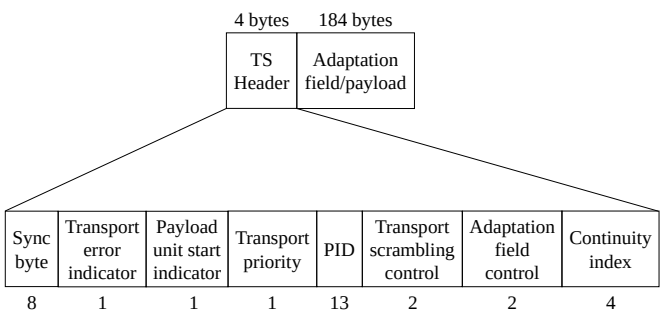

Fig. 2. TS packet structure, indicating the size in bits of each field

The most important header fields are Sync Byte and Program Identification (PID). Sync byte has a fixed value $(47)_h$ and indicates the beginning of the TS packet. The PID identifies the program that is inside the packet, such as audio, video, and closed caption, etc. This parameter is important for the re-multiplexer to correctly filter the PID for audio and video, Program Clock Reference (PCR), and data from each encoder.

B. Multiplexer / re-multiplexer

All TS data encoders and data carousels are re-multiplexed, resulting in an output of 204-byte TS packets. This output signal is called the Broadcast Transport Stream (BTS) because its bit rate is constant and equal to four times the sampling frequency of the IFFT modulator. The bit rate is then equal to 4 × 512/63 = 32.507937 Mb/s [12].

The final sixteen bytes of the BTS, i.e., the dummy byte, has a counter and a packet layer identifier [13], and can optionally have a Reed Solomon block code (RS) shortened to (204,196,4) with a correction capacity of up to 4 bytes in a TS packet.

The BTS packet sequence of each layer depends on the guard interval, the convolutional encoder rate, the number of segments, and the modulation of each layer. This sequence, termed multiplex frame is repeated at equal intervals that only depend on the guard interval and mode, as can be seen in Table I [4]. Besides the packets of each layer, there are null packets that are generated by the multiplexer, which do not correspond to any hierarchical layer and serve to maintain the constant bit rate 32.507937 Mb/s regardless of the input. Identified in the final 16 bytes of the BTS, the corresponding hierarchical layer of each packet coming from the encoders are configured in ISDB-T_B multiplexer so that the modulator can transmit that packet in the layer correctly.

TABLE I
NUMBER OF PACKETS IN A MULTIPLEX FRAME

Mode	Guard Interval			
	1/4	1/8	1/16	1/32
1 (2k)	1280	1152	1088	1056
2 (4k)	2560	2304	2176	2112
3 (8k)	5120	4608	4352	4224

Because there can be up to three hierarchical layers with different modulation parameters and convolutional encoder rate, the bit rate must be calculated for each of them. With that, the encoder bit rate can be properly configured to not exceed the limit of each layer. It is also worth noting that if data is transmitted, the encoder bit rate should be adjusted so that the sum of these two rates do not exceed the maximum allowed. Equation (1) shows the calculation of segment bit rate [4].

$$bit\ rate = \frac{N_s \times N_c \times M_d \times R_{cc} \times R_{RS}}{T_u \times (IG+1)} \quad (1)$$

The useful time T_u of the OFDM symbol, the number of useful carriers N_c and the Reed Solomon encoder ratio R_{Rs} are calculated by Equations (2), (3) and (4), respectively [4].

$$T_u = \frac{2^{mode-1} \times 63}{250} \quad (2)$$

$$N_c = 2^{mode-1} \times 96 \quad (3)$$

$$R_{RS} = \frac{188}{204} \quad (4)$$

Combining Equations (2), (3), and (4) into (1) results in equation (5), which can be used to calculate the bit rate of each layer or segment.

$$bit\ rate = \frac{N_s \times M_d \times R_{cc} \times 376000}{1071 \times (IG+1)} \quad (5)$$

In Equation (5), the N_s, M_d, and R_{cc}, and GI parameters represent the number of segments, the number of bits per

doi: 10.18580/setijbe.2015.4 Web Link: http://dx.doi.org/10.18580/setijbe.2015.4

symbol, the convolutional encoder rate, and the guard interval, respectively. The number of bits per symbol M_d is 2 for DQPSK or QPSK, 4 for 16QAM, and 6 for 64QAM. As this number increases, the greater the total bit rate, but the distance between these points decreases, decreasing the signal robustness [8].

C. BST-OFDM modulator

The BST-OFDM modulation allows the thirteen segments to be distributed in up to three hierarchical layers with different protection against errors. In Table II the transmission parameters for the Brazilian digital television system can be found [4].

TABLE II
CONFIGURATION PARAMETERS IN ISDB-T_B

Mode	1,2 or 3
Guard Interval	1/4, 1/8, 1/16 or 1/32
Partial reception (1seg)	On or off
Total number of segments	13
Maximum number of layers	3
Layer modulation	DQPSK, QPSK, 16QAM or 64QAM
Layer convolutional encoder rate	1/2, 2/3, 3/4, 5/6 or 7/8
Layer time interleaving	0, 400, 800 or 1600 ms (Mode 1) 0, 200, 400 or 800 ms (Mode 2) 0, 100, 200, 400 ms (Mode 3)

It can have up to three layers and these are identified by the letters A, B, and C. When it is used only one layer, this is designated as A. If there are two layers, the layer that has fewer segments is A and the other is B. In this case, the central segments correspond to layer A and the outer layers correspond to layer B. If three layers are used, the layer designated as A has less or an equal number of segments as layer B, which in turn has a lower or equal number of segments compared to C. It is shown in Figures 3, 4, and 5 [4] [14], the identification of the segments and their respective layers, in the case of one, two, and three layers, respectively. Fig. 4 is used in the 1 + 12 configuration (Layer A with one segment and B with twelve segments) and in Fig. 5, the 1 + 3 + 9 configuration (Layer A with one segment, B with three segments, and C with nine segments).

A configuration widely used in São Paulo has two layers, with Layer A for 1seg service and B for high-definition content. The guard interval is 1/16 in Mode 3, with the following configuration in Layer A: one segment, QPSK modulation, convolutional encoder rate of 2/3, and time interleaving of 400ms. Layer B has twelve segments, 64QAM modulation, convolutional encoder rate of 3/4, and time interleaving of 200ms. It is possible with this configuration to also have multiprogramming in Layer B, up to eight programs in SD (Standard Definition) or two programs in (HD) high definition.

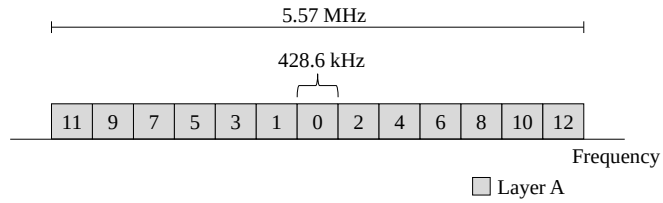

Fig. 3. Segments arrangement in the case of one layer

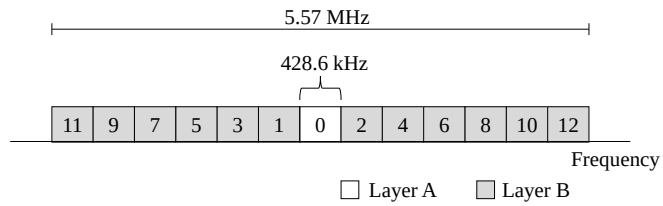

Fig. 4. Segments arrangement in the case of two layers (12 + 1)

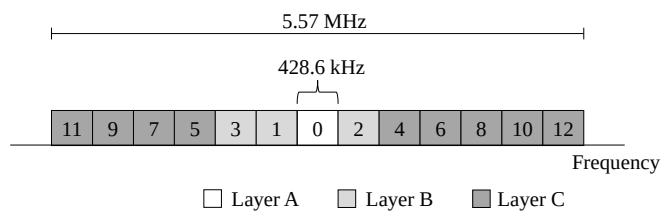

Fig. 5. Segments arrangement in the case of three layers (1 + 3 + 9)

III. IP SERVICES

Some services that use the IP protocol for transmission are Digital Video Broadcasting - Handheld (DVB-H) and Internet Protocol over Television (IPTV).

A. DVB-H

DVB-H is a terrestrial system with an application for portable receivers and it is based and compatible with Digital Video Broadcasting - Terrestrial (DVB-T), which is used for fixed receivers. DVB-H was created because the DVB-T system had problems due to the mobility of portable receivers receiving the signal [15] [8]. In this system is transmitted IP datagrams within the Multi-Protocol Encapsulation (MPE) sections with or without the option of using Forward Error Correction (FEC). Using the MPE-FEC resulted in a signal more robust [15]. To reduce energy use in portable receivers, time slicing was developed. This technique consists of transmitting only one service at a time with a high bit rate, i.e. each service is transmitted sequentially at different times. There is an energy saving because the receiver does not need to receive the data all the time. However, to know when data is desired, there is Transmission Parameter Signaling (TPS) that tells the receiver if time slicing and MPE-FEC are being used [8].

B. IPTV

IPTV is a system used to transmit digital television services to broadband users, through the IP communication network, i.e. it not uses radio frequency directly. Thus, the content is encoded in the desired video and audio standard to be multiplexed in IP [16]. IPTV is responsible for transmitting videos generated for one or more terminals (users) and

doi: 10.18580/setijbe.2015.4 Web Link: http://dx.doi.org/10.18580/setijbe.2015.4

depending on the programming, this service can be VOD (video on demand) or broadcast [17]. In the first case, the content transmitted by IP has just one destination point, i.e. unicast mode. In broadcast, the mode used is multicast because there are several users who can access this content at the same time. Thus, there is an IP network bandwidth saving by transmitting single content to multiple users.

IV. PROPOSAL

The purpose of this work is to transmit data encapsulated in UDP/IP through the ISDB-T_B system. Fig. 6 shows how the encapsulations are arranged. Within MPEG2-TS, Multi-Protocol Encapsulation (MPE) is used to transmit data in IP/UDP format. Fig. 7 shows the bit structure of the MPE [18]. It can be seen that the MPE is within the MPEG2-TS payload, and, for this reason, a multi-protocol encapsulation packet occupies multiple TS packets.

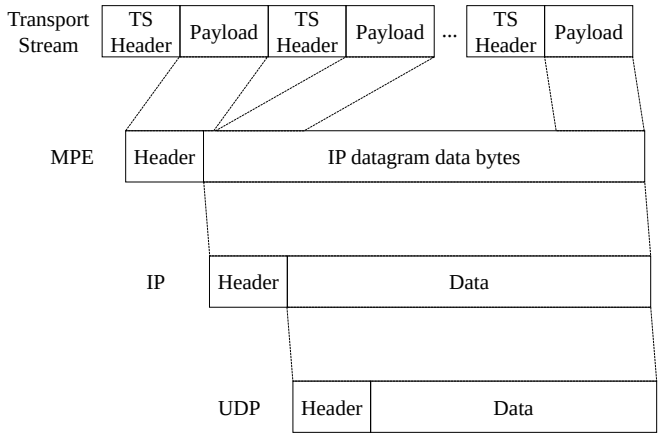

Fig. 6. Encapsulations

An important MPE field is the section length because, with an indication of the section size, it is possible to identify IP/UDP bytes. As for the fields payload scrambling control and address scrambling control, they allow to identify the absence or presence of a private shuffling method of useful information and Media Access Control (MAC) address, respectively [18].

Within each MPE datagram, there is an IP/UDP packet. This protocol contains source and destination address and IP port information. It is desired that the destination IP address is multicast, i.e., to multiple receivers. Thus, it is transmitted in multicast. The identification field of the IP protocol identifies the protocol used after its header; in this case is UDP and the field value is 17. Fig. 8 shows the data structure of IP [19] and UDP [20] packets.

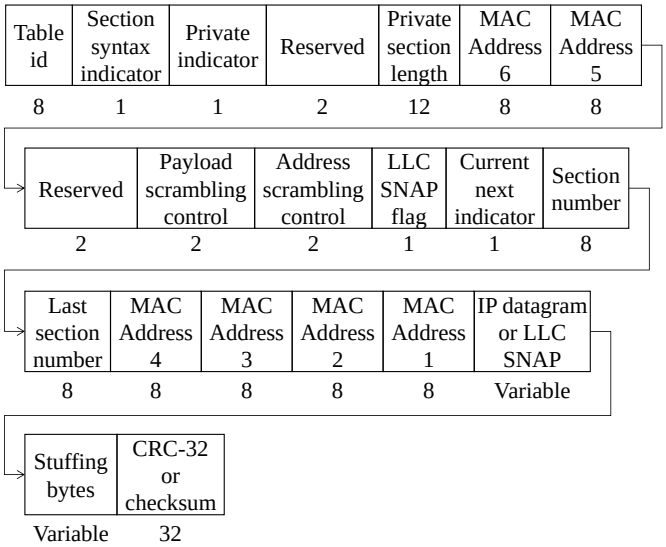

Fig. 7. Structure of Multi-Protocol Encapsulation (MPE), with size indicated in bits

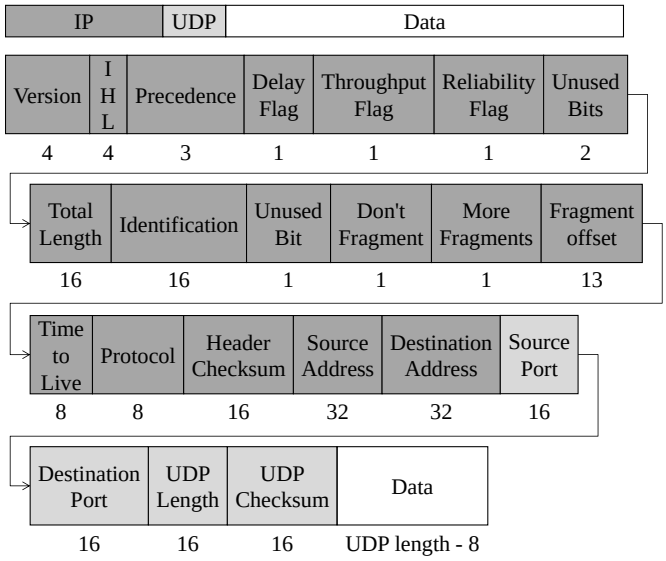

Fig. 8. IP and UDP packet structure, with size in bits. Data sizes in bytes

The block diagram in Fig. 9 shows from IP/UDP data encoding to the computer. Initially files, free games, applications, and audio/video, etc, are encapsulated in the format shown in Fig. 6 and are multiplexed, modulated, and transmitted in the ISDB-T_B standard. The IP receiver demodulates and decapsulates these, and the resulting IP/UDP signal is directed to the Ethernet output connected to the computer. Data received by the computer is processed by a manager, and the updated information is shown on the computer screen. Thus, the IP content transmitted by the ISDB-T_B is available for download or streaming of audio/video. Just updating the computer video codecs allows the computer to decode videos in various patterns, for example, VC-1, Dirac, DIVX, and RMV, etc. transmitted by ISDB-T_B for streaming. The channel exchange is also completed via Ethernet. Fig. 10 shows the IP receiver development board connected to the computer.

doi: 10.18580/setijbe.2015.4 Web Link: http://dx.doi.org/10.18580/setijbe.2015.4

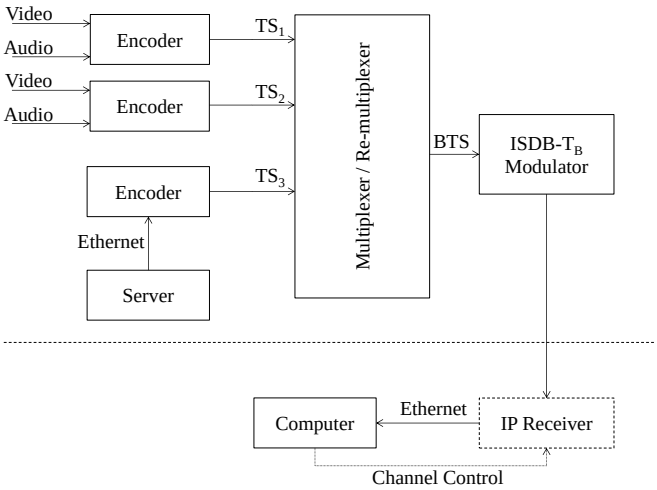

Fig. 9. Block diagram showing the IP transmission of ISDB- T_B

Fig. 10: IP receptor connected to a computer

V. Conclusion

In this study, it was proposed to transmit IP/UDP data over ISDB-T_B, allowing a high bit rate compared with the speed of the Internet currently offered. Informative content can be transmitted through streaming audio/video and files; applications, and free games can be loaded and ran by a computer, only requiring an update in the computer to open certain file types or video.

The useful bit rate when transmitting data in IP/UDP decreases due to the size of the MPE and IP/UDP headers. Using just one hierarchical layer in the most common configuration, the maximum bit rate achieved was approximately 18.6 Mb/s.

This same proposal could be used for an IP USB Full Seg receiver, with the only difference being, that the receiver itself would have an IP output through USB.

Acknowledgment

The authors would like to thank RH-TVD CAPES and friends at the Digital Television Research Center at Mackenzie Presbyterian University.

References

[1] *Televisão digital terrestre – Codificação de vídeo, áudio e multiplexação Parte 1: Codificação de vídeo*, ABNT NBR 15602-1:2007, Abr. 2007.
[2] *Televisão digital terrestre – Codificação de vídeo, áudio e multiplexação Parte 2: Codificação de áudio*, ABNT NBR 15602-2:2007, Abr. 2007.
[3] *Televisão digital terrestre – Codificação de dados e especificações de transmissão para radiofusão digital Parte 2: Ginga-NCL para receptores fixos e móveis – Linguagem de aplicação XML para codificação de aplicações*, ABNT NBR 15606-2:2007, Ago. 2008.
[4] *Televisão digital terrestre – Sistema de transmissão*, ABNT NBR 15601:2007, Abr. 2007.
[5] M. Takada; M. Saito, "Transmission System for ISDB-T", *Proceedings of the IEEE*, vol. 94, no 1, pp. 251-256, Jan. 2006.
[6] M. Kornfeld; G. May, "DVB-H and IP Datacast—Broadcast to Handheld Devices," *IEEE Transactions on Broadcasting*, vol. 53, no. 1, pp. 161-170, Mar. 2007.
[7] M. Zahid; M. A. Qadeer; A. Iqbal, "Deployment of IPTV over IMS architecture," *2nd IMSAA*, 10-12 Dec. 2008, pp.1-6.
[8] B. Furht; S. Ahson, editors. *Handbook of Mobile Broadcasting: DVB-H, DMB, ISDB-T, and MediaFLO*. , Boca Raton: Auerbach Publications, 1ª ed., 2008, ch. 1 and 4.
[9] *Generic coding of moving pictures and associated audio: Systems*, ISO/IEC 13818-1, Nov. 1994.
[10] *Televisão digital terrestre – Codificação de vídeo, áudio e multiplexação Parte 3: Sistemas de multiplexação de sinais*, ABNT NBR 15602-3:2007, Abr. 2008.
[11] J. O. Noah, "A rational approach to testing MPEG-2," *IEEE Spectrum*, vol. 34, no. 5, pp. 67-72, May 2007.
[12] C. Akamine; Y. Iano; G. M. Valeira; G. Bedicks, "Re-multiplexing ISDB-T BTS over DVB TS for SFN", to be published.
[13] *Transmission System for digital terrestrial broadcasting*, STD-B31 V1.6 E2, Nov. 2005.
[14] M. Uehara, "Application of MPEG-2 Systems to Terrestrial ISDB (ISDB-T)", *Proceedings of the IEEE*, vol. 94, no 1, pp. 261-268, Jan. 2006.
[15] D. Plets, *et al.*, "Influence of Reception Condition, MPE-FEC Rate and Modulation Scheme on Performance of DVB-H," *IEEE Transactions on Broadcasting*, vol.54, no.3, pp.590-598, Sept. 2008.
[16] I. Há, et al, "Adoption of IPTV under the Convergence of Broadcasting and Telecommunications," in *11th International Conference on Advanced Communication Technology*, Phoenix Park, Feb. 15-18 2009.
[17] J. Maisonneuve, *et al*, "An Overview of IPTV Standards Development," *IEEE Transactions on Broadcasting*, vol. 55, no. 2, pp. 315-328, Jun. 2009.
[18] *Televisão digital terrestre – Codificação de dados e especificações de transmissão para radiodifusão digital Parte 3: Especificação de transmissão de dados*, ABNT NBR 15606-3:2007, Aug. 2008.
[19] J. Postel, "Internet Protocol," RFC 791, Set. 1981.
[20] J. Postel, "User Datagram Protocol," RFC 768, Ago. 1980.

Gustavo de Melo Valeira received his BS in Electrical Engineering from Mackenzie Presbyterian University (São Paulo, Brazil) in 2007. He is currently working on his Master's Degree in Electrical Engineering - Telecommunications at Mackenzie Presbyterian University (São Paulo, Brazil). He is one of the researchers from the Digital TV Laboratory at Mackenzie Presbyterian University, where he had the opportunity to test digital television systems in Brazil (ISDB-T_B) and Japan (ISDB-T).

Cristiano Akamine has a Master's degree in Electrical Engineering from the Universidade Estadual de Campinas (2004) and a degree in Electrical Engineering from Mackenzie Presbyterian University (1999). He is currently a professor and researcher at the Escola de Engenharia at Mackenzie Presbyterian University. He has experience in Electrical Engineering with an emphasis in Telecommunication Systems, mainly in the following areas: Digital TV, ISDB-T_B, and DVB-T systems.

doi: 10.18580/setijbe.2015.4 Web Link: http://dx.doi.org/10.18580/setijbe.2015.4

Edson Lemos Horta holds a degree in Electrical Engineering from the Escola Politécnia da Universidade de São Paulo (1989), a masters degree in electrical engineering from the Escola Politécnia da Universidade de São Paulo (1995) and a PhD in Electrical Engineering from the Escola Politécnia da Universidade de São Paulo (2002), with a one-year internship at Washington University in St Louis (USA), funded by CNPq. He is currently an Assistant Professor at the Pontifica Universidade Católica de São Paulo, an Assistant Professor III at Mackenzie Presbyterian University and a visiting Professor at the Escola Politécnia da Universidade de São Paulo. He is also a member/company consultant at Napali Engenharia S/C LTDA, specializing in hardware design (reconfigurable logic and embedded processors). He has experience in Electrical Engineering with an emphasis in Programmable Logic Devices (FPGAs, CPLDs, etc), working mainly in the following areas: reconfigurable computing, partial reconfiguration, programmable logic devices, logic synthesis.

Fujio Yamada is a Professor at the Escola de Engenharia at Mackenzie Presbyterian University and a researcher at the Digital TV Laboratory. He has participated in several events as a speaker and moderator at conferences and symposiums.

Rodrigo Eiji Motoyama received his BS in Electrical Engineering from Mackenzie Presbyterian University (São Paulo, Brazil) in 2007. He is currently working on his Master's Degree in Electrical Engineering - Telecommunications at Mackenzie Presbyterian University (São Paulo, Brazil). He is one of the researchers in the Digital TV Laboratory at Mackenzie Presbyterian University and works in both field and laboratory tests areas.

Cite this article:
de Melo Valeira, G., Akamine, C. , Lemos Horta, E., Yamada, F., and Motoyama, R.E.; 2015. IP Transmission over ISDB-TB. SET INTERNATIONAL JOURNAL OF BROADCAST ENGINEERING. ISSN Print: 2446-9246 ISSN Online: 2446-9432. doi: 10.18580/setijbe.2015.4 Web Link: http://dx.doi.org/10.18580/setijbe.2015.4

Objective Analysis of HDTV H.264 x MPEG-2 with and Without Packet Loss

Eduardo Santos Bueno, Cristiano Akamine, Renato de Mendonça Maroja, and Gustavo de Melo Valeira

***Abstract*—This article aims to compare video quality between H.264 and MPEG-2 compression methods through an objective analysis. The method used to assess the video in the test is through comparison with the reference video. The tests were conducted using Picture Quality Analysis (PQA) equipment. The PQA has the following methods for an objective evaluation: Picture Quality Rating (PQR) and Differential Mean Opinion Score (DMOS). The PQR and DMOS methods are objective evaluations approaching subjective evaluations.**

By only analyzing the video compression imperfections, i.e., no packet loss, it can be seen that H.264 presents video quality equivalent to MPEG-2 with a transmission rate about two times smaller. However, the study completed for this article relates to video quality with packet loss in the transport layer of the ISDB-T_B transmission system, this shows that H.264 suffers a bigger loss in video quality than MPEG-2 with the same value in relation to signal-to-noise ratio (SNR) in the transmission channel, into the ISDB-T_B receiver. To generate error packets in the transmission, white noise was added between the transmitted and received signal. The test results show that H.264 provides superior video quality when compared to MPEG-2, with no packet loss, but with packet loss, MPEG-2 provides better video quality than H.264.

***Index Terms*—Differential Mean Opinion Score (DMOS), H.264, MPEG-2, Packet loss, Picture Quality Analysis (PQA), Picture Quality Rating (PQR).**

I. Introduction

TERRESTRIAL digital television was first broadcast in Brazil in December 2007 in São Paulo; it is based on the Japanese digital television system Integrated Services Digital Broadcasting - Terrestrial (ISDB-T). The main differences between the systems adopted in both countries are the audio/video encoding, middleware, and channel allocation [1] [2] [3].

The video compression system used by the Brazilian system is the Moving Picture Expert Group (MPEG-4 part 10) known as H.264 and MPEG-2 is another encoding method, which is used in other digital television systems like the Advanced Television System Committee (ATSC), Digital Video Broadcasting (DVB), and ISDB-T.

Recommendation H.264 is a document published by the International Telecommunication Union (ITU) and International Organization for Standardization / International Electrotechnical Commission (ISO/IEC) [4] [5].

The H.264 standard was published in 2003 and is based on the concepts of previous standards, such as MPEG-2 and MPEG-4 part 2, and offers better efficiency in video compression, i.e., better image quality and more flexibility in compression, transmission, and video storage [6]. H.264 can be used in many applications, including video conferencing, television transmission, and data storage. Therefore, it is obtained using a variety of video compression algorithms that compact an image sequence forming a digital video that uses a lower bit transfer rate than the original video.

However, with a constant increase in the information to be transmitted, there is also a need for greater video compression, which can cause minor degradation in the picture, but it is possible to assess this loss in image quality through a subjective or objective evaluation.

The criteria used in a subjective evaluation of image quality must comply with the standards established by ITU-R BT.500-11 [7].

In video compression, the criteria used in an objective evaluation of picture quality must be in accordance with the standards established by the ITU and ISO/IEC, which are both independent organizations for the global standardization of telecommunications.

The objective of this study is to compare the objective video quality of video compression methods H.264 and MPEG-2. The objective comparison was carried out using the Picture Quality Analysis (PQA) equipment, and the metrics used were Picture Quality Rating (PQR) and Differential Mean Opinion Score (DMOS).

This required using video encoders for both H.264 and MPEG-2 at different compression rates. From the results, it was possible to assess the performance of each compression system by the video rate, and so compare H.264 in relation to MPEG-2.

Several articles in the literature say the H.264 video compression method is more efficient than MPEG-2 [4] [6] [8]. Therefore, this study quantifies these differences. Knowing these differences, it is possible to determine the quality gain versus bit rate.

Eduardo Santos Bueno is a researcher at Mackenzie Presbyterian University, São Paulo, Brazil (e-mail: duardo.bueno@mackenzie.br).

Cristiano Akamine is a professor at Mackenzie Presbyterian University, São Paulo, Brazil (e-mail: cristiano.akamine@mackenzie.br).

Renato de Mendonça Maroja is a researcher at Mackenzie Presbyterian University, São Paulo, Brazil (e-mail: rmmaroja@gmail.com)

Gustavo de Melo Valeira is a researcher at Mackenzie Presbyterian University, São Paulo, Brazil (e-mail: gustavo.valeira@mackenzie.br).

doi: 10.18580/setijbe.2015.5 Web Link: http://dx.doi.org/10.18580/setijbe.2015.5

II. Objective Measures

In a video system, there are many video processing devices that can affect image quality, including the stages of encoding and decoding, which can cause some image degradation.

It is considered that the best assessment of video quality is done by human evaluators since the important thing is to meet the viewer's needs. However, assessing video quality by a subjective evaluation requires a large amount of time and has a high cost. Furthermore, the subjective analysis can only detect visible degradation, and result variations occur due to the evaluators. Thus, what is needed is the development of objective evaluation methods for video quality based on subjective image analysis, and the methods used in this paper are based on this.

The objective analysis of the image quality can be performed with the PQA equipment that can perform the PQR and DMOS measurements.

The PQR and DMOS methods analyze the perceptual contrast difference between a reference video and a test video. The PQR measurement is an assessment of image quality, which corresponds to the perceptual sensitivity measurement that only determines noticeable image differences, known as Just Noticeable Differences (JND) [9] [10].

The JND is based on human perception, which assesses the human reaction to variations in image quality so that it is possible to assess the quality of an image in relation to another [8]. For example, to measure JND, two images or videos are compared, i.e., a reference video and a test video, where this video is derived from the reference video, which in turn has some defects. The lower the JND value, the lower the differences between the test video and the reference video are. 1 JND corresponds to 1 PQR.

A difference of 1 JND is approximately 0.1% of the contrast difference perception between the reference video and the test video [10] [11].* However, with this perceptive contrast difference, viewers do not easily distinguish which is the reference video and which is the test video, therefore, they are practically equal.

However, the perceptual contrast difference between a reference video and a test video becomes clearer with values above 2 JND. If the reference video and the test differ by 3 JND or more, viewers will always notice the video differences, in 100% of cases [10] [11].

It can be concluded that the smaller the PQR, the better the quality of the test video with respect to the reference video will be.

The DMOS measurement corresponds to the subjective evaluations of picture quality, which are completed by evaluators, using the ITU procedure ITU-R BT.500. This is possible because the PQA generates a map of the perceptual contrast differences between the reference video content and the test, which contains information about the differences that viewers will notice between the reference video and the test video [10] [11].

However, unlike subjective image analysis, in which evaluators are used, PQA produces a DMOS result for the sequence of each picture frame. Thus, the DMOS analyzes the contents of the entire video.

The grade is given, based on a five-point scale to assess both the reference video and the test video as in Fig. 1 [10] [11].

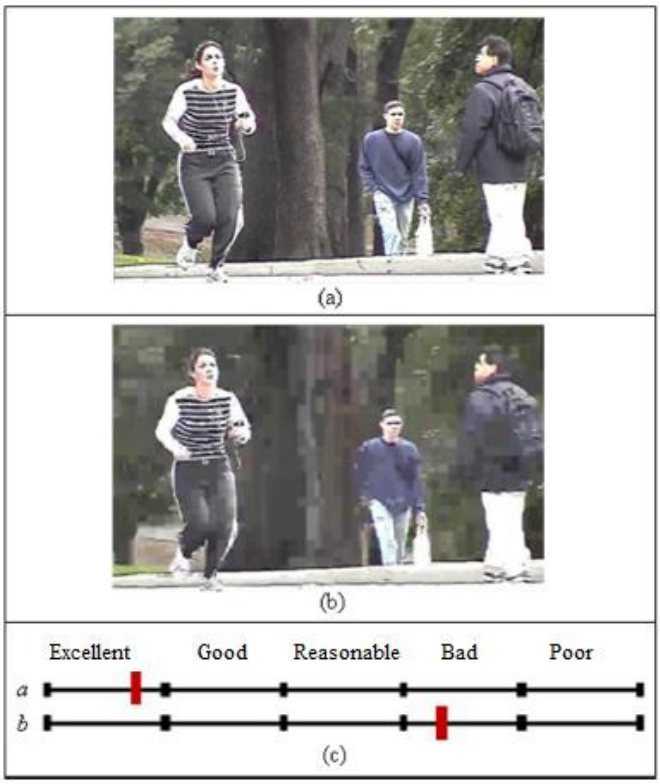

Fig. 1. Demonstration DMOS assessment (a) reference video, (b) test video and (c) note scale. Source - Tektronix - PQA500.

In Fig. 1 (c) the *a* scale is for reference video and the *b* scale is for the test video. The scale in Fig. 1(c) refers to the video quality of Fig. 1(a) and Fig. 1(b). The grade is displayed with a mark added to the scale. From the results, the Mean Opinion Score (MOS) is calculated, i.e., the average result given by the evaluators. The values obtained using the scale are converted into a numerical value, which is the score that the PQA analyzed. To obtain the DMOS, it is necessary to subtract the reference video MOS from the test video's MOS [10] [11].

Values between 0-20 are classified as "excellent" and the test video is good in relation to the reference video [10] [11].

Values between 21-40 mean that the test video is "good" and the video quality is fairly good compared to the reference video [10] [11].

Values between 41-60 indicate that the test video is "reasonable" and the video quality is only acceptable in relation to the test video, but the quality is not good, so the viewer feels uncomfortable when watching the video [10] [11].

Values between 61 to 80 are categorized as "bad" and the test video quality is simply bad in relation to the reference video. For this reason, the image defects are clearly perceived [10] [11].

Values over 81 indicate that the test video has several defects and is classified as "poor" [10] [11].

doi: 10.18580/setijbe.2015.5 Web Link: http://dx.doi.org/10.18580/setijbe.2015.5

III. Test Model Objective

The test was designed to objectively analyze video quality for the following variables: encoding standard, bit rate without packet loss, and bit rate with packet loss. For each of the video encodings H.264 and MPEG-2, the bit rates selected were 3 Mb/s to 15 Mb/s with intervals of 1 Mb/s. With packet loss, the bit rate chosen was 13 Mb/s with a variation in the signal-to-noise ratio between 17.9 dB and 17.2 dB with an interval of 0.1 dB. Tests were performed on three different videos without being compressed, as in Table I. The HDTV video sources are available from Tektronix.

TABLE I
Description of Videos

Name	Size	Time	Frames	Description
Eighth Ave	5.11GB	44.18s	1325	A video that has many people walking on a boulevard. However, the camera is stable.
Stripy jogger	1.87GB	16.18s	486	The camera spends all his time focused on a woman running in a park, therefore, has the movement of people and the camera.
Times Square	2.94GB	25.43s	763	It has no movement in the video content only camera circular motion when shooting buildings.

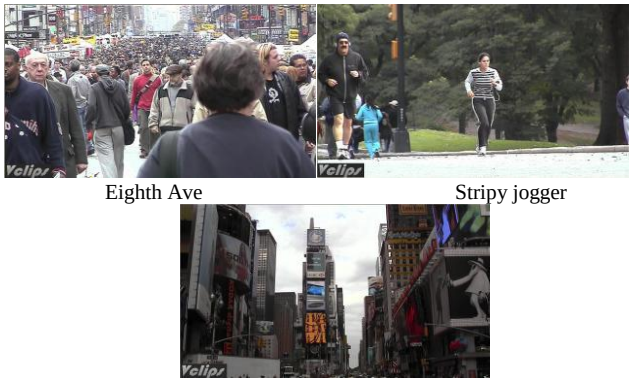

Fig. 2. One frame from each of the 3 video sources used. Source - Tektronix - PQA500.

The tests were conducted using the full-reference measuring method. The full-reference measurement compares the reference video sequence with the test video sequence. The reference video is the original video, and the test video is the video after the encoding of the reference video, and the comparisons are made frame by frame.

The MPEG-2 and H.264 encodings are performed with the use of encoders in real time, i.e., the same type used by television broadcasters. For the Group of Picture (GOP) configuration, the values used were values recommended by the encoders of HDTV encoding. For MPEG-2, a distance was adopted for frame I (with 5 frames), and another distance for frame P (with 3 frames). For H.264, a limited distance was adopted for frame I (between 1 and 255 frames), and for frame P (between 1 and 3 frames).

The MPEG-2 and H.264 encodings were performed with the standard configuration profile/High for video encoding 1080i 30fps (i.e. 1920 pixels by 1080 lines interspersed, 30 frames per second).

The first test was to verify the video quality of the MPEG-2 and H.264 encoders without packet loss. The setup for this test is shown in Fig. 3.

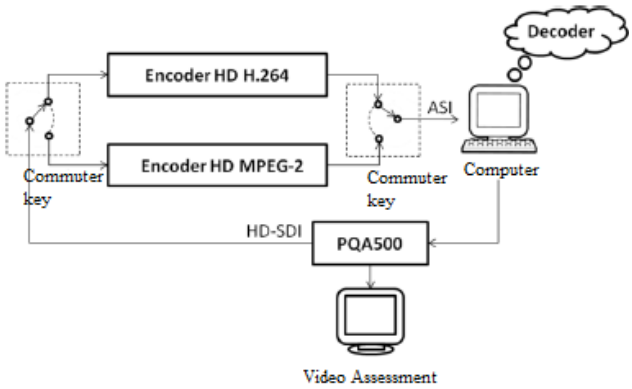

Fig. 3. Block diagram of the first test configuration

As shown in Fig. 3, PQA generates the reference video in a HD signal format by the High Definition - Serial Digital Interface (HD-SDI) which is then encoded by one of the encoders. The encoding is performed on both H.264 and MPEG-2 separately. The computer has a card that receives the Transport Stream (TS) via the serial interface known as Asynchronous Serial Interface (ASI) and writes the TS. This operation is performed at various compression rates and after recording the compressed videos, they are decoded for comparison with the original video, in PQA.

In the first test, the three encoded video sequences shown in Fig. 2 were encoded, which only allowed the comparison of encoding quality, with different bit rates. The decoding was performed in the software.

The second test was to determine how much video quality degradation occurred using MPEG-2 and H.264 encoders when there is packet loss in the transport layer of the ISDB-T_B transmission system. To generate error packets in the transmission, white noise was added to the modulated signal applied to the receiver. The use of white noise is effective because it has a constant spectrum along the frequency. The setup for this test is shown in Fig. 4.

doi: 10.18580/setijbe.2015.5 Web Link: http://dx.doi.org/10.18580/setijbe.2015.5

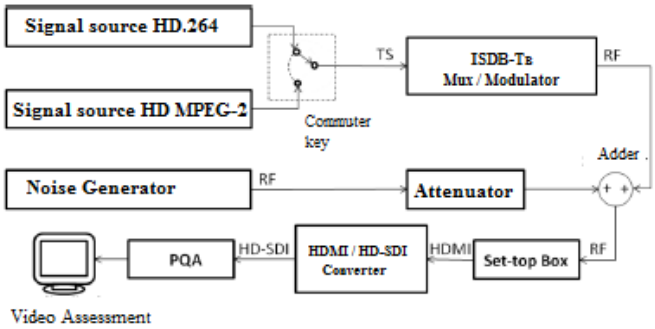

Fig. 4. Block diagram of the second test configuration

In Fig. 4, the signal source generates a HD video in both the H.264 standard and in MPEG-2. In both compression methods, a bit rate of 13 Mb/s has been used. The encoded video signal is multiplexed and modulated in the ISDB-T_B transmission system, to be received by the set-top box. The transmission configuration used is shown in Table II. However, to generate error packets in the transmission channel, white noise is added to the signal. PQA receives the signal decoded from the Set-Top Box, which was necessary to convert High-Definition Multimedia Interface (HDMI) to HD-SDI. This operation is performed with various signal-to-noise ratio values (SNR). After PQA receives the video, the comparison of the encoded video is performed at a rate of 13 Mb/s, but with some packet loss.

TABLE II
ISDB-T_B TRANSMISSION CONFIGURATION

Mode	3
Guard Interval	1/16
Layer	1
Hierarchical layer digital modulation	64QAM
Temporal interleaver	0.2s
Convolutional encoder rate	3/4

The completion of the objective tests was completed with PQA using the PQR and DMOS methods.

IV. Results Analysis

The video quality analysis was performed considering an ideal communication channel and a channel with varying SNR. The variation of SNR causes bit errors within the ISDB-T_B transport layer of the digital channel. The results obtained are presented in the next section:

A. Assessment without packet loss

The tests were performed with three video sequences and present the average results for both the PQR and DMOS methods.

Fig. 5 shows the graph for the PQR method, comparing the H.264 (blue line) and MPEG-2 (red line) encodings with a bit rate variation.

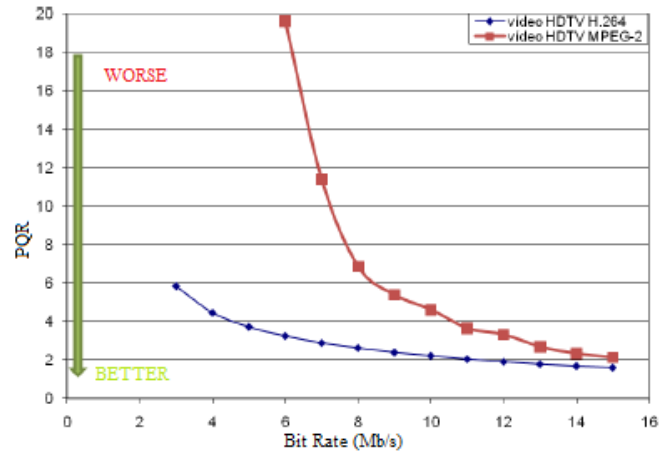

Fig. 5. PQR assessment of H.264 and MPEG-2 encoding without packet loss

As shown in Fig. 5, the H.264 encoding method is of a better quality than the MPEG-2 encoding at any compression ratio for HD video. Therefore, it is possible to transmit H.264 video at 7 Mb/s with the same quality of MPEG-2 video at 13 Mb/s.

It can be concluded that the HD video with MPEG-2 encoding is of a good quality with a low bit rate. However, the HD video with H.264 encoding is of a good quality in relation to the original video with a rate higher than 11 Mb/s with a score between 1 and 2 PQR, where the difference between the test video and the original video is barely noticeable when compared.

Fig. 6 shows the DMOS method graph, comparing the H.264 (blue line) and MPEG-2 (red line) encodings with a bit rate variation.

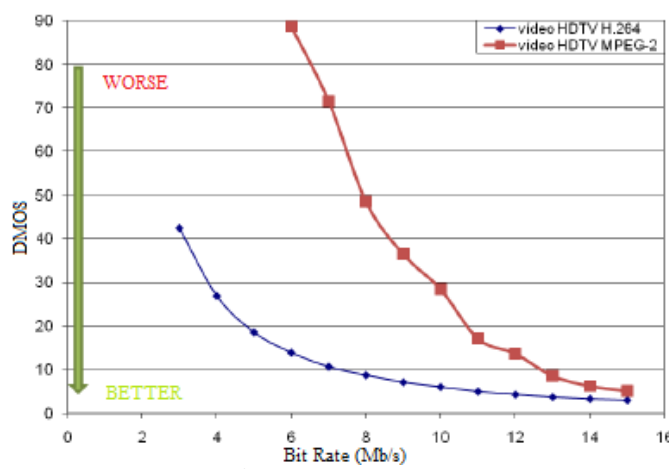

Fig. 6. DMOS evaluation of H.264 and MPEG-2 encoding without packet loss

As shown in Fig. 6, the H.264 encoding method is of a better quality than the MPEG-2 encoding at any compression ratio for HD video. Therefore, it is possible to transmit H.264 video at 7 Mb/s with the same quality of MPEG-2 video at approximately 13 Mb/s.

It can be seen that the HD video with MPEG-2 encoding is not of good quality with a low bit rate. However, the HD video with H.264 encoding is of a good quality in relation to the original video with a rate higher than 8 Mb/s and is of an

excellent quality, while the MPEG-2 acquires this degree of quality from 13 Mb/s.

B. Assessment with packet loss

The following tests were performed with the three videos shown in Fig. 2. Despite using the same video sequences, for these tests they were recorded with 1800 frames, lasting 60 seconds, with a rate of 13 Mb/s, to achieve this the same video was repeated a few times. In addition, various tests were completed with the same videos and the results shown are the average for each video for both the PQR and DMOS methods.

Figs. 7 and 8 show graphs for the PQR and DMOS assessment results, respectively, comparing H.264 (blue line) and MPEG-2 (red line) encodings with a change in signal-to-noise ratio.

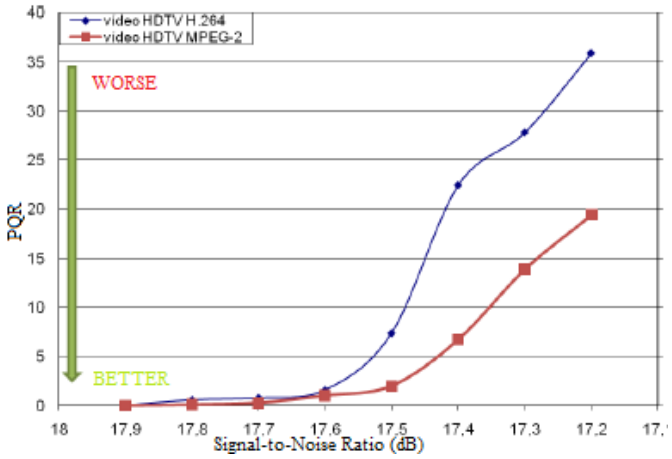

Fig. 7. PQR Evaluation of H.264 and MPEG-2 encoding with packet loss

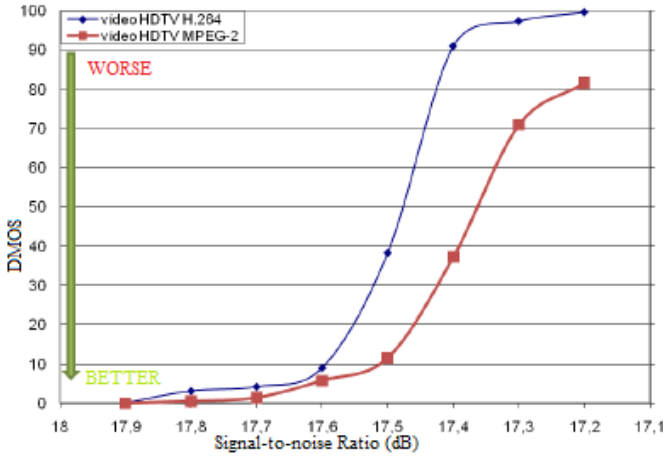

Fig. 8. DMOS evaluation of H.264 and MPEG-2 encoding with packet loss

These results show that H.264 is more sensitive to packet loss than MPEG-2. It is observed that when the SNR value is between 17.9 dB and 17.6 dB the encoders are similarly affected. However, H.264 is shown to be more sensitive to packet loss than MPEG-2, from an SNR value of 17.6 dB.

This occurs because the H.264 decoder is slower to recover from packet loss. Moreover, the degradation shown by the MPEG-2 decoder in response to packet loss had a minor impact.

V. Conclusion

The PQR and DMOS objective evaluations ensure accurate control of video quality. The DMOS assessment helps determine the differences in the test video in relation to the reference video based on subjective quality ratings. Therefore, the PQR measurement helps determine how viewers perceive the differences in the test video in relation to the reference video, an efficient high-quality video, when the differences are close to the visibility threshold.

The test results are consistent, where the H.264 encoding provides a similar quality to the MPEG-2 encoding at approximately half the bit rate. However, H.264 decreases its advantage at a high bit rate, namely above 15 Mb/s, here there is little difference between MPEG-2 and H.264.

However, packet loss in test results also demonstrates that the H.264 encoding quality drops sharply while the quality of MPEG-2 encoding in response to packet loss had a minor impact. This sensitivity seems to be partly caused by the GOP structure, where the H.264 decoder takes a longer time to recover. This can be seen when viewing the number of wrong frames that the video encoded in H.264 generates when packets are lost, whereas the video encoded in MPEG-2 was shown to be better.

Acknowledgment

The authors would like to thank their friends in the Laboratorio de Televisão Digital at Universidade Presbiteriana Mackenzie.

References

[1] *Televisão digital terrestre – Codificação de vídeo, áudio e multiplexação Parte 1: Codificação de vídeo*, ABNT NBR 15602-1:2007, Abr. 2007.
[2] *Televisão digital terrestre – Codificação de vídeo, áudio e multiplexação Parte 2: Codificação de áudio*, ABNT NBR 15602-2:2007, Abr. 2007.
[3] *Televisão digital terrestre – Sistema de transmissão*, ABNT NBR 15601:2007, Abr.2007.
[4] B. Farmer, "Video Compression using ITU-T Recommendation H.264‖." M.S Dissertation, Faculty of Engineering & Surveying. University of Southern Queensland, Queensland, 2005.
[5] *Information technology, Coding of audio-visual objects — Part 10: Advanced Video Coding. n.2*, ISO/IEC 14496-10, 2004.
[6] I. E. G. Richardson, *H.264 and MPEG-4 Video Compression*. England: Wisley, 2003, p. 281.
[7] *Methodology for the subjective evaluation of the quality of television pictures*, ITU-R BT.500-11, 2002.
[8] R. Arthur, "Avaliação Objetiva de Codecs de Vídeo," M.S. Dissertation, Faculdade de Engenharia Elétrica e de Computação. Universidade Estadual de Campinas. São Paulo, 2002.
[9] *Measuring and Interpreting Picture Quality in MPEG Compressed Video Content*. Tektronix. S.L. 2001. Available at: <http://www.tek.com/Measurement/App_Notes/25_14675/eng/25W_14675_0.pdf>
[10] *Perceptual-Based Objective Picture Quality Measurements*. Tektronix. S.L. 2008.
[11] *Understanding PQR, DMOS, and PSNR Measurements.* Tektronix. S.L. 2008.

Cite this article:
Santos Bueno, E., Akamine, C. , de Mendonça Maroja, R., and de Melo Valeira, G.; 2015. Objective Analysis of HDTV H.264 x MPEG-2 with and Without Packet Loss. ISSN Print: 2446-9246 ISSN Online: 2446-9432. doi: 10.18580/setijbe.2015.5 Web Link: http://dx.doi.org/10.18580/setijbe.2015.5

Passive Reception of Digital TV Signals with an Antenna

Fujio Yamada, Cristiano Akamine, Rodrigo Eiji Motoyama, and Gustavo de Melo Valeira

***Abstract*—This article aims to present a passive repeater for transmitting digital TV signals. In this article, some projects that indicate the limitations in this type of repeater are presented and in what situations it becomes suitable for use.**

***Index Terms*—Band Segmented Transmission - Orthogonal Frequency Division Multiplexing (BST-OFDM), Electric field strength, Mobile reception.**

I. Introduction

THE Brazilian Digital TV System (SBTVD) signal is immune, to a limited extent, to interference and disturbances such as Gaussian noise, multipath signal, impulsive noise, the Doppler effect, and fading, due to the numerous technological resources available [1]. However, for a good image to be received, the signal presence must be above a certain level with a good quality measure in relation to Carrier-to-Noise (C/N) [2]. Situations occur in digital television reception where although there is a high-intensity Digital TV signal nearby, the location where the signal is received is in a shadowed region. The solution is to redirect this signal to the desired location via a signal relay device. However, it is not always possible to install an active relay in this high-intensity location, due to a lack of infrastructure with electricity, a high installation cost or for equipment security reasons (theft). In this case, it is desirable to develop a low-cost solution for both the installation and maintenance, that is unlikely to be stolen or vandalized. Depending on the signal level at the location, a passive repeater can be installed, this only uses antennae installed in a back-to-back configuration without the use of an amplifier [3]. It is a low-cost solution that solves the problem, in some cases. This paper presents some situations where a passive repeater is a solution.

The two most common situations for applying a passive repeater for digital TV signals are:

a) a high-intensity signal in a certain location where it is required to be redirected to a relatively distant shadowed region. For example, the summit of a hill or the top of a building, but due to the obstruction, this signal does not reach the desired location.

b) a high signal intensity on the outside of a wall or the top of the building, but due to the attenuation caused by the wall or slab the signal does not reach the internal environment where the receiver is installed.

Fujio Yamada is a researcher at Mackenzie Presbyterian University, São Paulo, Brazil (e-mail: fujio.yamada@mackenzie.br).

Cristiano Akamine Yamada is a professor at Mackenzie Presbyterian University, São Paulo, Brazil (e-mail: cristiano.akamine@mackenzie.br).

Rodrigo Eiji Motoyama is a researcher at Mackenzie Presbyterian University, São Paulo, Brazil (e-mail: rodrigo.motoyama@mackenzie.br).

Gustavo de Melo Valeira is a researcher at Mackenzie Presbyterian University, São Paulo, Brazil (e-mail: gustavo.valeira@mackenzie.br).

II. Passive Repeater Development

This chapter presents a demonstration of the development and the implementation of a passive repeater for digital television using only antennae mounted in a back to back configuration. Due to the various scenarios whose parameters vary, such as the distance between the transmitter and the repeater, the location of the receiver, the power involved, and the channel frequency, this work shows the received signal conditions across the simulations adopting certain values. For conditions with other parameter values, the viability can be estimated using interpolation values. For cities that use transmitters with lower interpolation power an estimation can be made considering the ERP power in dBm between this simulation and the actual condition and adding or subtracting this value to the results shown in the subsequent tables.

A. Signal Repeater Located far from the Receiver

The field intensity threshold of a SBTVD receiver to decode a signal is 51dBμV/m, 90% of the time [1]. Considering a margin of 6 dB, this value becomes 57BμV/m, which corresponds to the voltage at the receiver input (37dBμV) for a TV channel in the 500MHz band [4].

One solution is to use a pair of passive antennae in a back-to-back configuration, separated by a metal plate to isolate the electromagnetic field in order to avoid mutual interference and pointing the receiving antenna in the direction of the best signal strength from the transmitter and directing the relay antenna to the location where you want to install the receiver. The output of the receiver from the transmitter antenna (A) must be connected to the input of the relay antenna (B) as shown in Fig. 1. The coaxial cable for connecting the antenna (C) must have the lowest attenuation possible, for example, RG6. Fig. 2 shows the repeater installation.

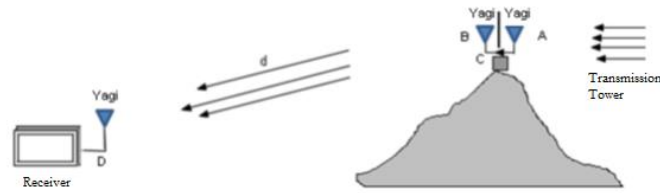

Fig. 1. Installation diagram of back-to-back passive repeater

doi: 10.18580/setijbe.2015.6 Web Link: http://dx.doi.org/10.18580/setijbe.2015.6

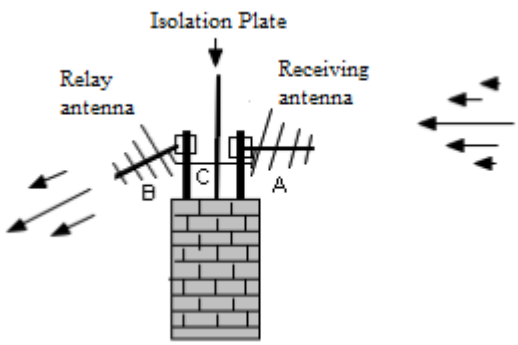

Fig. 2. Image of a back-to-back antenna installation

Table I shows the calculation of the minimum field intensity required for signal capture in the area near the receiving antenna (A) for the signal repetition to be viable, for a receiver that is located 100m, 300m or 1000m from the retransmission location and can still decode the signal.

To calculate Table I, the following assumptions were used:

- Yagi-Udo antennae were used for the repetition location, with a minimum gain of 12 dB [3] across the UHF band for both reception and retransmission. The interconnection cable between the two antennae is an RG6 with attenuation of 1 dB. Care should be taken to put the antennae in the same polarization as the antenna from the signal generating station.
- To ensure that there is no mutual interference between the antennae reception and retransmission fields, a metal plate should be placed between the two antennae of the back-to-back repeater and if possible grounded.
- A Yagi-Udo external antenna was used with the television receiver; this has a gain of 12 dB and the attenuation due to the cable connectors used is estimated at 4dB.
- It was assumed that there was no obstruction between the transmitting station antenna and either the location of the signal repeater or the TV antenna.

In practice, the system proves feasible for short distances between the reception location and the TV antenna, up to 1000m depending on the distance between the transmitting tower and the repeater location. Longer distances require active repeaters, such as a Gap Filler.

For stations located in São Paulo that installed 15kW transmitters with an approximate gain of 12 dB antenna and installed 150m high, the maximum possible distance between the transmitting tower and the repeat point is shown in Table I. For this calculation a 3dB attenuation in transmission line between 15kW transmitter, antenna, and other associated devices was considered, resulting in 81.7 dBm ERP. For this calculation, a Yagi-Udo external antenna was used with a gain of 12 dB and the attenuation of the cable and connectors was estimated at 4dB. It was assumed that there was no obstruction in visibility between the transmitting tower and repeat location. For signal conversion of dBm to BµV/m the following [4] equation can be used:

$$P(dBm) = E(dB\mu V/m) - 113(dB) + 10\,log\left(\frac{\lambda}{\pi}\right)^2. \qquad (1)$$

The free space attenuation is calculated by: $A_{el} = \left(\frac{4\pi d}{\lambda}\right)^2$ where λ is the wavelength and d is the distance in meters.

B. *Distance between the transmitter and repeater location*

Often the maximum distance that the passive repeater can be installed from the transmitter is wanted to be known. This information can be obtained by calculating the distance in which the signal attenuates from the transmitter until reaching the repeater location level (A). In most cases, this type of signal repetition is valid when using an external antenna with the receiver.

TABLE I
MAXIMUM DISTANCE BETWEEN THE TRANSMITTER AND THE REPETITION LOCATION FOR AN EXTERNAL ANTENNA

Distance from B to the receiver	100			300			1000		
Channel frequency (MHz)	400	600	800	400	600	800	400	600	800
Transmission distance for 15kW (km)	39.4	26.9	20.2	13.6	8.9	6.6	4.1	2.6	2.0
Transmission distance for 5kW (km)	26.7	18.8	13.3	7.7	5.1	3.8	2.3	1.5	1.1
Transmission distance for 1kW (km)	10.2	6.8	5.1	3.4	2.3	1.7	1.0	0.7	0.5

The results in Table I show that the possibility of success with passive repetition depends substantially on the distance between the repetition location and the receiver antenna and the frequency of the measured channel. Table I shows that this kind of repetition is feasible for a transmitter within 5 km.

C. *Distance between the transmitter and repeater location for internal antenna at the receiver*

This situation is more difficult to solve because the walls and other obstacles cause additional attenuation. Research by the Laboratorio de Televisão Digital at Universidade Presbiteriana Mackenzie showed that this attenuation varies from 4 to 7 dB depending on the construction of the wall [5]. Furthermore, it is generally an internal omnidirectional antenna with a gain of zero to three dB against the 12 dB gain of a Yagi-Udo antenna. The difference in signal level between internal and external reception is in the order of 16 dB. This means that the signal intensity at the repeater location should also be higher by the same proportion. Calculating the maximum distance for this condition, we have Table II.

doi: 10.18580/setijbe.2015.6 Web Link: http://dx.doi.org/10.18580/setijbe.2015.6

TABLE II
MAXIMUM DISTANCE BETWEEN THE TRANSMITTER AND THE REPETITION LOCATION FOR AN INTERNAL ANTENNA

Distance from B to the receiver	100			300			1000		
Channel frequency (MHz)	400	600	800	400	600	800	400	600	800
Maximum transmission distance (km)	6.0	4.0	3.0	2.2	1.5	1.6	-	-	-

Table II shows that passive repetition to a receiver with an antenna is only feasible if the shadow region is located near the tower, approximately 3 to 6 km and that the receiver is connected to a 100 or 200m repeater if a 15kW transmitter is used.

D. Signal repeater located near the receiver

Often within a building like a mall or a residence the signal level is insufficient for television signal reception. However, it is noted that externally the signal intensity is elevated. If the installation of a cable from the external antenna to the receiver device or a large antenna is not desired due to aesthetic reasons, the installation of a passive signal repeater on the external wall would be sufficient. The main function of the passive repeater in this case is to redirect the distribution of the field in the indoor environment improving coverage in certain areas while the total energy within the environment does not change [3]. This topic shows in which conditions this option is feasible. Fig. 3 outlines the signal being repeated in a closed environment.

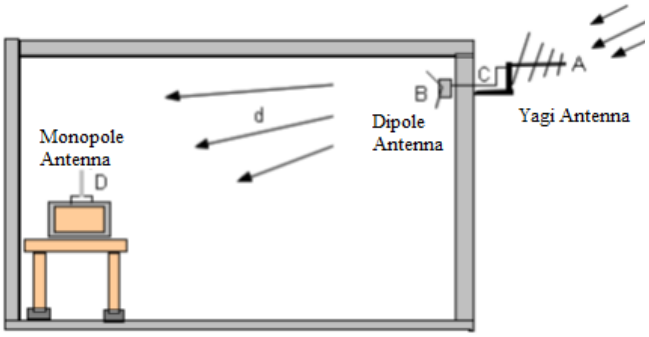

Fig. 3. Repeater near the receiver

For this version, the following assumptions were adopted:

- A Yagi-Udo antenna was used at point A with a presumed gain of 12 dB
- A dipole antenna was used as the relay antenna with a presumed gain of 5 dB
- The antenna type used was monopole omnidirectional with a 3 dB gain at the receiver.
- The reception threshold used was 57dBμV/m with a 6dB margin
- It was assumed that there was no obstruction between the relay antenna and the receiver antenna

TABLE III
MAXIMUM DISTANCE BETWEEN THE TRANSMITTER AND THE REPETITION LOCATION FOR AN INTERNAL ANTENNA

Distance B-D (m)	10			20			40		
Freq. (MHz)	400	600	800	400	600	800	400	600	80
Free space att. B-D (dB)	44.7	48.0	50.5	50.5	54.0	56.5	56.5	60.0	62.
Antenna gain A-B (dB)	17	17	17	17	17	17	17	17	1
Receiver gain monopole antenna (dB)	3	3	3	3	3	3	3	3	3
Cable repeater losses C (dB)	1	1	1	1	1	1	1	1	1
Total att. A-D (dB)	25.7	29.0	31.5	31.5	35.0	37.5	37.5	41.0	43.
Field strength in A (dBμV/m)	82.7	86.0	88.5	88.5	92.0	94.5	94.5	98.0	10

III. EXPERIMENTS COMPLETED

To confirm the validity of the above simulations, experiments were performed, a carrier at -31dB was generated using a Rohde Schwarz generator, model SMU200A and was transmitted with an Anritsu standard dipole antenna with a 3dBi gain. The measurements were performed in a Faraday cage to avoid any signal interference present in the environment. The signal was received at the reception site for an omnidirectional monopole antenna with a 3dBi gain and was measured with an Anritsu MS8901A spectrum analyzer. Fig. 4 shows how the test structure as it had been assembled in the laboratory and the results are presented in table IV.

doi: 10.18580/setijbe.2015.6 Web Link: http://dx.doi.org/10.18580/setijbe.2015.6

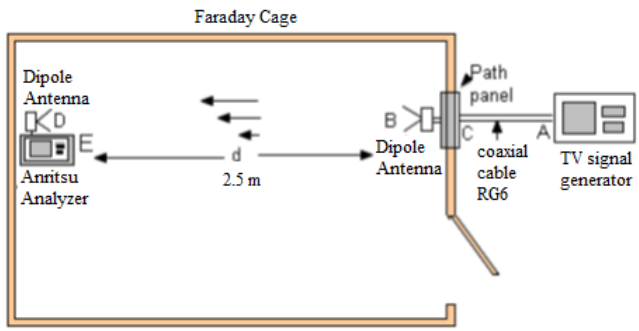

Fig. 4. Indoor signal repeater diagram

TABLE IV
MEASUREMENTS IN THE FARADAY CAGE

Description	Values				
Frequency (MHz)	470	500	600	700	800
Generator Level in A (dBm)	-31.4	-31.4	-31.4	-31.4	-31.4
Free space attenuation (dB)	-33.8	-34.4	-35.9	-37.3	-38.4
Antenna gain (dB)	6.0	6.0	6.0	6.0	6.0
Cable attenuation (dB)	0.4	0.4	0.4	0.5	0.5
Expected value (dBm)	-58.9	-60.2	-61.0	-62.3	-63.5
Measured value in E (dBm)	-58.7	-62.4	-62.9	-63.8	-63.7
Measured value in dBμV/m	68.2	65.0	66.3	66.5	67.9

The measured values match the expected values, within a measurement tolerance.

IV. CONCLUSION

This work gives an idea of how digital TV passive repetition can be implemented and the conditions in which it is feasible. This is the presence of a minimum signal level that is stable in the signal repeater location. Normally to achieve the signal level required for passive repetition it is necessary to have visibility between the transmission and reception locations. The example calculations presented allow an interpolation to be made to determine the values for other propagation conditions. Possibly being an excellent TV signal repeating system without large implementation costs, low maintenance, and little vulnerability to theft.

REFERENCES

[1] *Televisão Digital Terrestre: Sistema de Transmissão*, NBR 15601, 2008
[2] G. Bedicks Jr, F. Yamada, E. Horta, C. Akamine, and F. Sukys, "Brazilian DTTB Coverage Performance Evaluation," *in IEEE 58th Annual Broadcasting Symposium*, 2008.
[3] Y. Huang, N. Yi, and X. Zhu. "Investigation of Using Passive Repeaters for indoor radio Coverage Improvement," *Antennae and propagation Society International Symposium*, 2001.
[4] C.Y.W. Lee, *Mobile Cellular Telecommunications*, McGraw-Hill Inc., 1995.
[5] R.E. Motoyama, "Proposta de Procedimento de Teste de Recepção de TV Digital com Antena Indoor," M.S Dissertation. Engenharia Elétrica. Universidade Presbiteriana Mackenzie, 2010.

Cite this article:
Yamada, F. , Akamine, C. , Motoyama, R. E. , and de Melo Valeira, G.; 2015. Passive Reception of Digital TV Signals with an Antenna. ISSN Print: 2446-9246 ISSN Online: 2446-9432. doi: 10.18580/setijbe.2015.6 Web Link: http://dx.doi.org/10.18580/setijbe.2015.6

Experimental Investigation of Digital TV Signals with Multipath in Curitiba

Marco Antônio Costa de Borba, Carlos Eduardo Neves Mayer, Keiko Verônica Ono Fonseca, Alexandre de Almeida Prado Pohl, Karine de Ramos Good, Luciano Mildemberg, Deisi Luiza Wosch, and Ruth Angelina Martins

***Abstract*—This article describes experimental propagation measurements of DTV signals in the urban region of Curitiba. A digital TV analyzer manufactured by Rohde & Schwarz, model ETL was used [1], which is able to differentiate open TV channel signals received via different paths. At each measuring location, the geographical coordinates, the relative intensity, the relative delay of each of the ten most intense echoes received, the recording time, and the channel power were recorded. A vertical monopole antenna tuned to the channel frequency and mounted two meters above ground level on the top of a special purpose vehicle was used as the receiving antenna. Signal frequency spectrum and the subjective quality of the received signal were simultaneously observed. Both the path loss and the echo pattern were measured. 1580 samples were recorded, taken approximately five meters apart in various regions of the city and were compared with current propagation models. The power and delay of every multipath version was checked to evaluate the efficiency of the guard interval. The effects of distance and elevation of the reception site were investigated, as well as the presence of channel-modifying obstacles. Analysis of the results included the comparison of received power measurements with the Okumura-Hata model calculations. The multipath delay data was analyzed as per recommendation ITU-R P.1407 [2]. Preliminary results show the robustness of the ISDB-T_B system against UHF propagation in Curitiba. Some aspects of the measurements elicit further investigations that can be carried out with the same resources.**

***Index Terms*—Digital TV, Multipath, Measurements, Urban propagation, UHF.**

I. Introduction

THE main purpose of a broadcasting system is to maximize the number of receptors able to capture a signal that it is compatible with the acceptable quality standards established for the service from the technical point of view or the marketing point of view. Knowing the actual coverage provided by a transmitting station for digital TV is an area of interest for broadcasting managers. It is very unlikely that the signal quality is acceptable in the entire coverage area. Locations of failures and the reasons for failures in coverage is an area that broadcasting station technical teams continue to investigate. The advent of digital TV has brought doubts about the real effect of propagation on multiple path signals, characteristic of urban regions can have on a digital transmission. For the regions where the signals fails, is this because of the low received signal power or could this be caused by the arrival of successive versions of the signal that went through multiple pathways? In this study, an experimental approach was chosen in order to answer these questions.

Financial support provided by CAPES, through the project 'Formação de Pessoal Qualificado em TV Digital no Paraná' process 23038.2355/2008-16 AUX-PE-RH-TVD 249/2008

II. Materials and Methods

Given the dispersion values to be expected when measuring received power, a higher number of samples reduce uncertainties. For the measurements in this analysis, 1580 samples were collected. To enable accurate data collection and to eliminate human errors in transcription and annotation, an automated system was used. It is based on a ETL digital TV analyzer produced by Rohde & Schwarz Company [1].

A route was chosen for the test that presented various propagation conditions: direct sight, shading caused by the terrain or constructions, high relative signal intensity with multiple paths in some places, and low-intensity signals reflected in other regions of the route . The route taken can be identified in Fig. 1 with the received power within the range between -30 dBmW and -70 dBmW.

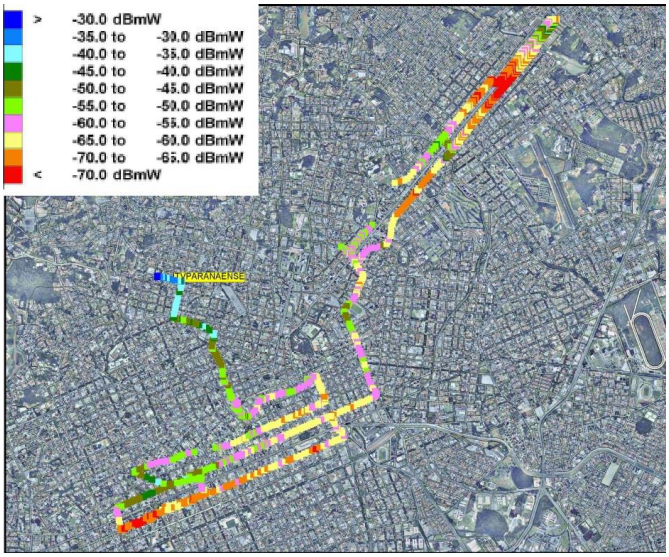

Fig. 1. Route taken in Curitiba by the reception vehicle

doi: 10.18580/setijbe.2015.7 Web Link: http://dx.doi.org/10.18580/setijbe.2015.7

The whole measuring system was mounted on a vehicle specially prepared for this activity. The vehicle boasts an inverter system, capable of providing adequate AC power for the measuring instruments on board. A GPS receiver is coupled to the measuring system so that the coordinates where the measurements were made were automatically incorporated into the table with the measured values without human intervention. For most of the trial, further measurements were taken approximately every thirty meters along the route. This separation to the order of 60, tends to maintain statistical independence between two adjacent measurements. A second spectrum analyzer, capturing the same signals by an equivalent antenna, but separate, was kept under observation during the experiment, in particular to indicate the regions where the received signal spectrum was no longer on a single plane, a fact that by itself is an indication of propagation by multiple paths.

The receiving antenna chosen was a vertical monopole antenna to reduce directionality reception influences. The idea is that all echoes are received with about the same gain, no matter the direction from which it comes. It was fixed on the vehicle two meters from the ground. The antenna used in the experiment measures 11cm, approximately $\lambda 4$ in the central frequency of 635 MHz in channel 41, granted to Rede Paranaense de Comunicacao, whose 8 kW transmitter, antenna tower and station were used as the signal source for testing. In this evaluation, a total loss of 1.28 dB was considered due to RF switches, connectors, and lines of transmission, which leads to a coherent EIRP with that reported in [3]. The additional loss of 0.17 dB is attributed to the fact that throughout the test, the receiving antenna is always found below the main beam of the transmitting antenna, outside the maximum gain direction. The power effectively radiated in dBm can be expressed by the following equation:

$$EIRP_{dBmW} = 60 + 10log_{10}(8kW) + 10.7dBd + 2.14dB - 1.28dB - 0.17dB = 80.24dBmW \quad (1)$$

For reception, the gain of the monopole was estimated at -1 dBd, due to the absence of a full grounding plane in the assembly of the vehicle. An additional loss of 7 dB was tentatively attributed to the difference in polarization used in the transmission (horizontal) and reception (vertical). A power splitter was used to send equivalent signals to the ETL and a digital TV receiver, which allowed a subjective evaluation of the received signal throughout the test. The loss in the power divider is 3.2 dB. Added to the loss in the cables, the total loss in reception of 9.42 dB. If d is the distance in km separating the receiver from the transmitter, and $L(d)$ is the loss due to propagation, the received power P_{dBm} in dBmW, it can be expressed by

$$P_{dBmW} = 71 - L(d) \quad (2)$$

Various propagation models were compared to measurements obtained. The received power values in each of the 312 simulations were calculated using equations available in [4], or generated by EDX software [5]. For example, in the region of Av. Canada the models in Table I were simulated, with the average error and the standard deviation expressed in dB.

The variation of $L(d)$ with d is dictated by the model chosen, as detailed in the following section.

III. Reviewed Models

With the volume of measurements and models experimented with, it was necessary to delimit the analysis of those situations with more elucidatory character. The following subsections discuss these choices.

A. Free Space Model

In this model, the received power is given by

$$P_{dBmW} = 71 + 20log_{10}\left(\frac{\lambda}{4\pi d}\right) \quad (3)$$

The free space model is represented, along with other information, in Fig. 2.

TABLE I
Propagation models with EDX software used on Av. Canada

Propagation Model	Mean error (dB)	Standard deviation (dB)
Anderson 2D v1.00	15.54	10.22
FCC – EDX	31.22	9.65
FCC – FCC	31.33	9.69
FCC – Pt22	31.22	9.65
FCC + RMD	21.81	9.60
Free Space + RMD	20.22	8.74
Hata-extended-open	14.59	9.33
Hata-extended-suburban	-3.44	9.33
Hata-extended-urban	-12.68	9.33
ITU-R 1546 cold sea curves with delta H	41.90	9.11
ITU-R 1546 cold seas curves without delta H	41.90	9.11
ITU-R 1546 Land curves with delta H	27.86	9.34
ITU-R 1546 Land curves without delta H	27.86	9.34
ITU-R 1546 Warm sea curves with delta H	41.90	9.11
ITU-R 1546 Warm sea curves without delta H	41.90	9.11
ITU-R 370 Cold sea curves with delta H	41.97	9.12
ITU-R 370 Cold sea curves without delta H	41.97	9.12
ITU-R 370 Land curves with delta H	41.97	9.12
ITU-R 370 Land curves without delta H	41.97	9.12
ITU-R 370 Warm sea curves with delta H	41.97	9.12
ITU-R 370 Warm sea curves without delta H	41.97	9.12
ITU-R 370 + RMD Cold sea curves with delta H	32.14	8.60
ITU-R 370 + RMD Cold sea curves without delta H	32.14	8.60
ITU-R 370 + RMD Land curves with delta H	32.14	8.60
ITU-R 370 + RMD Land curves without delta H	32.14	8.60
ITU-R 370 + RMD Warm sea curves with delta H	32.14	8.60
ITU-R 370 + RMD Warm sea curves without delta H	32.14	8.60
Longley rice v1.2.2	17.64	10.30
Okumura-Hata-open	23.95	9.50
Okumura-Hata-suburban	5.92	9.50
Okumura-Hata-urban	-3.32	9.50
TIREM – EDX	17.13	10.03

doi: 10.18580/setijbe.2015.7 Web Link: http://dx.doi.org/10.18580/setijbe.2015.7

B. Free Space Model with diffraction

It is equivalent to the previous model, with the following refinements [5]: the passages with direct view will be considered as the vectorial sum of the radius directly to that reflected in the ground; and the route segments beyond the direct view, rounded up to ten obstacles has its attenuation by diffraction added, according to the Epstein-Peterson technique of successive triads [5].

C. Okumura-Hata Model

The Okumura-Hata model used in this study, to verify its adequacy for experimental measurements was the 'big cities in frequencies above 300 MHz', as shown in [4]:

$$P_{dBmW} = 71 - (69.55 + 26.16log_{10}(f) - 13.82log_{10}(h_t) - (3.2(log_{10}(11.75h_r))^2 - 4.97) + (44.9 - 6.55log_{10}(h_t))log_{10}(d)) \quad (4)$$

In this expression, f is the frequency of the carrier in MHz, h_t is the height in meters of the center phase of the transmitting antenna, and h_r is the height of the receiving antenna in meters. The actual height that the antenna was effectively fixed to the vehicle was two meters in relation to the ground. To verify agreement with the experimental data, five curves were drawn using the Okumura-Hata model. Three of them used the correct height of the transmitting antenna, and three different values for the height of the receiving antenna: 2, 9, and 14 m. In the other two curves, the actual height of the receiving antenna at 2 m was maintained, and the height of the transmitting antenna was varied to the fictitious values of 30 and 1000 m, in order to investigate the effect of average land elevation on the propagation path. This information is detailed in Fig. 2. As can be seen by the monotonic decrease and constant rate of these curves, the Okumura-Hata model referred to in this subsection does not take into consideration the effects of diffraction.

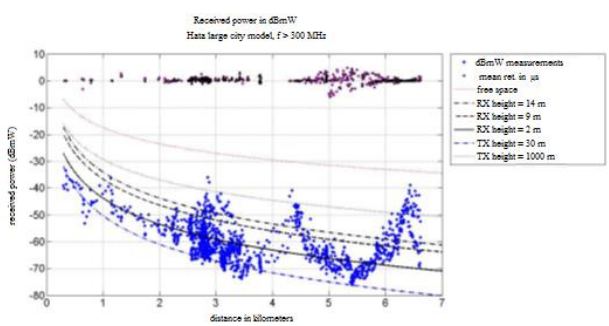

Fig. 2, Comparison between the received power measurement values with those predicted by the free space and Okumura-Hata models

D. Hata model with diffraction

The tool [5] in the Hata-extended-open and Hata-extended-suburban models, adds loss due to the effects of diffraction to the model described above through the Epstein-Peterson technique. A comparison of the measurements taken on Av. Canada is shown in Figs. 3 and 4.

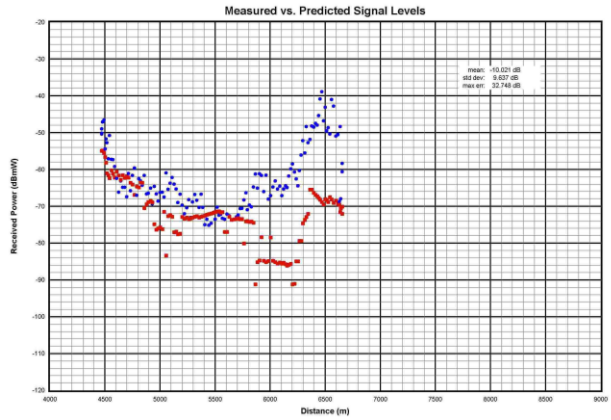

Fig. 3. Measured values of received power (blue circles) and the predictions made using the Hata-extended-suburban model, which includes the effect of diffraction following the Epstein-Peterson technique (red squares).

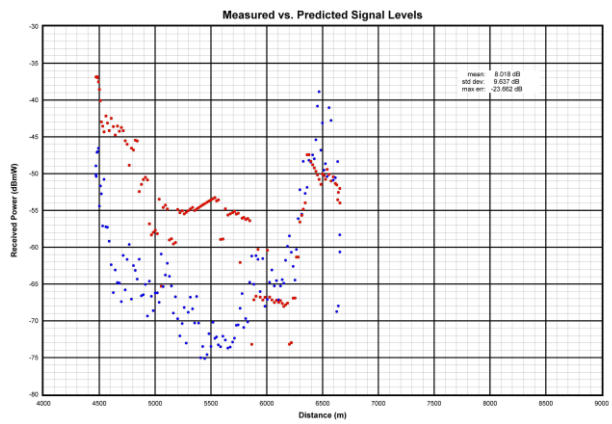

Fig. 4. Measured values of received power (blue circles) and those predicted by the Hata-extended-open model, which includes the effect of diffraction following the Epstein-Peterson technique (red squares).

IV. Echo Profiles

Besides the analysis of the received power, in the same trial information about the propagation by multiple paths was collected.

The ETL instrument is able to discern digital TV signals displaced in time and superimposed on the main signal. It is possible to measure the delay and intensity of each COFDM version. The version with a higher received power is chosen as a reference; it is assigned the intensity of 0 dB. The other copies of the received signal have their intensities measured in dB with respect to most intense version, so the values in dB are always negative. Their delays are also referred to the stronger version, even if it had not been the first to be received. In the chosen mode for the test, the ten echoes perceived to be the most intense are presented, each with a specific delay in relation to the most powerful. It means that there may be echoes with negative delays if the most intense version had not been the first to arrive. Sometimes these signals with a negative delay are called pre-echoes. A profile of typical echoes, as shown by ETL is shown in Fig. 5.

doi: 10.18580/setijbe.2015.7 Web Link: http://dx.doi.org/10.18580/setijbe.2015.7

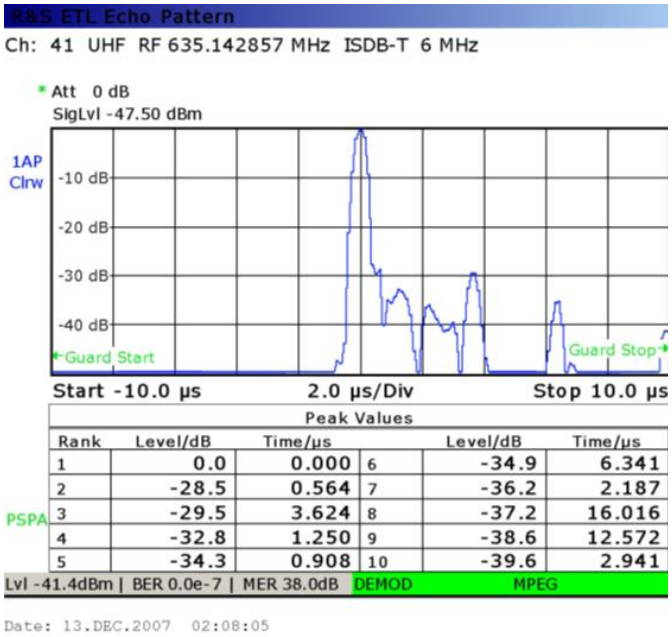

Fig. 5. Typical echo profile

Each of the 1580 measures taken during the test is associated with twenty figures relative to echoes. Ten of these are the intensities, in dB, with relation to the most intense. The ten other values are the delays in microseconds, also relatively to the most intense echo.

In order to summarize the information contained in these 31,600 numbers, the formulation of ITU-R was used [2], the so-called 'average delay' T_D and '*rms* scattering delay' S, for convenience is repeated below:

$$T_D = \frac{\sum_{i=1}^{N} P_i t_i}{\sum_{i=1}^{N} P_i} \tag{5}$$

$$S = \sqrt{\frac{\sum_{i=1}^{N} P_i t_i^2}{\sum_{i=1}^{N} P_i} - \frac{\left(\sum_{i=1}^{N} P_i t_i\right)^2}{\left(\sum_{i=1}^{N} P_i\right)^2}} \tag{6}$$

Note that the average delay T_D is a weighted average of the N delays taken into consideration (in our experiment there were ten). The weight of each delay in the media formation is its relative power. It is a central tendency measure.

The *rms* spreading is a dispersion measure that evaluates how much the delays are spreading in time.

V. Results Analysis

The measurements collected were analyzed from two points of view: the power received, and the echo profile caused by multipath. The following two subsections discuss each aspect.

A. Received power results analysis

By observing Fig. 2, we can see that the Okumura-Hat model, although providing a reasonable adjustment to the measurements of distances between 1.2 and 2.2 km, it could not model the signal propogation that is caused by the terrain and buildings. In particular, in the range between 3.5 and 4.4 km, and again between 5.4 and 6.4 km, the received power increases in distance; such behavior cannot be reproduced in the Okumura-Hata model.

To adapt the model for the above behavior, it is necessary for the model to consider the diffraction effect, and take into account the topographic data. This refinement is incorporated, among others, into the 'free space + RMD', 'Hata-extended-suburban' and 'Hata-extended-open' models. A comparison of the last two models with the measurements collected on the first pass on Av. Canada is shown in Figs. 3 and 4. In these, it can be seen that the models reproduce the weak signal ranges that, in the measurements is those taken between 5.4 and 5.7 km. This appears to be a better prediction with the 'Hata-extended-suburban' model until 5.65 km; after this distance, the 'Hata-extended-open' model best fits the experimental data.

B. Multipath results analysis

To better interpret the measured data, it is useful to imagine two similar situations, with the only exception being the direct signal; in the second scenario, the direct signal is 10 dB weaker than the first scenario. All the other reflected signals are the same in both situations. As the intensities are measured in relation to the most intense echo, which always evaluates to 0 dB, it is as if all the reflected echoes had suffered a tenfold increase in their power in the second scenario, compared to the first. It means that the weights of all the delays of the reflected signals become ten times larger. As a consequence, the average delay T_D had a considerable increase, even if the echoes have remained exactly the same.

Based on this reasoning, it is possible to conclude that a reduction in the direct signal is accompanied by an increase in the 'average time delay' parameter. Conversely, one elevation of the average delay is an indication of direct signal weakening, possibly a consequence of the loss of direct sight between the transmitter and receiver.

The measurements collected support this consideration. The route areas that have a perceptible increase in the average delay correspond to regions where there has been a reduction or even a suppression of the direct signal. In Fig. 2, in the area between 5 and 6 km, the increase of the average delay coincides with a decrease in received power. Both alterations occurred in a region of lower land, reinforcing the indication of the direct signal loss.

Another direct signal weakening indication is the occurrence of pre-echoes. The existence of negative delays signifies that the most intense echo was not the first to arrive. Therefore, the direct signal is not as strong, which indicates a likely obstruction in the first Fresnel ellipsoid.

C. Guard interval verification

The guard interval used by the digital TV transmitter that served as a signal source for the test is 63 µs.

It must be ascertained whether echoes that came after this interval have sufficient intensity to provide some risk of disturbance. In Fig. 6, the greatest delays found for each measurement are shown.

The capacity of a delayed signal to produce a disturbance depends on its intensity and its delay with respect to the main signal. In an ISDB-T_B system, a test [6] quantified the potential for a single echo and is shown in Fig. 7.

doi: 10.18580/setijbe.2015.7 Web Link: http://dx.doi.org/10.18580/setijbe.2015.7

A significant gap can be seen between the maximum delays measured in relation to the adopted guard interval.

VI. Conclusion

The analysis of 1580 signal intensity measurements and the echo profile and in each of them allows, among other considerations, the following conclusion:

- The Okumura-Hata model for large cities and frequencies above 300 MHz, while having provided an adequate approximation for small distances, it seems unable to cope with the Curitiba terrain variations, which were not very strong in the areas covered during the test. Errors higher than 30 dB are noted in Fig. 2.

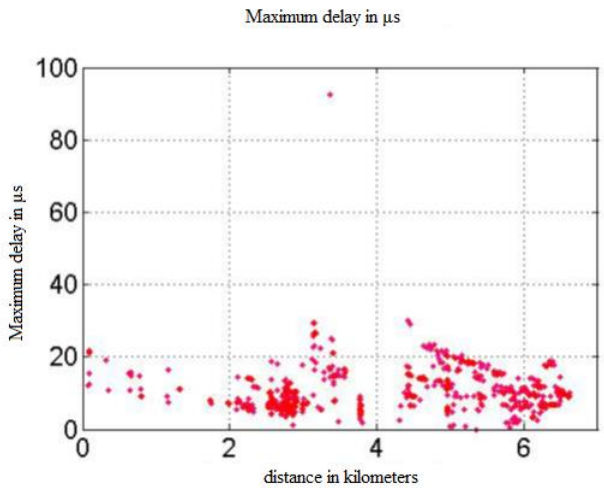

Fig. 6. Maximum delay value found for each measurement

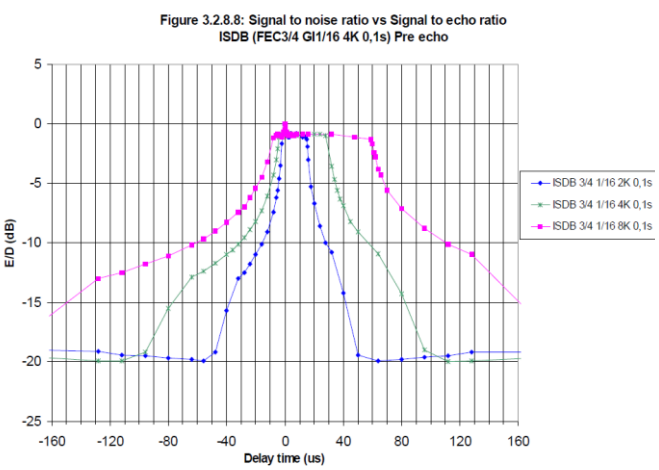

Fig. 7. Maximum admissible values for echo intensity in the ISDB-T_B system [6].

- It is important that the propagation model considers the topography and the diffraction in order to predict shadow areas within the area of coverage.
- Rare occurrences of degradation in image quality occurred in the exact locations where the signal level was low, comparable to the tuner sensitivity of -77 dBm used in the test. This fact is a strong indication that degradation is solely due to signal weakness; the measured multipath signals do not cause, per se, perceptible degradation in the received image.
- In the few regions where it was found, the signal weakening extended over several wavelengths. This means that the cause is the obstruction of the direct path (shadowing) by terrain or constructions. It is not caused by fast fading, as a result of multipath.
- In Fig. 2, it can be seen that an increase in the average delay measured correlates with a reduction in direct signal.
- Before the break found in the measurements, an eventual reduction in the guard interval can be considered, with the consequent possibility of an increased bit time rate.
- The occurrence of multipath is not always harmful; their existence allows reception in some locations that without the contribution of multiple paths would only have a signal with a power lower than the sensitivity of the receivers.
- The automated collection system used for measurements in the field proved to be practical in use. Measurements can be taken with the vehicle in motion, and a sensible number of locations can be assessed in a relatively short time, about 800 locations per hour. This allows a confident knowledge of the broadcasting coverage, in a fast way with greater accuracy than the models.

VII. Future Research

Some additional aspects can be analyzed concerning digital TV propagation in the urban region of Curitiba. The inclusion of the effect on the topography of the land caused by buildings in the model is one of them. Also intriguing is the fact that two models were necessary to obtain good adaptation to a single measured area. Another useful target for future research is the ability of the DTV signals to be captured within buildings since most broadcast television receivers make use of internal antennas.

Acknowledgment

The team that carried out this would like to express gratitude to Rede Paranaense de Comunicação, who kindly provided human resources and material, without which the work would not have been possible; the professors and LCD laboratory researchers of the Post Graduation Program in Electrical Engineering and Industrial Computing UTFPR, Curitiba campus, whose guidance and encouragement initiated and continued throughout the project.

References

[1] R. Schwarz, R&SR ETL TV Analyzer Operating Manual Volume 1.
[2] *Recommendation P.1407*, ITU-R P.1407, 1999.
[3] Anatel, "Descrição do sistema - características técnicas de operação da estação 690881088."
[4] T. S. Rappaport, *Wireless Communications Principles and Practice*, 2nd ed.,Prentice Hall PTR, 2002.
[5] E. W. LLC., *EDX Signal: Comprehensive Engineering Software for Wireless Communication System Design*, 10th ed., Oregon USA, 10 2008, rev. 018.

[6] U. M. A. S. Anatel, "Relatório final de testes de TV digital," Anatel, Tech. Rep.2, 2000.

Cite this article:
Costa de Borba, M. A., Neves Mayer, C. E., Ono Fonseca, K. V., de Almeida Prado Pohl, A., de Ramos Good, K., Mildemberg, L., Wosch, D. L. , and Martins, R. A. ; 2015. Experimental Investigation of Digital TV Signals with Multipath in Curitiba. ISSN Print: 2446-9246 ISSN Online: 2446-9432.doi: 10.18580/setijbe.2015.7 Web Link: http://dx.doi.org/10.18580/setijbe.2015.7

Factors that Influence the Performance of Digital Terrestrial TV Receivers in São Paulo

Paulo Guedes Esperante, Raquel Cymrot, Cristiano Akamine, Fujio Yamada, Rodrigo Eiji Motoyama, and Fabio Raia

***Abstract*—This article presents the factors that may degrade the reception of a digital TV signal, through the analysis of a communication channel. Methodologies and factorial experimental results with the communication channel are presented, and the analysis of meteorological factors that influence the reception quality of the ISDB-T_B system based on data regarding the quality of the digital signals collected from some TV stations in São Paulo. From the data obtained, statistical techniques were applied, such as planning and analysis of factorial experiments, simple and multiple linear regressions tests for measurement equality in order to determine which factors had greater influence on the degradation of digital TV signal.**

***Index Terms*—Digital TV, Meteorology, Statistics.**

I. Introduction

ACCESS of digital TV signals by the general population is related in part to the quality of the signal received. A digital TV, with the use of its interactive possibilities, can provide services and information to citizens. With a better understanding of the factors that can influence the reception quality it is possible to better plan the receivers locations, to maximize coverage in the country, leading to the inclusion of this service for more Brazilian citizens.

One of the factors that influence the digital signal reception quality are the noises. The noises are spurious that disturb the transmission channel and signal reception processing and can be classified as external system factors, for example, atmospheric noise, galactic noise, manmade noise or the internal system factors, for example, impulsive noise and thermal noise [1]. These noises are related to various meteorological factors and, therefore, cause disturbances in the transmission channel.

Based on this concept, data was collected simultaneously regarding both digital signal quality and meteorological conditions. By applying statistical methodologies to the results, it was possible to check the meteorological factor with the greatest influence on the degradation of the digital signal quality in the Integrated Services Digital Broadcasting-Terrestrial version B system (ISDB-T_B).

With the constant evolution of technology and having a predetermined system, further research should be conducted. When the survey includes quantitative data collection, it is necessary that the statistical analysis of the data is performed by a careful choice of the tools used, always testing the validity of the model assumptions necessary for the application of each analysis technique [2].

Among the possible statistical methodologies that may be used, experimental factorial designs 2^k stands out, which is very useful in preliminary investigations when it is necessary to determine the main factors and interactions that can influence the result of an experiment. In this case, each factor is presented in two distinct levels as reference [3]. This method is used by scientists and engineers aiming to improve systems, processes, and products based on the results obtained in these experiments.

Another application methodology is multiple regression analysis that aims to model and investigate the relationship between a dependent variable and one or more explanatory variables (regressive) [2].

For the two methods mentioned above it is essential to carry out residual analysis to verify the theoretical assumptions needed for their use were met [2].

II. Adopted Procedure

In order to relate the digital modulated signal in the ISDB-T_B standard with meteorological data, the meteorological variables analyzed that have the ability to contribute to noise generation in digital TV signal reception were: wind speed (m/s), wind direction, temperature (°C), Pressure (hPa), and light intensity (W/m²). To assess the quality of the digital signal the signal level and signal-to-noise ratio (C/N) for receiving data in each channel were observed. These measurements were made in São Paulo, in the Itambé campus of Mackenzie Presbyterian University, with a meteorological data collection system and a VHF/UHF antenna, connected to a demodulator, installed very close to each other. To evaluate the signal quality some TV stations in São Paulo with digital signal transmission were selected, and data collection was completed within one week for each TV station.

A statistical tool was applied to the collected data in order to check the level of influence of each variable under study.

Paulo Guedes Esperante is a Project Engineer at SBT, São Paulo, Brazil (e-mail: pauloesperante@gmail.com).

Raquel Cymrot is a professor at Mackenzie Presbyterian University, São Paulo, Brazil (e-mail: raquel.cymrot@mackenzie.br).

Cristiano Akamine is a professor at Mackenzie Presbyterian University, São Paulo, Brazil (e-mail: cristiano.akamine@mackenzie.br).

Fujio Yamada was a researcher at Mackenzie Presbyterian University, São Paulo, Brazil

Rodrigo Eiji Motoyama is an engineer at DTH service provider, São Paulo, Brazil (e-mail: rodgsp@gmail.com).

Fabio Raia is a professor at Mackenzie Presbyterian University, São Paulo, Brazil (e-mail: fabio.raia@mackenzie.br).

doi: 10.18580/setijbe.2015.8 Web Link: http://dx.doi.org/10.18580/setijbe.2015.8

In factorial experiments, it is common to use a table of contrasts to simplify calculations for checking existence of the main effects and interactions among the variables. The factorial experimental are also known for delimitation of L^k, where k stands for the total number of factors in this experiment and L is the number of levels tested for each factor, assumed equal, as reference [4].

Table I outlines the contrasts for an experiment design for 2^3:

TABLE I
CONTRAST COEFFICIENTS OF A 2^3 FACTORIAL DESIGN INPUT

Experiment	Interactions						
	A	B	C	AB	AC	BC	ABC
1	-1	-1	-1	1	1	1	-1
2	1	-1	-1	-1	-1	1	1
3	-1	1	-1	-1	1	-1	1
4	1	1	-1	1	-1	-1	-1
5	-1	-1	1	1	-1	-1	1
6	1	-1	1	-1	1	-1	-1
7	-1	1	1	-1	-1	1	-1
8	1	1	1	1	1	1	1

Source - Barros; Scarminio; Bruns (2003, p.111)

All factors begin with the value -1. The first factor (A) changes the signal every $2^0 = 1$ line. The second factor (B) changes the signal every $2^1 = 2$ lines. The third factor (C) changes the signal every $2^2 = 4$ lines. If it had more factors, the signals would follow these rules successively. In the interaction between the factors, the signal used is related to the multiplication of signals between its columns, in the corresponding lines.

The experimental design should provide the necessary answers, using the lowest possible number of experiments (runs). When economic conditions and time to perform the experiments permit, it is advisable that the design use at least two replicas so that it is possible to estimate the error without confusion. When the use of replicas is not possible, the error will be confused with minimum interactions to the order of three, because they are generally negligible [2].

In factorial experiment $2^{4,}$ on the threshold (-1) the variables were at their minimum, those being multipath, impulsive noise, white noise, and signal intensity. In this situation, the signal would not be suffering sufficient inference to cause degradation in the image decoded by the receiver. At level (+1) the signal would be suffering interference (the same commented previously). The C/N ratio used was 22 dB, the value adopted being slightly above that recommended by the Agência Brasileira de Normas Técnicas (ABNT), whose signal-to-noise ratio is 19 dB to determine the parameters of the variables, which can be seen in [5].

In the second experiment of this article, the Kruskal-Wallis test was used to decide whether the samples come from the same or different populations. This non-parametric test is used when the assumptions to perform parametric variance analysis do not exist and only requires that random errors have the same continuous distribution to all levels of the factor in question. In the Kruskal-Wallis test, each observation is replaced by its respective position as reference [6].

The Kruskal-Wallis test uses the H-statistic calculated by the expression (1):

$$H = \frac{12}{N(N+1)} \sum_{i=1}^{a} \frac{R_i^2}{n_i} - 3(N+1) \quad (1)$$

where N equals the total number of observations, n_i is the number of factor observations in the level i, and R_i equals the sum of the posts of factor observations in level i. If there is an equal value in posts, an average post is used and the expression changes to (2):

$$H = \frac{1}{S^2} \left[\sum_{i=1}^{a} \frac{R_i^2}{n_i} - \frac{N(N+1)^2}{4} \right] \quad (2)$$

where S^2 is equal to the posts variance.

Rejecting the equality hypothesis of the average in the various levels of factor if H is greater than the value of the chi-square with (a - 1) degrees of freedom, if a = 3 and $n_i \geq 6$ for all i or if a > 3 and $n_i \geq 5$ for all i seen in [2].

III. LABORATORY EXPERIMENTS

For the study of factors that can influence the internal antenna reception performance, emulations were completed with the following devices: a Rohde & Schwartz SFU-Broadcasting Test System signal source model, a Spirent TAS Signal Simulator 4500 Flex RF Chanel emulator model, a Rohde & Schwarz RF step attenuator, two Huber + Suhner combiners, a TAS-impulsive noise generator, a Micronetics white noise generator, a demodulator plate developed by Mackenzie, a HP VSB/QAM HP89441-V Spectrum Signal analyzer, and a Huber + Suhner impedance detector ("Ballun").

The emulation for transmitting the digital signal was performed in channel 15 with a frequency of 479 MHz +1/7 MHz. The transmission parameters used in the tests were: 1/16 guard interval, 64 QAM modulation, Mode 3, 3/4 of FEC (Forward Error Corrector), and time interleaving of 0.2 seconds. Such standards are commonly used in practice by many broadcasters, and these characteristics were the same in both experiments. Emulations were made within a Faraday cage present in the Digital TV Research Laboratory at Mackenzie Presbyterian University in order to avoid adjacent channel interference and co-channel of digital TV signals broadcast in São Paulo.

Experiments with a 2^4 factor design were performed, in which the variables were analyzed: signal level (-64.02 dBm power just below the threshold and -61.02 dBm just above the threshold), the presence of white noise interference (with -92.78 dBm power just below the threshold and -90.00 dBm just above the threshold), the presence of impulsive noise interference (with a power of -88.4 dBm, 10 ms periods and window width varying between 1 ms and 3 ms, respectively below and above the threshold), the presence of multipath (63 µs delay with 6 dB attenuation with respect to the main signal just below the threshold and 3 dB just above the threshold), with an ISDB-T_B receiver.

Statistical tests were performed with the help of Minitab® statistical software, with a significance level equal to 5%.

doi: 10.18580/setijbe.2015.8 Web Link: http://dx.doi.org/10.18580/setijbe.2015.8

IV. Results

Two experiments were conducted at the Digital TV Research Laboratory at Mackenzie Presbyterian University. In the first experiment, 2^4 factor, there were three replication of each treatment with the following factors, multipath, white noise interference, signal strength, and impulsive noise interference. Variables collected were signal level, C/N rate, bit error after the convolutional decoder (Layer A), Layer A packet error after the Reed Solomon Decoder (number of erroneous packets in the layer).

Table II presents the descriptive factor levels and interactions that were significant for any of the variables measured. The number of Layer A error packets was not submitted because their values were mostly zero, and not having such adequate data precision. Residual did not show Normal distribution.

TABLE II
Descriptive Levels of Some Effects and Interactions

Term	Signal level	C/N	Layer A
multipath (A)	0.002	0.000	0.000
white noise (B)	0.400	0.000	0.000
signal intensity (C)	0.673	0.050	0.165
impulse noise (D)	0.000	0.000	0.000
A*B	0.4000	0.000	0.000

The researchers decided it would be better to only investigate the multipath factors and impulse noise, because they are the ones who have the greatest influence on the reception quality of the Brazilian digital TV system using four levels of each variable.

To find a limit for each threshold and determine which form of noise is predominant over the signal, another experiment was performed with impulsive noise and multipath factors, but with four levels each. The values used for the impulsive noise level was -84.4 dBm for a period of 10 ms and a window width of 3 ms, and the four levels ranged from -37 dBm to -46 dBm in 3 dBm increments. The reception threshold in the presence of multipath was completed by adjusting the main signal to -54 dBm in the presence of a delayed echo signal of 62.2 µs with respect to the main signal. In this test, the echo level was attenuated from 0 to 6 dB with a variation of 2 dB in relation to the principal signal level. The initial value of the C/N ratio established for this test was 23 dB.

Only the C/N and bit error variables after the convolutional decoder (Layer A) could be evaluated, once the variable signal level is kept constant for each multipath level, the number of packet errors in Layer A were not precisely adequate. For the C/N variable, the residual did not show a Normal distribution ($P < 0.005$), nor equal variances ($P = 0.011$ for the Levene test). The variable bit error after the convolutional decoder (Layer A) had two main effects, as well as its significant interaction, all with $P = 0.000$. Its residual had a Normal distribution ($P = 0.107$), but the variances equality assumption was not observed ($P = 0.029$ for the Bartlett test). As can be seen in [7], test F is robust.

Fig. 1 presents bit error residual after the convolutional decoder (Layer A).

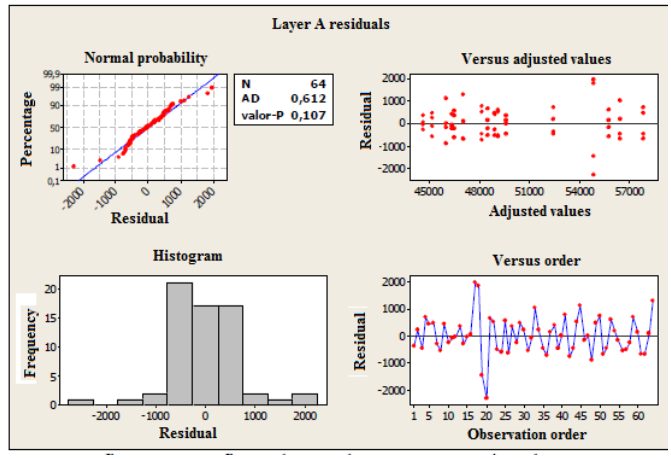

Fig. 1. Residual plots for the variable Layer A

It was decided to perform only a descriptive analysis by analyzing the charts of individual values for the variables signal level, C/N, and bit error after the convolutional decoder (Layer A), and Layer A packages errors after the Reed Solomon decoder (number of error packets in Layer A) as shown in Figs. 2, 3, 4, and 5.

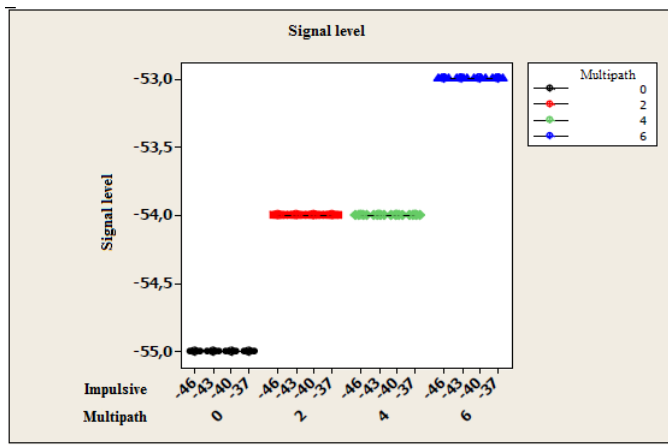

Fig. 2. Individual values for signal level, varying multipath and impulsive noise

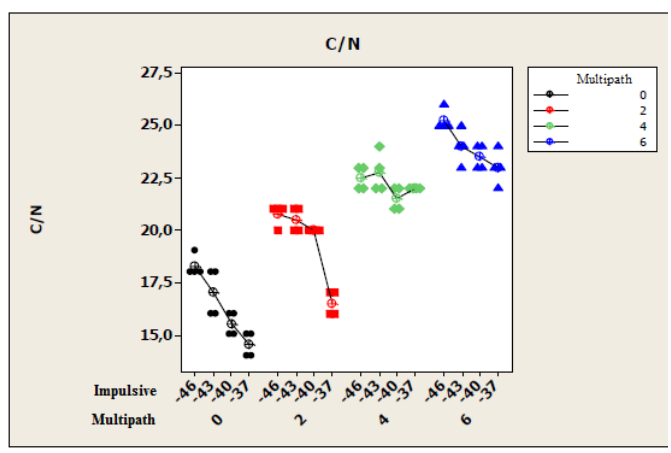

Fig. 3. Individual values for C/N, varying multipath impulse noise

doi: 10.18580/setijbe.2015.8 Web Link: http://dx.doi.org/10.18580/setijbe.2015.8

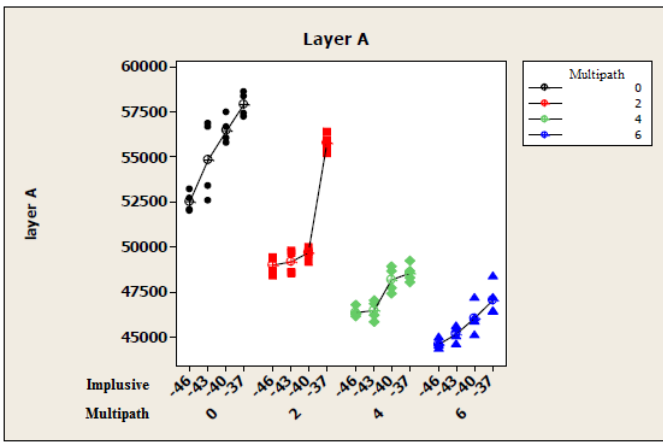

Fig. 4. Individual values for Layer A, varying multipath and

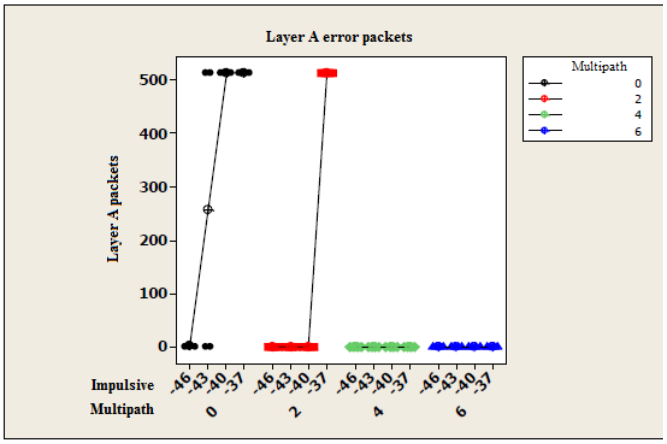

Fig. 5. Individual values for the number of the error packets in Layer A, varying multipath and impulsive noise.

The results show that for the signal level, when enhancing the echo power of the multipath, the signal was less degraded. In this case, the variation in the intensity of impulsive noise did not influence the results. The signal level remained constant for the same multipath even though the impulsive noise varied. For the C/N rate, when enhancing the echo power of the multipath, the signal was less degraded, but by increasing the intensity of the impulsive noise the signal suffered more degradation. When a signal is less degraded fewer errors occurred (Layer A), as the signal level of the echo is increased and by the fact that the echo signal boosts the received signal the number of errors decreases. The opposite occurs by increasing the intensity of impulsive noise. For multipath 4 dB and 6 dB (attenuation), there were no error packets in Layer A after the Reed Solomon decoder.

In the second part of the research, based on data collected by the external antenna, the transmissions are made by stations A, B, C, D, E, F, G, and H are divided into three clusters. Fig. 6 shows the arrangement of the clusters:

Mean equality tests were carried out for the C/N and the signal level, using the non-parametric Kruskal-Wallis test, in both cases, the equality assumptions for all measurements were rejected (P = 0.000).

In the C/N analysis, stations with the highest average were those of cluster 2 with two stations that obtained the highest C/N, followed by a station in cluster 1 and a station in cluster 3. Stations with a lower level response are three stations in cluster 1 and a station in cluster 3. One possible reason for cluster 2 obtaining the highest average is the fact that these are located closer to the Mackenzie receiver. In turn, the lowest average may have occurred due to the signal power transmitted by such stations.

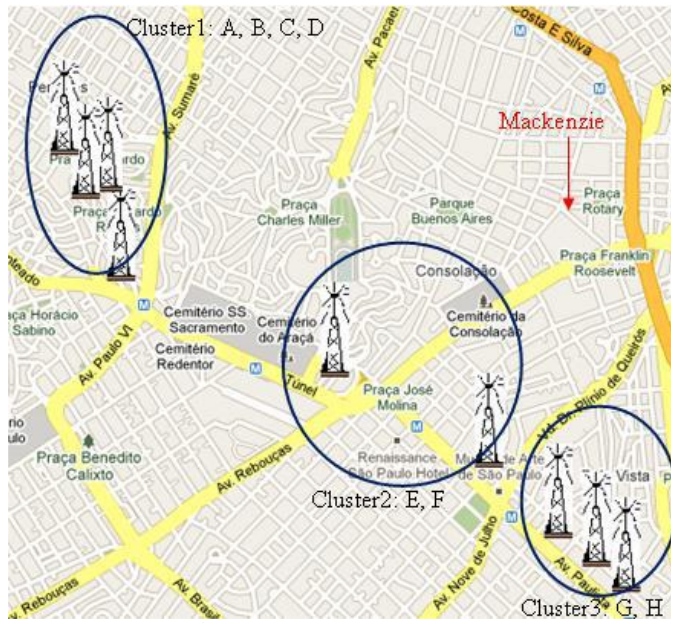

Fig. 6. Arrangement of clusters

Simple and multiple regressions were performed for C/N and the signal level using possible regressive variables like temperature, wind speed, wind direction, pressure, and intensity of light. The humidity variable, though presumably important, cannot be used because of strange values presented in its measurements.

In all possible regressions, the residuals did not adhere to the Normal distribution, nor was there independence between them. Due to the model assumptions not being satisfied their use was not possible. This article merely studied the linear correlations between the variables temperature, wind speed, wind direction, pressure and intensity of light, with a C/N and signal level variable for each station, presented in Tables III and IV.

TABLE III
METEOROLOGICAL VARIABLES, LINEAR CORRELATION COEFFICIENT AND P-VALUE FOR C/N

Issuer	Variables	Correlation	P-value
H	Temperature	-0.269	0.000
G	Temperature	-0.333	0.000
H	Wind speed	-0.292	0.000
F	Wind speed	0.268	0.001
G	Wind speed	-0.29	0.000
F	Wind direction	0.486	0.000
G	Wind direction	-0.154	0.047
E	Pressure	0.328	0.000
G	Light intensity	-0.171	0.027

Stations G and H showed decreasing linear relation between C/N and the temperature, which can be explained by the

doi: 10.18580/setijbe.2015.8 Web Link: http://dx.doi.org/10.18580/setijbe.2015.8

thermal noise of the receiver. With increased temperature, the C/N ratio decreases. Another possible reason is that stations G and H are subject to the adjacent channel effect, since both are close in terms of frequency range. Furthermore, the physical location is next to one another, are thereby subject to the same temperature variation. Possibly the light intensity variable at station G had a negative correlation with the C/N, as a warmer day tends to have higher brightness.

TABLE IV
METEOROLOGICAL VARIABLES, LINEAR CORRELATION COEFFICIENT AND P-VALUE FOR THE SIGNAL LEVEL

Issuer	Variables	Correlation	P-value
F	Temperature	-0.570	0.000
B	Temperature	0.239	0.002
C	Temperature	0.400	0.000
E	Wind speed	-0.213	0.009
F	Wind speed	0.241	0.003
G	Wind speed	-0.196	0.011
C	Wind speed	0.153	0.033
F	Wind direction	0.246	0.002
H	Pressure	-0.346	0.000
E	Pressure	0.352	0.000
F	Pressure	0.220	0.006
B	Pressure	-0.375	0.000
C	Pressure	-0.153	0.033
F	Light intensity	-0.557	0.000
B	Light intensity	0.184	0.017
C	Light intensity	0.192	0.007

At the same time, it was found that the wind speed and wind direction are related in the same way with C/N, having a positive or negative correlation, depending on the station. One possible reason for this situation is the balance of the receiving antenna, which changes the directivity beam of the antenna (the receiving antenna is directive). The correlation was, therefore, positive for certain other stations, and in fact negative for other due to the distance and location of each transmitter relative to the receiver antenna having the wind speed and wind direction favoring or hampering the transmission.

Another possible explanation could be the fact that the humidity may have influenced this result since the humidity in some situations varies the azimuth of the horizontal plane favoring or hampering the signal level. However, the data concerning the humidity had to be discarded, being a suggestion for the development of another study where this variable can be measured more reliably.

The pressure variable appeared with linear correlation significantly different from zero, possibly being indirectly related to humidity and as the humidity factor cannot be considered due to problems found in data collection, in addition the pressure variable cannot be considered as a precise variable. There are cases where the pressure interferes with the transmission, but its occurrence would be in frequency waves above 1 GHz, which is not the case for standard Brazilian digital TV broadcasts.

Stations F, B, and C were significantly different from a zero correlation between the signal level and temperature, which may again be explained by the thermal noise in the receiver. Together with the presence of thermal noise, depending on the distance between the transmitter antenna and the receiving antenna, the temperature correlation with the signal level can be positive or negative. The distance contributes to the existence of this correlation since varying the distance of the station's antenna to the receiving antenna, changes the azimuth of the horizontal plane and, therefore, the intensity of the electric field. Again in the analysis of correlations between the C/N and the light intensity accompanying the temperature in correlation with the signal level. Thus, stations F, B, and C contain linear correlation between the signal level and the light intensity significantly different from zero. The fact that stations B and C are subject to the adjacent channel effect also contributed to this similar behavior.

The wind speed was also one of the factors that influenced the reception of some stations (C, E, F, and G), interfering with the signal level. The correlation with the wind velocity was at certain stations positive and negative for others because the wind speed at certain stations promotes or hinders the transmission due to the distance from the transmitter. Similar to the C/N ratio, humidity could possibly be influencing these results. Only for station F was the wind direction positively correlated with the signal level, probably due to its location. One possible factor for this relationship is the balance of the receiving antenna that changes the directivity beam of the antenna.

V. CONCLUSION

In this article it was concluded that digital TV is a communication system that must be studied. As a over-the-air transmission, different types of interference can occur, causing changes in thousands of receivers (Set-Top Box).

It can be seen in laboratory tests completed, in which values for certain variables were applied, that the variables that occur with greater frequency in the receiver are multipath and impulse noise, and the results showed signal level loss and value in relation to C/N, when subjected to certain power levels as mentioned above.

Linear correlations were found between the meteorological variables such as temperature, speed, wind direction, and light intensity with variables representing the signal quality such as signal level and C/N ratio for the reception of digital TV, but these depended on location the each station's antenna in relation to the receiving antenna.

In Kruskal-Wallis non-parametric analysis, the relation of C/N ratio and the signal level were evaluated, it was concluded that by analyzing the results and map of station transmission antennae, the distance between the station antennae and the receiving antenna influences the reception.

How much the signal function is effected by meteorological variables indicates that this study should be repeated, measurements of humidity could not be used due to failure in the measure and a possibly prolonging the period of the data evaluation.

Therefore, by applying statistical methods, it was possible to show in numbers, the factor of influence each type of meteorological data has on the degradation of reception quality of the digital signal.

ACKNOWLEDGMENT

The authors acknowledge the support of the Instituto Presbiteriana Mackenzie (PIBIC/Mackenzie) for this research, teachers, and friends of the Digital TV Research Laboratory at Mackenzie Presbyterian University.

REFERENCES

[1] S. Haykin, *Sistemas de Comunicação Analógicos e Digitais.* 4th ed. Porto Alegre, Brazil: Bookman, 2004.
[2] D. C. Montgomery, and G. C. Runger, *Estatística Aplicada e Probabilidades para Engenheiros*. 4th ed. Rio de Janeiro, Brazil: LTC, 2009.
[3] N. B. Barros, I. S. S. Scarminio, R. E. Bruns, *Como Fazer Experimentos: Pesquisa e desenvolvimento na ciência e na indústria*. Campinas, Brazil: Unicamp, 2003.
[4] A. W. Ramos, *Melhorando o processo: delineamento de experimentos.* In: R. G. Rotondaro, "Seis Sigma: estratégia gerencial para a melhoria de processos, produtos e serviços." São Paulo, Brazil: Atlas, 2002.
[5] *Receptores*, NBR 15604, 2008.
[6] W. J. Conover, *Practical Nonparametric Statistics.* New York: John Wiley and Sons, 1999.
[7] J. Neter, W. Wasserman, M. H. Kutner, *Applied Linear Statistical Models,* 5th ed. New York: McGraw-Hill, 2005.

Paulo Guedes Esperante received his BS in Electrical Engineering at Mackenzie Presbyterian University, did graduate studies in Networks and Telecommunications at INATEL, and received his MS in Electrical Engineering at Mackenzie Presbyterian University. He is working at SBT as Project Engineer. He is focused on broadcasting areas (production), studies of digital television broadcasting system, microwave, and satellite communications.

Raquel Cymrot received her BS and MS in Statistics from the Mathematics and Statistics Institute at São Paulo University. She is currently a professor at Engineering School of Mackenzie Presbyterian University and a member of the Research Ethics Committee – Humans at Mackenzie Presbyterian University. She has published several articles and book chapters and participated in several national and international conferences.

Rodrigo Eiji Motoyama received his BS and MS in Electrical Engineering from Mackenzie Presbyterian University (São Paulo, Brazil) in 2007 and 2010. From 2006 to 2010, he was a researcher at Digital TV Research Laboratory at Mackenzie Presbyterian University. He is currently an engineer at DTH service provider and involved in the area of video coding and transmission technologies.

Cristiano Akamine He received his M.Sc. and Ph.D. degree in Electrical Engineering from the State University of Campinas (UNICAMP), São Paulo, Brazil, in 2004 and 2011 respectively. He is a professor of Embedded Systems, Software Defined Radio and Advanced Communication Systems at Mackenzie Presbyterian University. He is a researcher in the Digital TV Research Laboratory at Mackenzie Presbyterian University since 1998, where he has had the opportunity to work with many digital TV systems. His research interests are in system on chip for broadcast TV and Software Defined Radio.

Fujio Yamada was holder of the title Professor Doctor at the Engineering School at Mackenzie Presbyterian University and a researcher at Digital TV Research Laboratory at Mackenzie Presbyterian University. He has participated in several events as a speaker and moderator at conferences and symposia presentations.

Fabio Raia graduated in Physics at Mackenzie Presbyterian University, he has a Master's degree in Computer Science at Mackenzie Presbyterian University and a Ph.D. in Reactor Technology at the Institute of Energy and Nuclear Research (IPEN). He is currently a teacher at Mackenzie Presbyterian University. He has published several articles in Engineering.

Cite this article:
Guedes Esperante, P., Cymrot, R., Akamine, C., Yamada, F., Motoyama, R. E. , and Raia, F.; 2015. Factors that Influence the Performance of Terrestrial Digital TV Receivers in São Paulo. ISSN Print: 2446-9246 ISSN Online: 2446-9432. doi: 10.18580/setijbe.2015.8 Web Link: http://dx.doi.org/10.18580/setijbe.2015.8

Digital TV Signal Reception Testing in a Device with Spatial Diversity

Eduardo Romani, Wyllian Bezerra da Silva, Marco Antônio Costa de Borba, Keiko Verônica Ono Fonseca and Alexandre de Almeida Prado

***Abstract*—This paper presents the test results performed in internal and external environments employing tuner demodulator hardware with spatial diversity. Two types of antennae were used: monopole and hemispherical helical. The results demonstrated the superior performance of the system with spatial diversity.**

***Index Terms*— Digital TV, Spatial diversity.**

I. Introduction

THE introduction of Digital TV transmissions in Brazil, in December 2007 has motivated this research, the development and testing of systems and equipment for the processing, transmission, and reception of video and audio signals [1] [2] [3] [4]. In particular, the development of reception systems has been the focus of many studies [5] [6]. The requirements for receiving LD signals (Low-Definition) and HD signals (High-Definition) in fixed and mobile environment can vary dramatically. The reception of HD signals is usually performed with an external directional antenna placed on the roof of a residence with an average height of 10 meters. If placed on a building whose height is variable, the signal will have to be distributed among the apartments with the use of a network of cables and amplifiers. However, there is a tendency to avoid external antenna and to make use of an internal antenna, generally coupled to an amplification system. On the other hand, LD signal reception in a mobile environment typically employs a smaller size and omnidirectional antenna with lower gain. It is also at a lower height from the ground, between 1 and 1.5 meters. In addition, the mobile signal is subject to fading and Doppler effects, making the received signal strength vary abruptly and with greater intensity fluctuation. The robustness of the modulation system (QPSK) used in LD signals compensates for these effects allowing its reception in adverse conditions. However, there is a tendency also to receive HD signals in the mobile environment. However, this would create new challenges for the reception of the signal. One solution to improve performance is to employ a system with spatial diversity reception, which can use two or more antennae. In this case, the signals from different antennae are evaluated and processed using specific algorithms to increase the carrier-to-noise ratio (C/N) at reception. A Project carried out between 2009 and 2010 by a group of universities (Inatel, Unicamp, Mackenzie, PUC-RS, UFSC, UTFPR), with participation of the Centro de Tecnologia de Informação (CTI), developed and tested a tuning demodulation system, using a market chipset [7]. The system developed allows reception with diversity through two antennae and uses a combination technique with a maximum ratio between the signals (Maximum Ratio Combining, MRC). This paper relates to the results of system tests performed on internal and external reception in Curitiba.

The paper is organized as follows: Section II describes the methodology for conducting the tests. Section III describes the results of tests considering reception with two different pairs of antennae used with the tuner demodulation system. Section IV contains the conclusion.

II. Methodology

The tuner demodulation system test was performed in internal and external environments with the use of two different pairs of antennae, namely, a pair of monopole antennae and a pair of hemispherical helical antennae (HHA), these antennae were developed by the Centro de Pesquisa em Tecnologia Wireless (CPTW) of the Pontifíca Universidade Católica de Rio Grande do Sul [8]. The design of the tuner-demodulator board was developed by the Laboratório de Desenvolvimento de Hardware do Inatel [9]. During the tests in Curitiba a RF spectrum analyzer (Agilent) and a TV signal analyzer (Rohde & Schwarz) were used to check the signal level and certain features, such as echo pattern and the measurement locations.

The tests were carried out with the application of two different procedures: one for internal measurements, carried out inside the Universidade Tecnológica Federal do Paraná (UTFPR) and the others are field measurements, carried out in various parts of the city of Curitiba, both are detailed in the following sub-sections:

A. Test Procedure for internal measurements

In preparation for this procedure, the expected behavior of a home user when trying to receive a digital TV signal through an internal antenna was used as the criteria, in this case, the pair of antennae has been kept close to the tuner, but the antennae were separated by a half wavelength (in the case of monopole antennae). The assembly was placed in the environment to maximize the received signal level at the input of the spectrum analyzer.

The test configuration is seen in Fig. 1. The pair of antennae (monopole or HPA) is connected to the tuner input. An ASI connection (Asynchronous Serial Interface) has been developed especially on the tuner card to allow the signal

doi: 10.18580/setijbe.2015.9 Web Link: http://dx.doi.org/10.18580/setijbe.2015.9

output to go to a Dektec (STP-225), which allows analysis of transport stream (TS) of the received signal. In turn, an output of the DTU is connected to a laptop, which can access the analytics platform provided by the DTU and collect data that is recorded in a log file, in an automated manner. These values are recorded in a cvs file and subsequently transferred to a spreadsheet for analysis and processing. The ASI connection between the tuner and the DTU also allows the recording of TS, thanks to StreamXpert software.

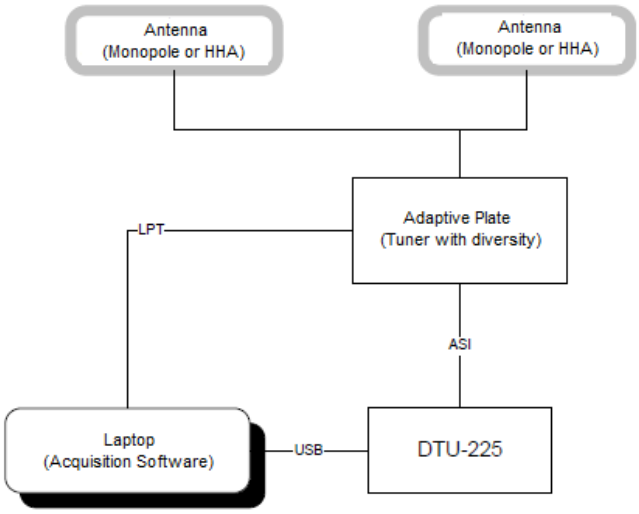

Fig. 1. Assembly diagram of equipment for internal measurements

Due to the extreme variability of the signals in the indoor environment, the following antenna alignment procedure was adopted and repeated in each of the locations measured:

• With a monopole antenna (less directional) in an upright position, connected to the spectrum analyzer input (programmed to indicate the total power received in the channel with 6 MHz bandwidth), seeks the position that provides the maximum received power. Thus, defines the position of the antenna called Av; recording the received power value of the spectrum analyzer, determined by the function averaging 100 scans. The averaging time is 10 seconds.

• Repeating the same procedure with the second monopole antenna coupled to the analyzer input; in a vertical position, the position being defined the Bv antenna;

• The previous two steps are repeated, with the monopole antenna in horizontal position, determining the positions Ah and Bh;

• A procedure analogous to the maximization of the received signal is adopted with the two HHA antennae. As both are mounted on the same vertical mast, after finding the optimal position for the upper antenna, the lower antenna turns itself until it points in the direction of maximum reception, following a reading taken by the spectrum analyzer. Registering the azimuth at each location, and the received power value of the spectrum analyzer, smoothed by the averaging function in 100 scans. The azimuth recorded is the angle between the directions of maximum antenna gain relative to the perpendicular direction to the north wall of the room, measured clockwise for those who look up at the antenna.

• After the maximization of the power points being carried out at the chosen location, the analyzer antenna is disconnected and, the tuner system connected. Tune to the chosen channel through the software that comes with the tuner that runs on the Linux operating system, and emulated by VMWare Player. If the signal can be accessed by the decoder, the DCT-320 StreamXpert software is used for accessing the signals in LD (Low Definition) and HD (High Definition) resolution.

• If the signal can be accessed at the measurement point, the TS and data logs received by tuner are recorded, such as AGC (Automatic Gain Control), SNR (Signal-to-Noise Ratio), BER (Bit Error Rate), and MER (Modulation Error Rate). This data is recorded individually in files for the master modes (main tuner), slave (secondary) and combined mode.

B. Test Procedure for external measurements

To perform the external measurements apply the same procedure for aligning the antenna for internal measurements as described, however for the external measurements are taken at several locations in Curitiba, setting up the equipment and positioning the antennae with the aid of the test vehicle on loan from Rede Paranaense Comunição (RPC). Measurements were performed with the vehicle stationary and with the aid of a Rhode Schwartz spectrum analyzer [10], whose output was coupled to a laptop through an Ethernet connection. The laptop has software developed by UTFPR, which performs the collection and storage of received data. The plotting of the data is graphically performed overlaying it on a map via a Google Maps API (Application Programming Interface). The geographical position of each measured location is obtained using a GPS unit that is connected to the same laptop through a USB connection, as seen in Fig. 2.

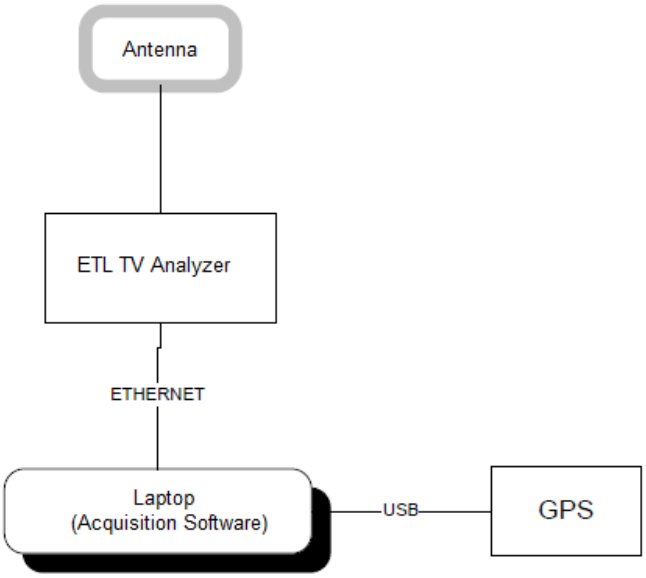

Fig. 2. Field trial system diagram

III. RESULTS

In the following sub-sections, the results are described,

doi: 10.18580/setijbe.2015.9 Web Link: http://dx.doi.org/10.18580/setijbe.2015.9

using the above procedures.

A. *Internal measurement results*

Indoors measurements were completed at 13 locations inside the UTFPR buildings, located in the center of Curitiba, at an approximate distance of 3.3 km from the transmitting antenna (channel 41). Fig. 3 shows a plan of the buildings in which the measurements were performed, noting that eight of them were taken on the ground floor, four on the first floor, and one in the basement.

Fig. 4 shows a graph of the received power at the input of the spectrum analyzer in the search function at the measurement location. The locations plotted on the horizontal axis begin with the basement location, continuing based on the height of the measurement location. From the results, it is evident that the HHA antenna provides better reception quality than the monopole antenna. The comparison shows that in only two locations did the monopole exceeded the performance of the HHA antenna, but in only one of these locations was it possible to access the signal. The HD signal could be accessed in 4 of the 13 locations with the HPA antenna while it could only be accessed in only 1 location with the monopole antenna. Note that the signal threshold to display the video is -74 dBm.

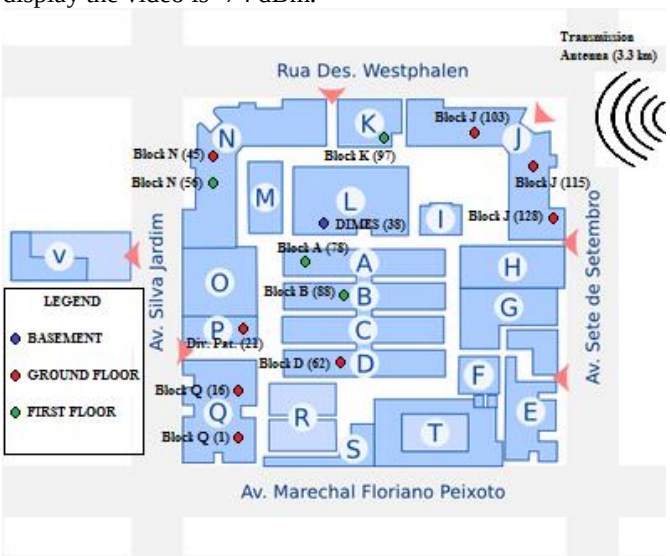

Fig. 3. SNR in each of the 202 samples in log 128.

Specifically, a comparison between the measurements can be stated as:

• In 5 of the 13 sites it continues to not be possible achieve reception of the signal, even with the use of spatial diversity and the use of more directive antennae;

• In locations closer to an opening (door, window, etc.) directive antennae performed better than the monopole antennae, and its optimal direction was related to the opening position: either pointing directly at it or a wall or object that more effectively reflects the signal that had passed through the opening;

• Where it was not possible to access and display video, the signal level was very close to or below the sensitivity threshold of the tuner (-77 dBm).

• As the measurements were carried out during normal university hours, people were moving in the vicinity of the antennae. At least one of the sites (log 21, Block P) this influence, was perceived; there was some variation in received power dB by the spectrum analyzer. However, no effect on the image was noticed.

As an example, Fig. 5 shows the signal-to-noise ratio (SNR) measured at Block J - Ground floor (log 128) with the tuner. The curves show the behavior of the SNR at each input (master and slave) and the combined SNR of the two antennae. It appears that the combined SNR is a few dB greater than the SNR of the individual antennae. In particular, it is observed that the combined value is valid until sample 140, and after this there is a loss of signal reception in the master antenna (probably due to the existence of a disconnection), causing the combined SNR value to agrees with the SNR value originating from the slave antenna.

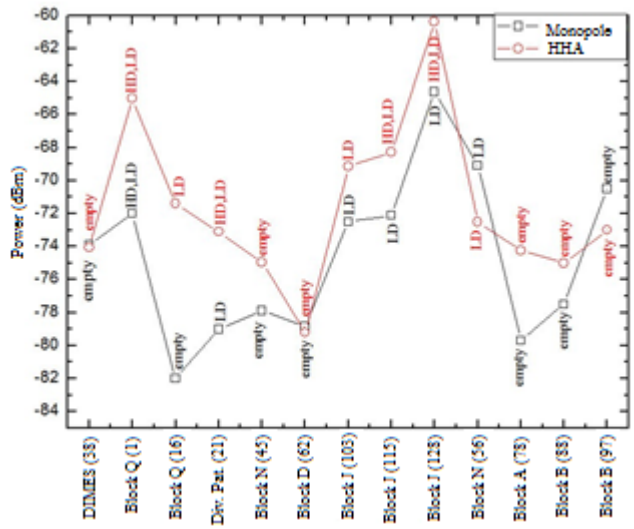

Fig. 4. Power measurements (dBm) in the indoor environment with an indication of accessing LD and HD signals

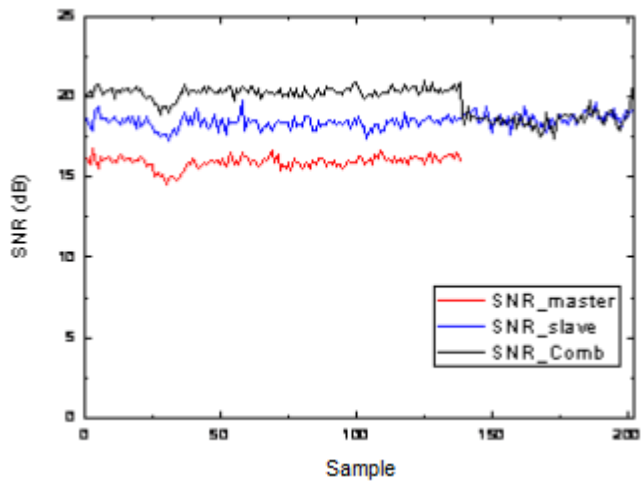

Fig. 5. SNR in each of the 202 samples of log 128

B. *External measurement results*

Nine (9) locations in the region of Curitiba were chosen to carry out the external measurements; these points had already been at locations with reception difficulty during when

doi: 10.18580/setijbe.2015.9 Web Link: http://dx.doi.org/10.18580/setijbe.2015.9

measurements were conducted in 2008 [3]. The purpose was to verify the performance of the tuner with spatial diversity at these locations. Initially, the signal characterization at the sites was performed with an ETL analyzer.

Table I provides information on the distances between the locations and the transmitting antenna, as well as the received power in the spectrum analyzer with each of the antennae.

TABLE I
DESCRIPTION OF THE LOCATIONS AND SIGNAL POWER AT RECEPTION

Location	Distance to the Antenna (km)	Altitude (m)	Signal amplitude (dBm)	
			HHA	Monopole
16	0.71	915.2	-29.75	-32.2
34	1.05	928.3	-46.79	-39.72
38	2.09	942.6	-47.53	-43.25
53	4.07	908.5	-51.45	-51.16
55	3.99	898	-50.72	-64.3
56	3.94	895.4	-61.92	-72.87
75	5.92	919.3	-64.05	-73.58
79	6	949.1	-59.87	-68.63
93	9	901.1	-80.05	-86.05
94	8.04	931	-53.63	-62.94

The distribution of the nine sites can be seen in Fig. 6, this also shows the measured power of the signals received by the HHA antenna using the TV analyzer. Note that at one location (93) the level was below the -70 dBm threshold established in the software. (However, it notes that the tuner sensitivity was observed at around -77 dBm).

The use of the ETL analyzer allows other parameters to be measured, such as the MER and the echo patterns related to multipath problems.

Fig. 6. Signals picked up with a HHA by an ETL TV Analyzer

The behavior of the received power as a function of the distance from the transmitting antenna can be seen in Fig. 8. Note the progressive decay of the largest signal level as the distance increases from the transmitting antenna. This decay theoretically occurs in an inversely proportional manner to the distance from the transmitting antenna, but in the chart it can be observed that some locations further away from the antenna have a greater signal amplitude than some closer locations, this occurs due to medium interference, such as buildings, vehicle movement near the measurement location, and also by multipath signals. In Fig. 7 the best performance of the HHA antenna in relation to the monopole antenna can be seen.

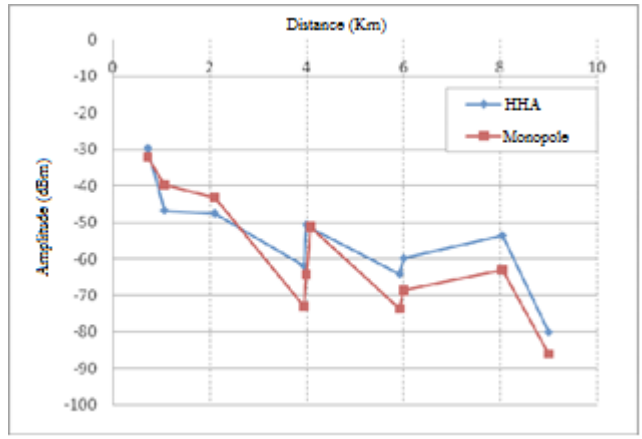

Fig. 7. Signal amplitude measurements (dBm) versus distance (km) in the external environment

The ETL analyzer allows the recording of standard echo signals at the measurement location, enabling the characterization of the multipath, that is, channel signals arriving at the receiving antenna along different paths. Figs. 8 and 9 show the relative echo amplitude (dB) versus time. The measurement is performed by taking the maximum received value as a reference for time t = 0. Negative values on the time axis represent lower amplitude signals that arrived at the analyzer first in relation to the highest measured signal amplitude. It can be seen that the amplitude of the echoes decreases the greater the delay time. It is observed that the maximum verified time delay in both cases, with reduced amplitude of 40 dB is relation to the maximum value, is less than the guard interval of the transmitted signal, which is 64 µs.

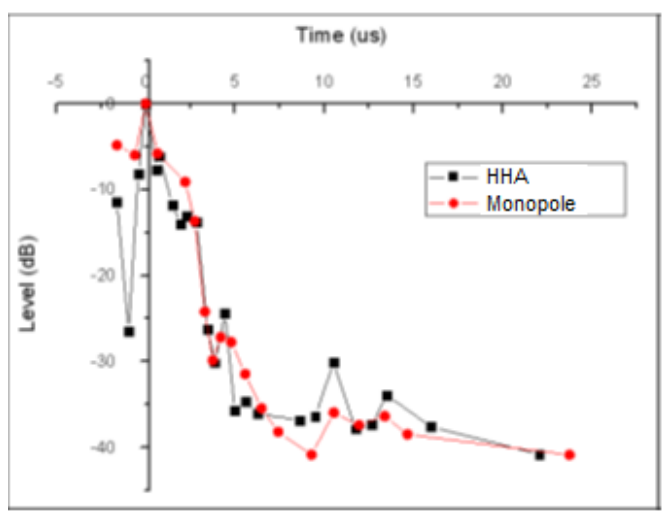

Fig. 8. Multipath signal measurements at location 79

doi: 10.18580/setijbe.2015.9 Web Link: http://dx.doi.org/10.18580/setijbe.2015.9

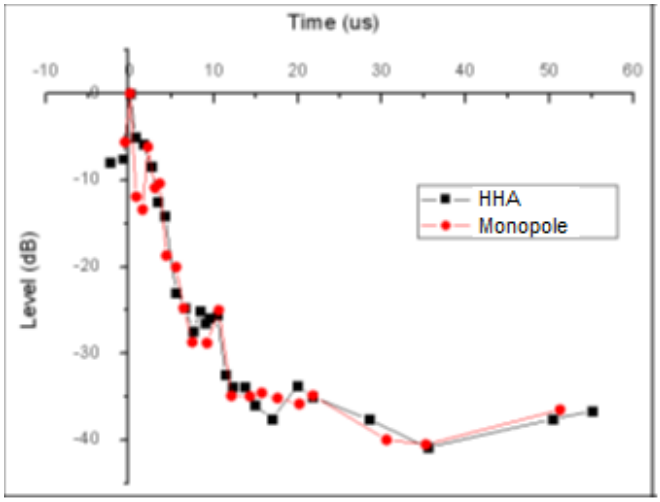

Fig. 9. Multipath signal measurements at location 94

The tuner-demodulator system was employed to make measurements at selected points, using, in this case, the HPA antennae. As noted in the internal measurements, the result of combining the master and slave signals produces a greater SNR value. This gain can reach a few dB, as shown in Fig. 10.

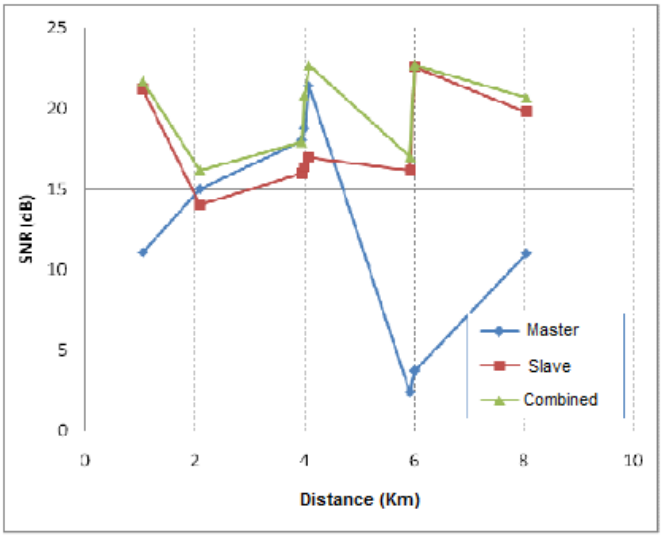

Fig. 10. SNR measurements (dB) versus distance (km) in the external environment

Another advantage of the system with spatial diversity is related to the fact that it provides the same SNR value, even when the signal at one of the antennae suffers a marked drop. In this case, the receiver will receive the antenna signal with the highest SNR. This situation is exemplified in the three most distant locations in Fig. 10, where the master antenna showed a sudden drop in SNR, while the slave input signal remained at acceptable levels, making the combined SNR acceptable.

IV. Conclusion

Field measurements were performed with HPA and monopole antennae using tuning modulation hardware with spatial diversity.

The measurement sites chosen were those previously selected for measurement in 2008, for both the UTFPR campus locations and the external locations.

The placement method chosen for the antennae tried to approximate the behavior of a home user seeking to receive TV signals with an internal antenna, who would try to achieve the positioning that provides the best reception.

In most places, the reception performance with the HHA antennae exceeded that observed with the monopole antennae.

It was difficult to obtain HD signals with power below -71 dBm while collecting the external measurements data. In addition, the reception of the high definition signal was subjected to variations in the master and slave channels, as well as disturbances at the measurement site. However, the use of spatial diversity provided a gain in the SNR of the combined signal of 2-3 dB when compared to those observed in the individual channels (master and slave).

Due to hardware difficulties of the HHA antennae on top of the test vehicle in Curitiba, signal capture could not be performed with the vehicle moving. Thus, the system performance faced a critical problem, the influence of the Doppler Effect and multipath could not be evaluated.

Acknowledgment

The authors acknowledge the research group at Laboratório de Desenvolvimento de Hardware do Inatel, coordinated by Prof. Luciano L. Mendes, responsible for the development of the tuner-demodulator board. The Centro de Pesquisas em Tecnologias Wireless, coordinated by Prof. Fernando César Comparsi de Castro, responsible for developing the HHA antenna and the Grupo Paranaense de Comunicação, in particular Mr. Ivan Miranda, for making the vehicle available for carrying out the tests in the external environment.

References

[1] G. Bedicks et al., "Results of the ISDB-T system tests, as part of digital TV study carries out in Brazil," *IEEE Trans. Broadcasting*, vol. 52, no. 1, pp. 38-44, 2006.

[2] B. P. Constanzo, and J. A. Neto, "Analysis of the Brazilian Digital TV System and Signal-Converting Devices," in *PICMET*, 6-9 August, Portland, 2007 pp. 1830-1838.

[3] C. L. Vasco et al, "Ensaios de Transmissão e Recepção de TV Digital Terrestre na Região Metropolitana de Curitiba," *Revista de Radiodifusão*, vol. 3, no. 3, pp. 63-76, 2009.

[4] W.B. da Silva e A. A. P. Pohl, "Framework de baixo custo para ensaios de TV digital", in *XXIX Simpósio Brasileiro de Telecomunicações*, Curitiba, 2-5 October, 2011.

[5] R. E. Motoyama, F. Yamada, C. Akamine e G. M. Valeira, "Método de Avaliação da Recepção do Sistema ISDB-Tb em Ambiente Indoor," *Revista de Radiodifusão*, vol. 3, no. 3, pp. 206-211, 2009.

[6] C. Akamine et al., "Field Trial for Brazilian DTV Using Space Diversity", in *IEEE International Symposium on Broadband Multimedia, BMSB 2010*, , Shangai, China, 24-26 March, 2010, pp. 1-11.

[7] Projeto SIRDAI, "Sistema de Recepção com Diversidade e Antenas Inteligentes para TVD desenvolvido no âmbito do Centro de Tecnologia de Informação e Comunicação (CTIC/MCT), gerenciado pela Rede Nacional de Pesquisas (RNP).

[8] http://www.pucrs.br/cptw/

[9] http://www.inatel.br/
[10] , R&S ETL TV Analyzer.

Cite this article:
Romani, E., Bezerra da Silva, W., Costa de Borba, M. A., Ono Fonseca, K. V. and de Almeida Prado, A.; 2015. Digital TV Signal Reception Testing in a Device with Spatial Diversity. ISSN Print: 2446-9246 ISSN Online: 2446-9432. doi: 10.18580/setijbe.2015.9
Web Link: http://dx.doi.org/10.18580/setijbe.2015.9

Results of Field Tests of the ISDB-T_B System at 8 MHz in Botswana

Eduardo S. Bueno, Gunnar Bedicks, Jr., Cristiano Akamine, and Edson L. Horta

***Abstract*—Botswana performed field tests of the Integrated Services Digital Broadcasting – Terrestrial version B (ISDB-T_B) system in order to choose which standard should be used by the country. This paper presents the results of performance tests of the ISDB-T_B system and an analysis of test results from the cities of Gaborone, Mahalapye, Maun, and Tsabong. The system was configured with an 8 MHz bandwidth and central frequency of 770.000 MHz. The system was evaluated with fixed reception using a single monopole antenna. Data collected in the field were used to analyze the power level, C/N ratio, Bit Error Rate (BER), and Quasi Error Free (QEF). The results corroborate in the adequate reception of the test signal.**

***Index Terms*—Bandwidth , Integrated Services Digital Broadcasting – Terrestrial version B (ISDB-T_B), Fixed reception.**

I. Introduction

THIS paper presents the results of performance tests for the ISDB-T_B standard, operating at 8 MHz, in four cities of Botswana: Gaborone, Mahalapye, Maun, and Tsabong. The system was evaluated on channel 58, with a frequency of 770.000 MHz. ISDB-T_B was designed to provide high quality audio and picture for fixed and mobile reception. It was also designed to deliver flexibility, interactivity, and expansion capabilities [1].

ISDB-T_B is derived from the Japanese ISDB-T system and employs the H.264 video codec, the MPEG-4 AAC HE audio codec, and a Brazilian middleware (DTVi). It uses VHF (channels 7-13) and UHF (channels 14-69) bands, with a 6 MHz bandwidth [2-8]. This system was developed in Brazil, where its performance operating at 6 MHz for fixed, mobile, and portable reception was demonstrated. [7-8]. The research conducted in order to approve the system also influenced its adoption by other countries, such as Peru, Argentina, Chile, Venezuela, Ecuador, Costa Rica, Paraguay, Philippines, Bolivia, Uruguay, and the Republic of the Maldives [7], [8]. Recently, Botswana adopted ISDB-T_B after analyzing the results presented in this paper.

Eduardo S. Bueno is a researcher at Mackenzie Presbyterian University, São Paulo, Brazil (e-mail: eduardo.bueno@mackenzie.br).

Gunnar Bedicks, Jr., is a professor at Mackenzie Presbyterian University, São Paulo, Brazil (e-mail: gunnar.bedicks@mackenzie.br).

Cristiano Akamine is a professor at Mackenzie Presbyterian University, São Paulo, Brazil (e-mail: cristiano.akamine@mackenzie.br).

Edson L. Horta is a professor at Mackenzie Presbyterian University, São Paulo, Brazil (e-mail: edson.horta@mackenzie.br).

II. ISDB-T 8 MHz

The ISDB-T system was developed in Japan. It uses BST-OFDM modulation with 13 segments and operates using 6, 7 or 8 MHz channels (BW_{TV}) [9]. Each segment contains a carrier set that occupies 1/14 x BW_{TV} [10]. Thus, the bandwidth of one segment is equal to 571.40 KHz when a BW_{TV} of 8 MHz is used. The 13 segments can be combined in up to three hierarchical layers, A, B, and C. The ISDB-T transmission system can be represented by three stages: re-multiplexing, channel coding, and modulation [11].

In the first stage, the MPEG-2 TS (188 bytes) coming from the multiplexing stage is responsible for BTS generation. The BTS is composed of a single TS of 204 bytes and a constant bitrate of 4 x Fs_{IFFT} (sampling frequency of the Inverse Fast Fourier Transform) at the modulator. This frequency is calculated from the IFFT size and the effective duration of the OFDM symbol. For 8 MHz, Fs_{IFFT} = 8192/756 µs = 10.8359 MHz, yielding a BTS bitrate of 43.3439 Mbps. BTS is composed of the TSP from each layer and null packets, called BTS frames. The packets must be ordered to guarantee the hierarchical transmission of a single TS and to minimize processing by the receiver [12]. The null packets are inserted to maintain the constant bit rate independent of the modulation parameters [11]. The channel coding is formed from a Reed Solomon block (188,204,8), an energy dispersal block formed by a 15-bit PRBS generator, a byte convolutional interleaver, a convolutional coder with a mother code rate of 1/2 (G1 = 171oct; G2 = 133oct) and puncture adjust for the rates R = 1/2, 2/3, 3/4, 5/6 or 7/8.

At the modulation stage, the channel coding signal is parallelized and processed by a MUX convolutional interleaving. Mapping is done for QPSK/DQPSK, 16-QAM or 64-QAM modulations. The layers are combined and time interleaved using 0 ms, 100 ms, 200 ms or 400 ms intervals [1], [9], [13]. The second stage of the modulation consists of one OFDM modulator operating with an inverse fast Fourier transform. The carrier amount (Nc) is 1405 in mode 1 (2K), 2809 in mode 2 (4K) or 5617 in mode 3 (8K) [9]. The output of the OFDM modulator is appended with a cyclic prefix formed by a copy of the end of the OFDM symbol. This prefix can be adjusted for GI 1/4, 1/8, 1/16 or 1/32, providing robustness against Inter-Symbol Interference (ISI) [14].

As the Fs_{IFFT} is directly related to the modulator bandwidth, this stage determines the occupation of the OFDM spectrum. The useful bandwidth BW used by the 13 segments is 7.43 MHz. Independent of BW_{TV}, the re-multiplexing, channel coding, and modulation stages are the same. The useful bitrate

doi: 10.18580/setijbe.2015.10 Web Link: http://dx.doi.org/10.18580/setijbe.2015.10

for segment Rb can be calculated using (1). D_{cs} is the data carrier amount: 96 in mode 1, 192 in mode 2 or 384 in mode 3. Nb is number of bits per symbol: 2 for QPSK, 4 for 16-QAM or 6 for 64-QAM. RS, the Reed Solomon code ratio, is 188/204.

$$Rb = \frac{1}{Tu} \cdot Dcs \cdot Nb \cdot R \cdot RS \cdot GI' \quad (1)$$

$$Tu = \frac{Nc-1}{BW} \quad (2)$$

$$GI' \frac{1}{GI+1} \quad (3)$$

ISDB-T was designed and tested at 6 MHz [2], [4], [10], and [15-17]. However, the performance does not change at different bandwidths. Planning criteria, including protection indices, for terrestrial digital television services were designed and tested at 8 MHz [18]. It is recommended that a receiver's tuner unit be compliant with ITU-R BT.1368-9, (see Tables I and II). The transmission parameters employed to obtain the measurements, which are presented in Table II, were 64-QAM modulation and an inner code of 3/4. Tables III and IV present the receiver parameters used in the tests.

The maximum signal level injected at the receiver input was -20 dBm in order to eliminate any risk of damage.

TABLE I
SENSITIVITY AT RECEIVER INPUT

Frequency [MHz]	UHF 600			
System	DQPSK 1/2	QPSK 1/2	16-QAM 3/4	64-QAM 7/8
P*min* [dBm]	-92	-93	-84	-76
(C/N) [dB]	6.20	4.90	14.60	22.00

TABLE II
PROTECTION RATIOS

Undesirable signal	Item	Protection ratio [dB]
Digital transmission ISDB-T	Co-channel	+20
	Lower adjacent channel	-30
	Upper adjacent channel	-30
Analog transmission I/PAL	Co-channel	+5
	Lower adjacent channel	*
	Upper adjacent channel	*

* Not established by a standard

TABLE III
SENSITIVITY AT RECEIVER INPUT [dBm)

Modulation Scheme	Inner-code coding ratio 1/2	2/3	3/4	5/6	7/8
QPSK	-94.2	-92.9	-91.3	-90.7	-89.9
16QAM	-89	-86.7	-85.9	-84.5	-83.7
64QAM	-84.1	-81.3	-80	-77.5	-76.1

TABLE IV
TRANSMISSION PARAMETERS AND REQUIRED C/N RATIO [dB]

Modulation Scheme	Inner-code coding ratio 1/2	2/3	3/4	5/6	7/8
QPSK	3.3	4.9	5.7	6.8	7.6
16QAM	8.9	11.2	12.3	13.4	14.3
64QAM	14.2	17.2	17.9	19.6	22

Prior to the field tests, some laboratory tests were made with two objectives in mind. The first was determining the receiver behavior for specific BER values. The second was analyzing the relationship between C/N and BER in a laboratory environment. This relationship can then be used as a reference for an analysis of the field tests. The laboratory tests were conducted in a controlled environment and were completely immune to external interferences.

During the field tests, the signal was transmitted from a tower 50 meters above the ground. In Gaborone, the transmission station was 1205 meters above sea level. In Mahalapye, the station was on a mountain with an altitude of 1245 meters. In Maun, the altitude was 950 meters, and in Tsabong, the altitude was 968 meters.

The same transmitter was used in each city. The RF transmission system is composed of an antenna, a transmission line, and high power amplifiers, all designed for the ISDB-T_B system. The transmission equipment includes a TS server, an ISDB-T_B exciter, RF amplifiers, and channel filters.

The system parameters were configured according the standards [9] and [19]. Table V shows the modulation parameters used in the tests. The transmitter used UHF channel 58 (center frequency of 770 MHz) with an 8 MHz bandwidth. The antenna was an omnidirectional Jampro Trunstile, with a gain of 8.23 dBd. The mean power level of the RF amplifiers was 1 Kw, with ERP ≅ 34 dBw (considering cable and conector losses).

TABLE V
ISDB-T PARAMETERS

Bandwidth	8 MHz		
Mode	3 (8K)		
Guard Interval	1/16		
Layer	A	B	C
Segments	1	3	9
Carrier Modulation	QPSK	16-QAM	64-QAM
Convolutional Coder	1/2	2/3	3/4
Time interleaving [ms]	=287	=287	=287
Bit Rate [Mbps]	0.44	3.52	17.84

The procedure used was based on test procedures from the evaluation of other DTV transmission systems, along with the recommendations and standards for this system. Based on [10], [20], and [21], the test plan was developed, and a measurement system was created in order to perform the field tests. The main task of the field tests was to measure the performance of a DTV system transmitting on UHF channel 58 (776 – 774 MHz). The mean signal power at an 8 MHz

doi: 10.18580/setijbe.2015.10 Web Link: http://dx.doi.org/10.18580/setijbe.2015.10

bandwidth, C/N ratio, BER, localization and perceived video quality, QEF [21], were measured. The subjective evaluation of the video quality was an adaptation of the ITU [20] using four grades (see Table VI). Grades "1" and "3" indicate intermittent reception, where "3" indicates that the image does not annoy the viewer and "1" indicates that the image does. BER values indicate an approximate range that would be measured at the receiver used in the tests. The BER values, obtained before the Reed Solomon coding, were measured in the laboratory.

TABLE VI
QUALITY RATING SCALE

Grade	Image	BER
5	error free	0.00E+00 – 2.00E-04
3	slightly annoying	4.50E-04 – 2.40E-03
1	very annoying	5.50E-03 – 1.20E-02
0	no lock	1.48E-02 – 1.00E+00

The field tests were performed in conjunction with the Department of Broadcasting Services (DBS) and the Botswana Telecommunications Authority (BTA), which provided the test vehicle (Fig. 1), equipped with measurement instruments for the ISDB-T_B system. The tests were performed at 41 locations in the four different cities. The reception measurements were obtained using a monopole antenna with -2.26 dBd gain, located 2.5 meters above the ground.

The setup used in the field tests is shown in Fig. 1. An ISDB-T_B receiver was used for channel decoding. Performance was measured using a subjective reception analysis, similar to [20]. An Anritsu MS8911B signal analyzer was used to measure the signal intensity level and analyze the signal characteristics. The system was calibrated, and the receiver was tested prior to the tests, in order to confirm that its sensitivity met specifications [17] and [18].

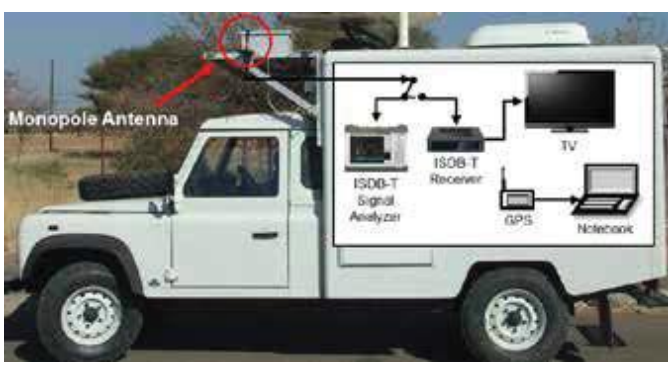

Fig. 1. Transmission System

The measurement methodology was based on [21] and other test procedures used to evaluate DTV transmission systems [10], [22-25].

The test vehicle was moved to each predetermined test site, where the following characteristics were recorded: time, geospatial coordinates, local environmental characteristics, urban density and traffic. The main reason for this was to characterize the test site with regard to the buildings and local traffic, which may cause unwanted effects on the signal reception. The power level, C/N and BER were also recorded for each test site. For each location, it was necessary to manually search for the receiver channel. The reception quality was measured using a subjective analysis. This analysis was performed by observing an image for sixty seconds, QEF, and grading it according to Table IV.

IV. DTV FIELD TEST RESULTS

This section describes the most important measurements for designing digital transmission systems. Many data sets were collected at each location in order to evaluate the signal reception quality under different interference and fading conditions in the field.

Four small cities in Botswana were analyzed, with a total of 41 measurement locations, covering the entire area of each city. In the results, DBA refers to the distance from the test site to the antenna, and the BER values were obtained before the Reed Solomon coding.

Gaborone, the largest city in Botswana, had 17 measurement locations (Fig. 2). In contrast to other cities in Botswana, Gaborone has many buildings and intense traffic, and some of the test sites did not have a direct line-of-sight to the transmission tower.

Fig. 2. Test Sites in Gaborne

In Gaborone, some test sites did not obtain adequate reception, as shown on Table VII. Test sites 1, 5 and 7 were graded "0", "0" and "1", respectively. These locations are urban areas and 10 km from the transmission tower. The buildings caused signal obstruction and reflection. Site 12 is an industrial zone and received a grade of "0". Site 14 is a residential zone and received a grade of "3". Both locations are approximately 15 km from the transmission tower and are obscured by buildings in the city center. Hence, test site 12 did not receive sufficient signal intensity, and site 14 had a close-in echo of -30 dB relative to the main signal (Echo to Carrier ratio = E/C = -30 dB), due to the existence of buildings.

TABLE VII
RESULTS OF FIELD TESTS AT GABORONE

Site	Location	DBA [Km]	Signal Level [dBm]	C/N [db]	BER	Grade
1	Civic Center	10.70	-79.0	7.5	1.65E-02	0
2	Tsholofelo P.	7.54	-67.0	24	0.00E+00	5
3	Broadhurst	7.62	-66.0	18	0.00E+00	5
4	Ledumang SSS	4.40	-44.6	24	0.00E+00	5
5	MMC	9.85	-78.7	11	1.65E-02	0
6	Block 7	8.90	-65.0	23	0.00E+00	5
7	Mogoditshane	10.90	-78.0	18	6.64E-03	1
8	Ledumadumane	9.09	-57.0	23	0.00E+00	5
9	Phakalane	4.30	-58.4	24	0.00E+00	5
10	Gaborone N	4.72	-67.5	22	2.20E-04	5
11	CBD	10.70	-63.0	21	2.50E-05	5
12	Gaborone W	15.35	-81.0	7	1.65E-02	0
13	Gaborone W	14.40	-74.0	21	0.00E+00	5
14	Old C. Hall	14.75	-77.8	17.1	2.50E-03	3
15	Old C. Hall	14.20	-76.6	19	4.50E-05	5
16	Block 9	14.60	-72.1	22	0.00E+00	5
17	SSKA	3.52	-59.6	20.6	0.00E+00	5

In Mahalapye, 7 measurements were performed (Fig. 3). This city has only houses and moderate traffic, and the transmission tower is on a mountain 1245 meters above sea level. Although there was a large distance from the city to the tower, every test site had a direct line-of-sight to the transmission tower.

Fig. 3. Test Sites in Mahalapye

Every test site in Malahapey obtained adequate reception, with grades of "5". The results are presented in Table VIII.

In Maun, a small city with low traffic, there were 10 measurements (Fig. 4). It has three districts far from the center of the city, which caused fading, and there is an airport in the center.

In Maun, only one location did not obtain adequate reception, as shown in Table IX. Site 5 is a rural zone, 32.9 km from the transmission tower, and obtained a grade of "3", due to the low intensity signal and multipath interference. The maximum echo, which was also a close-in echo, had an E/C = -20 dB.

TABLE VIII
RESULTS OF FIELD TESTS AT MAHALPYE

Site	Location	DBA [km]	Signal Level [dBm]	C/N [dB]	BER	Grade
1	D. Ward	10.90	-53.1	22	0.00E+00	5
2	Tshikinyega	12.20	-60.4	23.6	0.00E+00	5
3	Xhosa	13.90	-71.5	21.6	2.00E-06	5
4	Xhosa 1	13.50	-62.3	22.3	1.00E-06	5
5	Flowertown	16.30	-59.1	24.2	0.00E+00	5
6	T. Ward	14.60	-70.9	23.4	0.00E+00	5
7	Mahalapye W	12.50	-52.0	23.6	0.00E+00	5

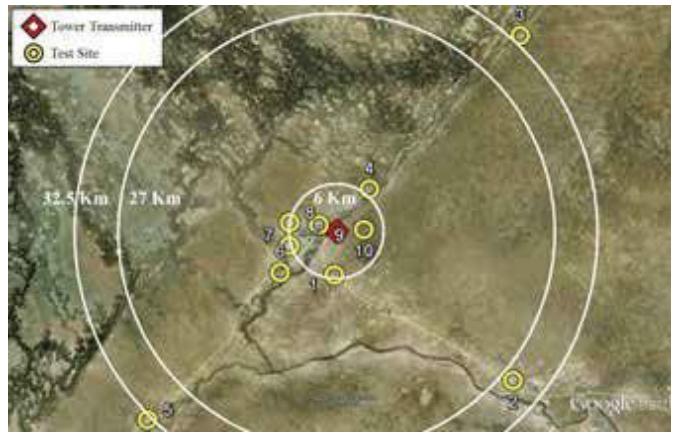

Fig. 4. Test Sites in Maun

TABLE IX
RESULTS OF FIELD TESTS AT GABORONE

Site	Location	DBA [Km]	Signal Level [dBm]	C/N [dB]	BER	Grade
1	Matshwane	5.40	-51.1	23	0.00E+00	5
2	Chanoga	28.40	-76.7	19.2	4.70E-05	5
3	Shorobe	33.30	-78.0	18.7	1.77E-04	5
4	Boronyane	6.60	-59.1	25.7	0.00E+00	5
5	Kimana	32.90	-77.7	18.5	1.21E-03	3
6	Shashe	8.67	-68.5	21.7	2.00E-06	5
7	Bomadi	6.13	-60.0	23.4	0.00E+00	5
8	Botshabelo	5.93	-63.0	23.2	0.00E+00	5
9	Airport	2.31	-68.6	19.7	2.20E-05	5
10	Disaneng	3.33	-50.4	23.3	0.00E+00	5

In Tsabong, a small city with low traffic, 7 measurements were made (Fig. 5). In this city, only one site did not obtain adequate reception, as shown in Table X. Site 7 is a rural zone, 26.1 km from transmission tower, next to the border with South Africa. It is surrounded by mountains and obtained grade of "3", due to low signal intensity.

doi: 10.18580/setijbe.2015.10 Web Link: http://dx.doi.org/10.18580/setijbe.2015.10

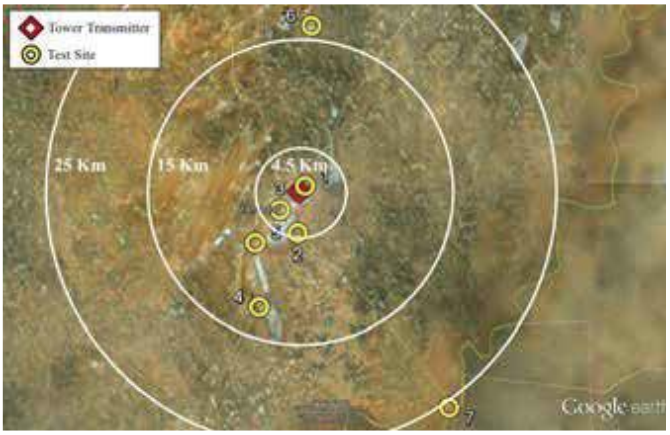

Fig. 5. Test Sites in Tsabong

TABLE X
RESULTS OF FIELD TESTS AT TSABONG

Site	Location	DBA [Km]	Signal Level [dBm]	C/N [dB]	BER	Grade
1	BDFCamp	0.60	-47.8	24.6	0.00E+00	5
2	Mokha	4.48	-67.7	21.5	3.00E-06	5
3	Tsabon M.	2.60	-47.7	24.5	0.00E+00	5
4	Logaganeng	12.30	-61.5	26	0.00E+00	5
5	-	6.87	-52.80	24.7	0.00E+00	5
6	Maleshe	15.80	-72.0	21.9	4.00E-06	5
7	MacCathy	26.10	-78.7	17.8	8.60E-04	3

Table XI provides a direct comparison between the signal reception qualities of the four cities in Botswana. Reception margin is an important parameter of DTV service. It indicates whether a digital TV signal can be received without errors and how many dB the C/N ratio may be degraded before reaching the reception limit (Fig. 6) [23], [25].

TABLE XI
FIXED SERVICES AVAILABILITY

Grade	Gaborone	Mahalapye	Maun	Tsabong	Total
5	70.59%	100.00%	90.00%	85.71%	82.93%
3	5.88%	0.00%	10.00%	14.29%	7.32%
1	5.88%	0.00%	0.00%	0.00%	2.44%
0	17.65%	0.00%	0.00%	0.00%	7.32%

In Fig. 6, C/N ration are on the horizontal axis, and BER measurements are on the vertical axis, using a logarithmic scale. The values above the points represent the grades. In Fig. 6, the curve represents the laboratory tests, performed in a controlled environment, completely immune from external interferences. From these results, it was observed that for C/N ration above 17.5 dB, no errors are seen at the receiver. Based on the field tests, C/N ration below 15 dB obtained a grade of "0". These values were discarded. C/N ration between 17 dB and 18.5 dB obtained grades of "3" or "1". C/N ration above 18.7 dB obtained a grade of "5".

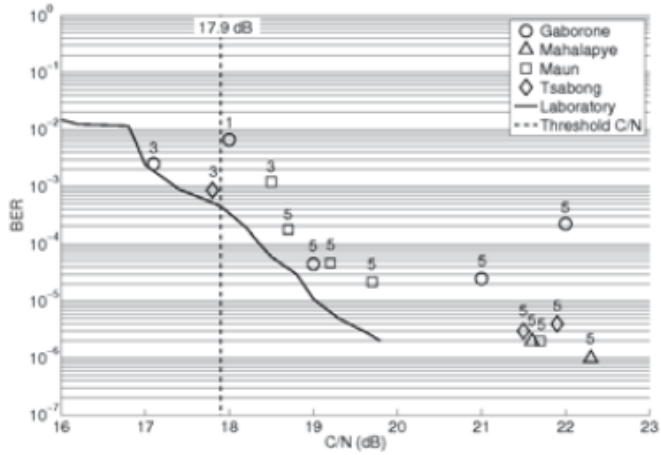

Fig. 5. BER x C/N (Comparison of Field and Lab Test)

V. DTV FIELD TEST ANALYSIS

With ISDB-T_B, the minimum C/N ration at the receiver in the tests was 17.9 dB (BER = 2.0E-4, before Reed Solomon coding), as characterized in the laboratory. Furthermore, the minimum field intensity for fixed reception was Pmin = -80 dBm. However, it is worth mentioning that this minimum C/N ration (17.9 dB) was obtained from subjective evaluations of video quality, QEF, under controlled conditions, without multipath interference. In the field tests, the threshold C/N ration may be higher [10], [23] and [25]. The C/N ration is an important factor for satisfactory reception (Fig. 6). The majority of test sites had the possibility of perfect reception when the C/N ratio was greater than 17.9 dB, the receiver protection ratio threshold. However, high C/N ration do not guarantee good reception. For example, a DTV receiver may fail when there is multipath interference. This is demonstrated by the existence of error in the reception signal at two test sites with C/N ratios greater than 17.9 dB.

The results for Mahalapye, Maun and Tsabong, which are shown in Table XI, are better than those for Gaborone because echoes are generally found in urban areas, where there is no direct line-of-sight without physical obstruction to the transmission tower from the reception location [10]. The effect of echoes can be seen at three test sites (1, 5 and 7) close to downtown Gaborone, 10 km from transmission tower. Test site 1 had a power level of -79 dBm, which is close to the reception threshold, and there was also a close-in echo with E/C = -4.5 dB, produced by the surrounding structures; the grade at this site was "0". Test site 5 had a power level of -78.7 dBm, which is close to the reception threshold, and there was also a close-in echo with E/C = -10 dB; the grade at this site was also "0". Test site 7 had a power level of -78 dBm, which is within the reception threshold, but there was a close-in echo with E/C = -10 dB. Its grade was "1", and its C/N ratio was 18 dB, which is close to the minimum value. Test sites 12 and 14 in Gaborone were approximately 15 km from the transmission tower and also did not obtain adequate reception. Test site 12 had a power level of -81 dBm, which is insufficient signal intensity, yielding a grade of "0". Test site 14 had a power level of -77.8 dBm, which is within the

doi: 10.18580/setijbe.2015.10 Web Link: http://dx.doi.org/10.18580/setijbe.2015.10

reception threshold, but there was an echo with E/C = -35 dB, and its grade was "3". Its C/N ratio was 17.1 dB, which is less than the minimum value.

Mahalapye had the best performance because it is a secondary city, and the transmission tower was on a mountain, with direct line-of-sight to all reception locations. Thus, the signal intensity ranged from -52 dBm to -71 dBm.

In Maun, test site 5 had a power level of -77.7 dBm, which is within the reception threshold, but there was a close-in echo with E/C = -20 dB. Its grade was "3", and its C/N ratio was 18.5 dB, which is greater than the minimum value. In Tsabong, test site 7 was 26.1 km from the transmission tower, and the power level was -78.7 dBm, which is close to the reception threshold. Its grade was "3", and its C/N ratio was 17.8 dB, which is less than the minimum value.

In the field tests, 34 of 41 locations obtained good reception quality using a monopole antenna. Among the seven locations with poor reception, two of them had a C/N ratio greater than 17.9 dB, but the reception was intermittent. This intermittent reception was due to distortion of the received signal caused by multipath interference in addition to the noise. The other five locations did not have sufficient signal intensity above the noise level.

VI. Conclusion

Field tests were performed at 41 location tests in Botswana for digital TV signal. These tests showed that the ISDB-T_B system had a service availability of 82.93% at the test sites. The urban zones have lower C/N ratios than other locations. Furthermore, in urban areas, the probability of signal distortion due to multipath interference is very high and yields a high probability of poor reception quality. It was verified that reception quality is determined mainly by the C/N ratio and signal distortion due to multipath interference.

A digital TV modulation system is chosen based on how well it can fulfill the particular requirements and priorities of a country. Additionally, other non-technical factors, such as geographic, economic and political relations with neighboring countries, have to be considered. Each country needs to determine its needs and then study the available information about the performance of different systems in order to choose the best one. On February 26, 2013, Botswana adopted the ISDB-T_B system as its standard for digital terrestrial TV. Botswana was the first country in Africa to adopt the ISDB-T_B system.

Acknowledgment

The authors would like to thank RH-TVD CAPES, their colleagues at the Mackenzie Digital TV and Radio Research Centre and Calvin Goiletswe from the Department of Broadcasting Services of Botswana.

References

[1] M.Takada and M.Saito, "Transmission system for ISDB-T," *Proc. of the IEEE*, vol. 94, no. 1, pp. 251–256, Jan. 2006.
[2] *Digital terrestrial television - Video coding, audio coding and multiplexing - Part 1: Video coding*, ABNT NBR 15602-1, Dec. 2007.
[3] *Information technology - Coding of audio-visual objects – Part 10: Advanced Video Coding*, ISO/IEC 14496-10, Oct. 2004.
[4] *Digital terrestrial television - Video coding, audio coding and multiplexing - Part 2: Audio coding*, ABNT NBR 15602-2, Dec. 2007.
[5] *Coding of audio-visual objects - Part 3: Audio*, ISO/IEC 14496-3, 2007.
[6] *Digital terrestrial television - Data coding and transmission specification for digital broadcasting Part 5: Ginga-NCL for portable receivers - XML application language for application coding*, ABNT NBR 15606-5, Apr. 2009.
[7] G. Bedicks Jr. et al., "Outlines of the brazilian digital terrestrial television broadcasting system," in *57th annual IEEE Broadcasting Symposium*, Washington, DC, Oct.1st Nov.2007.
[8] G. Bedicks Jr. et al., "Performance evaluation of brazilian DTV mobile reception," in *BMSB*. Bilbao, Guatemala, May 2009.
[9] *Transmission System for Digital Terrestrial Television Broadcasting*, ARIB STD B31, 2005.
[10] Y. Wu et al., "Comparison of terrestrial DTV transmission systems: The ATSC 8-VSB, the DVB-T COFDM, and the ISDB-T BST-OFDM," vol. 46, no. 2, pp. 101–113, 2000.
[11] C. Akamine et al., "Re-multiplexing ISDB-T BTS into DVB TS for SFN," vol. 55, no. 4, pp. 802–809, 2009.
[12] M. Uehara, "Application of MPEG-2 systems to terrestrial ISDB (ISDB-T)," *Proc.of the IEEE*, vol. 94, no. 1, pp. 261–268, Jan. 2006.
[13] G. Bedicks Jr. et al., "Field measurements for ISDB-T_B in the VHF band," *in BMSB*, Nuremberg, Jun. 2011.
[14] A. Peled and A. Ruiz, "Frequency domain data transmission using reduced computational complexity algorithms," p. 4, 1980.
[15] *Digital terrestrial television - Transmission system*, ABNT NBR 15601, Dec. 2007.
[16] *Digital terrestrial television - Video coding, audio coding and multiplexing - Part 3: Signal multiplexing systems*, ABNT NBR 15602-3, Dec. 2007.
[17] *Digital terrestrial television - Receivers*, ABNT NBR 15604, Dec. 2007.
[18] *Planning criteria, including protection ratios, for digital terrestrial television services in the (VHF/UHF) bands*, ITU-R BT.1368-9, Dec. 2011.
[19] *Error-correction, data framing, modulation and emission methods for digital terrestrial television broadcasting*, ITU-R BT.1306-6, Dec. 2011.
[20] *Methodology for the subjective assessment of the quality of television pictures*, ITU-R BT.500-11, Dec. 2011.
[21] Unified NorDig Test Specifications, NorDig.
[22] G. Bedicks Jr. et al., "Digital signal disturbed by impulsive noise," vol. 51, pp. 322–328, Nov. 2005.
[23] C. -C. Lin, C. -M. Chen, J. -H. Tarng, H. -M. Hang and H.-C. Yu, "Analysis of ATSC field test results in Taiwan," vol. 48, no. 1, pp. 38–43, 2002.
[24] P. Angueira et al., "DTV (COFDM) SFN signal variation field tests in urban environments for portable outdoor reception," vol. 49, no. 1, pp.81–86, 2003.
[25] P. Angueira et al., "DTV reception quality field tests for portable outdoor reception in a single frequency network," vol. 50, no. 1, pp. 42–48, 2004

Cite this article:
S. Bueno, E., Bedicks, Jr., G., Akamine, C., and L. Horta, E.; 2015. Results of Field Tests of the ISDB-TB System at 8 MHz in Botswana. ISSN Print: 2446-9246 ISSN Online: 2446-9432. doi: 10.18580/setijbe.2015.10 Web Link: http://dx.doi.org/10.18580/setijbe.2015.10